Realization of a miniaturized planar amperometric glucose sensor for biomedical applications

Dissertation
submitted to the Faculty of Sciences of the University of Neuchâtel
to obtain the degree of Doctor of Sciences

by

Samuel A. GERNET

Dipl. Phys. ETHZ

Institute of Microtechnology
University of Neuchâtel
Breguet 2, 2000 Neuchâtel
Switzerland

To my wife

IMPRIMATUR POUR LA THÈSE

Réalisation d'un capteur de glucose ampéro-métrique miniaturisé pour des applications biomédicales

de Monsieur Samuel Gernet

UNIVERSITÉ DE NEUCHÂTEL

FACULTÉ DES SCIENCES

La Faculté des sciences de l'Université de Neuchâtel sur le rapport des membres du jury,

MM. N. de Rooij, A. Shah, Mme M. Koudelka Hep, MM. J.-P. Randin (Neuchâtel) et H.L. Schmidt (Munich)

autorise l'impression de la présente thèse.

Neuchâtel, le 6 août 1990

Le doyen:

Cl. Mermod

Abstract

Glucose sensors may be applied for an improved control of diabetes mellitus. Moreover, they may be used in analytical chemistry as well as for bioprocess control applications. In the first field, sensor miniaturization plays an important role, especially when enzyme electrodes have to be used in vivo.

Glucose can be detected by a variety of methods. Simple enzyme electrodes consisting of an electrochemical cell and a membrane part offer the potential of highly specific, simple and accurate biosensors. One of the most successful method is the amperometric detection of hydrogen peroxide formed within a glucose oxidase enzyme membrane. Planar devices can be realized using thin film techniques, so that they are particularly suitable for mass production and miniaturization.

This thesis describes the development of a miniaturized planar amperometric glucose sensor. The electrochemical microcell consists of two platinum electrodes and one silver/ silver chloride reference electrode. An important objective is the study of the electrochemical behavior in order to draw a parallel between some technological parameters of thin film processing and the electrode surface properties. The membrane part consists of an inner glucose oxidase membrane and an outer dip-coated polyurethane membrane. The enzymatic layer can be deposited on individual sensor chips using a μ-pipette or by spin-coating the enzyme solution on wafer level.

On wafer deposited membranes show a well defined geometry and a good uniformity of membrane thickness and, thus, are particularly suitable for testing theoretical models of enzyme electrodes. Hence, an other important goal of this work is the modelization of the competitive effects of diffusion and bisubstrate enzyme reaction allowing thus a better analysis of sensor responses.

Contents

I
Introduction

1.0 Summary

This chapter reviews generally the disease and treatment of diabetes mellitus, presents the problems of insulin administration used so far and shows the necessity of developing implantable glucose sensors for an improved control of diabetes. Further, the environment of this project, its origin and evolution, is depicted. Finally the objective and the structure of this thesis are outlined.

1.1 Disease and treatment of diabetes mellitus

This section describes the pathophysiology of diabetes mellitus, gives a classification of the main types of diabetes, reviews the appropriate treatments and describes the methods for an improved control of diabetes. Moreover, the aim of developing implantable glucose sensor briefly will be discussed.

1.1.1 Pathophysiology

Diabetes mellitus is a disease manifested by the loss of control of the blood glucose level. It is not a single disease but a collection of disorders, all related by the presence of a chronically raised blood glucose concentration (hyperglycaemia) and due biochemically to a relative or absolute lack of insulin [1]. Insulin is a polypeptide hormone (molecular weight, 6000) which is synthesized, stored and secreted from the beta cells of the pancreatic islets of Langerhans. The best understood action of insulin is to lower the blood glucose concentration and this is mainly accomplished by suppressing glucose output from the liver, but insulin also stimulates glucose uptake into peripheral cells such as muscle and adipose tissue. The maintenance of blood glucose levels within a very narrow range (of about 3.5-6.5 mM in the human) is extremely important since the brain uses glucose as virtually its only source of energy and low levels (hypoglycaemia) cause mental confusion and, if sustained, coma and death. On the other hand, high blood glucose levels cause unpleasant short-term symptoms, such as frequent urination and thirst, and in the long term are probably a major factor in the development of tissue damage in the blood vessels, eyes, kidneys and nerves [2]. Moreover diabetic patients have a life expectancy of one-third less than the general population [3].

Blood glucose concentrations in the range of 1-30 mM may be observed in 'treated' diabetics. In normal subjects high levels of glucose stimulate insulin release from the islets of Langerhans and low levels inhibit secretion. Evidently, the beta cell has a glucose sensor but the full nature of this mechanism is not understood. Moreover, when hypoglycaemia occurs, the body releases a burst of 'counter regulatory' hormones (cortisol, glucagon, adrenaline, noradrenaline and growth hormone) which oppose the action of insulin and raise the concentration of blood glucose.

Insulin also has many metabolic actions distinct from glucose and carbohydrate pathways; in general it can be taken as the hormone of macromolecular synthesis, stimulating the conversion of small molecular weight fuels into their large storage forms, e.g. glucose into glycogen, fatty acids into triglycerides and amino acids into proteins. Insulin deficiency causes breakdown of these macromolecules and elevates levels of, for example, fatty acids and amino acids, as well as glucose.

1.1.2 Classification of diabetes mellitus

About one to three per cent of the population in affluent societies (five to ten per cent of those over 40 years) suffer from diabetes [4]. The two main types of diabetes are called insulin-dependent, juvenile-onset or type 1 diabetes and non-insulin-dependent, maturity-onset or type 2 diabetes. In addition, diabetes can occur for the first time during pregnancy, and on rare occasions it is secondary to other diseases such as chronic pancreatitis (long-standing pancreatic inflammation, often due to alcoholism) and over-secretion of the hormones which antagonise insulin (cortisol, glucagon, growth hormone and catecholamines).

About 20% of diabetic patients have type 1 diabetes. The onset of the disease is usually in childhood and early adulthood (under the age of 35 years) and the patients are usually lean. The pathology of type 1 diabetes is one of beta cell injury leading to complete destruction, so that blood levels of insulin are very low or absent. The cause of this ß-cell damage is not known but may be viral attack of the pancreas, autoimmunity (i.e. antibodies or cell-mediated immunity against the body's own tissues) and environmental toxins. Heredity also plays a complex and poorly understood part since diabetes tends to run in families. Current thinking is that a tendency to develop diabetes is inherited (perhaps a defect in the immune response system) and that additional environmental triggers (viruses, toxic chemicals) are necessary in later life for the development of the actual disease.

Type 2 diabetic patients comprise about 80% of the diabetic population and here the onset of the disease is usually between 50 and 70 years of age. Many of the patients are overweight. Again, the cause of this type of diabetes is unknown, but it is recognized that there is (a) resistance against the action of insulin at the target organs due, in part, to a decrease in receptor numbers and (b) impaired glucose-stimulated insulin secretion from the pancreas. However, the ß-cell mass is intact and blood insulin concentrations in this type of diabetes are normal or elevated.

1.1.3 Treatment of diabetes mellitus

Because type I diabetics have an absolute insulin deficiency they must receive insulin injections to live. Without them these patients become severely ill as the blood glucose and ketone body concentrations rise; they become dehydrated, acidotic, drowsy and eventually comatose, a syndrome known as diabetic ketoacidosis. Conventional treatment takes the form of several (one to four) daily insulin injections given into the subcutaneous tissues of the arms, legs, abdomen or buttocks.

Type 2 diabetics are usually managed by diet or by diet and oral hypoglycaemia agents. The latter are drugs which release insulin from the pancreas and sustain its action at the peripheral receptors. Occasionally, type 2 patients are transferred to insulin therapy when diet and oral agents have failed to produce sufficient lowering of blood glucose. Usually, these patients do not develop diabetic ketoacidosis.

Insulin, diet and oral hypoglycaemic drugs are able to control the acute symptoms of hyperglycaemia but in the long term complications may appear [5]. Small blood vessel disease (microangiopathy) results in impaired kidney function (nephropathy) and, in some cases, death from kidney failure. Microangiopathic changes in the eye (retinopathy) can lead to loss of vision, so that, nowadays, diabetes is the commonest cause of blindness in the Western World under the age of 65 years. Diabetic peripheral nerve disease is responsible for loss of or altered sensation, particularly in the limbs, and neuropathy affecting the autonomic nervous system for complications such as impotence and diarrhoea. Large blood vessel disease (macroangiopathy) causes accelerated coronary artery disease, strokes and circulatory impairment in the limbs.

In spite of the terrible consequences of micro- and macroangiopathy, the greatest fear of the insulin-dependent diabetic is probably hypoglycaemia. Most diabetic patients have impaired counter-regulatory hormone responses to hypoglycaemia so that metabolic recovery is delayed [6]. In addition, many also have no symptoms of hypoglycaemia, such as sweating, and fail to recognise that the blood glucose concentration is dangerously low. All insulin-dependent diabetics are at risk of unpredictable hypoglycaemic attacks which may be caused by factors such as erratic absorption of insulin from the subcutaneous tissue, exercise, missed meals and inappropriate insulin injection regimes.

1.1.4 Methods for an improved control of diabetes

It is certainly a fact that ordinary insulin therapy is unable to maintain normal blood glucose level throughout the entire day and, thus, does not mimic non-diabetic insulin secretion sufficiently closely to achieve normoglycaemia [7].

To improve metabolic control in diabetic patients more physiological strategies of insulin administration have been developed. The four most important approaches are (a) self-monitoring of blood glucose samples and adjustment of insulin dosages based on the results, (b) electromechanical open-loop devices for continuous insulin infusion, (c) closed-loop devices with feedback control of insulin delivery rates and (d) transplantation of the pancreas or isolated islets of Langerhans.

Blood glucose self-monitoring techniques involve placing a finger-prick sample of capillary blood on a strip impregnated with the enzyme glucose oxidase (e.g. Dextrostix, Ames; BM Test-Glycaemie, Boehringer). The hydrogen peroxide produced in this enzyme layer reacts with a dye in the presence of peroxidase giving a colour change. The intensity is then proportional to the blood glucose concentration. Values can be estimated by comparing the colour with a printed chart or by using a portable reflectance meter (e.g. Glucochek, Glucometer, Ames, Hypocount, Hypoguard). The basis of improved control using this technique is that the patient can close the loop himself by adapting the insulin injection or nourishment, according to the strip result.

The search for better methods of treating insulin-dependent diabetes led to the development of portable infusion systems for continuous insulin delivery. Such systems, known as open-loop devices, consist of an insulin pump, a reservoir, and a power supply but still are not self-regulated. Hence, the blood glucose is normalized by a pre-programmed insulin pump at a variety of pre-set rates. The physician or the patient decides the timing and magnitude of infusion rates based on the patient's sensitivity to insulin, intake of food and finger-prick samples of blood-glucose with reagent strips. Applying this method carefully, near normoglycaemia can be achieved. Among the intravenous, intramuscular and intraperitoneal routes of administration the most popular technique is that of continuous subcutaneous insulin infusion [8].

Conventional insulin therapy requires multiple daily insulin injections to achieve a near normal physiological regulation of blood glucose. Open-loop devices do not have this disadvantage, but they must be carried by the patient all the time. Both conventional insulin therapy and open-loop therapy need frequent glucose measurements by the patient to maintain adequate glycaemic control since diet and exercise demand an

adaption of the insulin doses. This deficiency led to the development of a portable self-regulated system, called a closed-loop system. Such a device consists of an insulin delivery system and an implantable glucose sensor. The main advantage of a closed-loop insulin delivery device is its independence of external glucose measurements and its ability to cope with the variations of insulin requirements.
A closed-loop device is available commercially (the Biostator, Ames-Miles) and is known as artificial endocrine pancreas (AEP). The AEP is a non portable bedside machine which withdraws blood from a peripheral vein and measures the glucose concentration. An on-board computer then calculates, according to pre-set algorithms, the amount of glucose or insulin to be infused into another vein to restore or maintain normoglycaemia. The AEP is especially suitable for the investigation of changes in intermediary metabolites and counter-regulatory hormones which accompany blood glucose control [9, 10]. Its long-term (more than a few days) application is limited by the intravenous insulin infusion route and the associated risks of thrombosis, embolism and septicaemia.
Among the components of a closed-loop device (insulin pump, glucose sensor and microprocessor that translates the information provided by the sensor into the required amount of insulin), the pump and the microprocessor are commercially available, but reliable implantable glucose sensors have still to be developed.

1.1.5 The aim of developing implantable glucose sensors

As seen above, implantable glucose sensors would enable feedback control of an external or implanted insulin-infusion pump. Moreover, as an alternative to finger-prick sampling, an implanted sensor might give a continuous read-out of diabetic control to aid in dosage adjustments, or making possible the recording of daily profiles.
Small, rapid and inexpensive glucose sensors would also be desirable for in vitro analysis of blood samples because the current generation of bench-top laboratory analysers for blood, serum and plasma glucose measurement are moderately bulky and expensive.
In addition, most insulin-dependent diabetics have an impaired perception of hypoglycaemia, so that an audible alarm of hypoglycaemia, triggered by an implanted biosensor, could alert the patient to this condition during the day and wake the patient in the event of nocturnal hypoglycaemia.

Another serious complication of type 1 diabetes is the ketoacidosis with a mortality up to 5% [11]. It is probable that an early warning of rising blood glucose values from an implantable biosensor would prevent further metabolic deterioration.

1.2 Environment of the work

In the beginning of 1984 "l'Association Neuchâteloise du Diabète (AND)" proposed the development of an artificial pancreas in Neuchâtel and initiated a collaboration between the Institute of Microtechnology of the University of Neuchâtel and the "Laboratoires de Recherches Métaboliques de la Faculté de Médicine (LMR)" of the University of Geneva. At the same time both university groups began a bibliographic study. In July 1984 the two groups decided to define a common project on glucose sensors as a main part of an artificial pancreas. In October 1984, the evaluation of the best sensing method for such a glucose sensor was undertaken. This work was supported by the AND. The literature study resulted in the internal report entitled "Stand der Forschung von implantierbaren Glukose-Sensoren". On the basis of this study the realization of an amperometric enzyme sensor was proposed. It was decided that the technological development would be carried out in Neuchâtel whereas the in vivo characterization would be taken up in Geneva.
In February 1985 a research request was submitted to the Swiss National Science Foundation (national program no. 18, "Biomedical techniques") entitled "Development of a specific glucose sensor for ameliorating the treatment of insulin-dependent diabetics". In August 1985 this request, now entitled "Development of a specific glucose sensor for an artificial pancreas", has been granted for a period of four years. In September 1985 an additional request was submitted to the Foundation Lord Michelham of Hellingly and has been accepted in February 1986. In automne 1986 the IMT and the company Disetronic Ltd. in Burgdorf submitted jointly a research request "Entwicklung eines klinisch-einsetzbaren Glukose-Monitors" to the Swiss Committee for the Promotion of Applied Scientific Research. It was granted in summer 1987.
The results of this research have been presented at the following conferences:

Journées de Microtechnique et de Génie Médical, 8.-9. September 1986, Lausanne, Suisse:

"A Planar Enzymatic Sensor for the Determination of Glucose"

Transducers 87, 2.-5. Juni 1987, Tokyo, Japon:

" Voltammetry - A powerful tool for evaluation and process control of thin film electrodes "

Eurosensors II, 2.-4. November 1988, Twente, Pays-bas:

" A planar glucose enzyme electrode"

Int. Symp. on Electroanalysis and Sensors, 6.-9. April 1987, Cardiff, Wales:
"Fabrication and characterization of a planar microelectrochemical cell"

172nd Meting of Electrochem. Soc., 18.-23. October 1987, Honolulu, Hawaii
"Immobilized enzymes studies using a thin planar electrochemical cell"

Moreover the following papers have been published:

S. Gernet, M. Koudelka and N.F. de Rooij
A planar glucose enzyme electrode
Sensors and Actuators, Vol.17, No.3/4, p.537 (1989)

S. Gernet, M. Koudelka and N.F. de Rooij
Fabrication and characterization of a planar electrochemical cell and its application as glucose sensor
Sensors and Actuators, Vol.18, No.1, p.59 (1989)

M. Koudelka, S. Gernet and N.F. de Rooij
Planar amperometric enzyme-based glucose microelectrode
Sensors and Actuators, Vol.18, No.2, p.157 (1989)

1.3 Outline

In **Chapter 2** the most common methods of glucose measurement are reviewed and their features are discussed.

Chapter 3 describes the principle of amperometric glucose detection. Further, the structure and reaction scheme of the enzyme glucose oxidase and its specificity to the β-D-glucose isomer are detailed. In order to understand the basic behaviour of an enzyme electrode, the different enzyme kinetics are briefly described. Since the enzyme glucose oxidase obeys the two-substrate reaction scheme (glucose and oxygen), the thermodynamics of dissolved oxygen is presented.

Chapter 4 treats the major immobilization methods of enzymes. The further properties of immobilized enzyme layers depend on the immobilization method used. The kinetics as well as the mass transfer effects are described and applied to treat the enzyme membrane behaviour theoretically.

Chapter 5 presents the different designs of the planar electrochemical microcells used for the amperometric detection of hydrogen peroxide. The fabrication procedures of these three electrode devices are detailed and their electrochemical behaviour is described. The electrochemical cell is then combined with an enzymatic membrane, and in order to render the sensor response less dependent on partial pressure of O_2, an additional outer polyurethane membrane is dip-coated. The thus completed device is characterized in physiological solutions and tested in vivo, subcutaneously implanted in rats.
Furthermore, thin enzyme membranes are also deposited on wafer level by the IC compatible lift-off technique and their reproducibility (homogenity, thickness, sensor response) is discussed.

In **Chapter 6** the amperometric response of the glucose sensitive electrode is modelized by combining the bisubstrate ping-pong enzyme kinetics and internal mass transport. The method of finite differences is then applied to solve the time dependent differential equations numerically. In order to determine the model parameters, digital simulation is used to fit theoretical calibration curves to experimental ones.

Chapter 7, finally, summarizes the most important conclusions of this work.

1.3 References

[1] WHO, Expert Commitee on Diabetes Mellitus, Second report, Technical Series 646 (1980), WHO, Geneva.

[2] A.P.F. Turner and J.C. Pickup, Diabetes Mellitus: Biosensors for Research and Management, Biosensors, 1 (1985) 85-115.

[3] Report of the National Commission on Diabetes to the Congress of the United States, U.S. Dep. Health, Educ., Welfare, Public Health Service, Nat. Inst. of Health, DHEW Publication No.(NIH) 76 (1976) 1021-1028.

[4] R.F. Hamman, Diabetes in affluent societies, in Diabetes in epidemiological perspective, eds. J.I.Mann, K.Pyorala and A.Teuscher, Churchill Livingstone, Edingburgh (1983) 7-42.

[5] H. Keen and R.J. Jarrett, Complications of Diabetes, Edward Arnold, London (1982).

[6] P.E. Cryer and J.E. Gerich, Relevance of glucose counter regulatory systems to patients with diabetics: critical roles of glucagon and epinephrine, Diabetes Care, 6 (1983) 95-99.

[7] G. Tchobroutsky, Relation of diabetic control to development of microvascular complications, Diabetologia, 15 (1978) 143-152.

[8] J.C. Pickup, H. Keen, J.A. Parsons and K.G.M.M. Alberti, Continuous insulin infusion: an approach to achieving normoglycaemia, Brit. Med. J., 1 (1978) 204-207.

[9] D.L. Horwitz, B. Gonen, J.B. Jaspan, B.G. Langer, D. Rodmand and A. Zeidler, An 'artificial beta cell' for control of diabetes mellitus: effect on plasma glucagon levels, Clin. Endocr., 11 (1979) 639-644.

[10] R. Nosadini, G. Noy, M. Nattrass, K.G.M.M. Alberti, D.G. Johnston, P.D. Home and H. Orskov, The metabolic and hormonal response to acute normoglycaemia in type 1 (insulin-dependent) diabetes: Studies with a glucose controlled insulin infusion system (artificial endocrine pancreas), Diabetologia, 23 (1982) 220-228.

[11] K.G.M.M. Alberti and T.D.R. Hockaday, Diabetic coma: reappraisal after five years, Clin. Endocr. Metab., 6 (1977) 421-455.

II

Glucose measurement

2.0 Summary

The principal methods used to assay blood samples for glucose have undergone an evolution from general chemical assays for reducing sugars, through the more specific biochemical approach, to the present numerous proposals for biosensors.
Simple enzyme electrodes consisting of an electrochemical cell and a membrane part offer the potential of highly specific, simple and accurate biosensors. Nowadays, devices based on either amperometric hydrogen peroxide detection or electrochemical oxidation of an electron transfer mediator are the most successful. Furthermore, planar devices can be realized by using thin film techniques, so that they are particularly suitable for mass production and miniaturization.

2.1 Detection methods

Diabetes is classically considered a disorder of glucose metabolism, since glucose was the first abnormal metabolite to be recognized. Therefore, a specific glucose sensor is generally regarded as the most appropriate device and the efforts in biosensor development have been concentrated in this field. However, as seen in chapter 1, blood and probably tissue levels of many other intermediates of carbohydrate, fat and protein metabolism are disturbed [1] and may offer alternative measures of control [2]. Since most clinical information in diabetes concerns blood glucose levels it would be of most interest to be able to sense metabolic activity in this compartment. An overview of the different glucose detection methods is given in Fig.2.1.

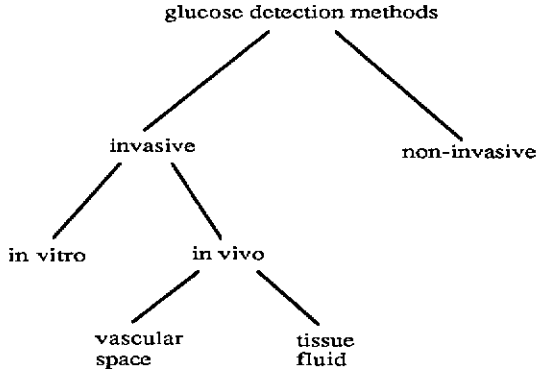

Fig. 2.1: Glucose detection methods

Non-invasive glucose sensing has been achieved by measurement of the optical properties of the aqueous humour of the eye [3]. Recently, a novel blood glucose monitoring system has been developed by applying a SOS/ ISFET (silicon on sapphire/ ion-sensitive field-effect transistor) biosensor to a SEF (suction effusion fluid) [4]. It seems that the SEF, collected through the skin by evacuation, contains almost the same amount of glucose as that in the serum. Hence, such a system enables non-invasive transcutaneous blood glucose monitoring.

The invasive methods can be divided into in vitro and in vivo detection methods. Applying the former means withdrawing samples of blood or tissue fluid and measuring the glucose level by chemical assays or by the use of biosensors. In vivo measurements are carried out by implanting biosensors directly in the vascular space or another suitable implantation site.

Unfortunately, long-term implantation within the vascular space is associated with thrombosis and infection. It is generally assumed that the tissue fluid in the subcutaneous, intramuscular or even intraperitoneal sites will be in dynamic equilibrium with plasma glucose, through diffusion across the capillary wall, and that they would therefore be suitable sensor implantation sites. There is little information on the actual glucose concentration of these positions because of the difficulty of obtaining tissue fluid samples without disturbing the local architecture, vascular permeability and flow.

In addition to the concentration of glucose or changes in other variables at the implantation site, the interaction between the sensor and the biological environment must be considered. This especially refers to interfering chemicals which affect the sensor response. Moreover, the sensor behaviour is also influenced by proteinases which may degrade component enzymes in the sensor, and proteins, as well as cells and blood components (such as fibrin and platelets) which may encapsulate and/or physically or chemically foul the implant. Such interactions will probably be markedly different at various potential implantation sites as well as highly dependent on the nature of the sensor.

Nowadays most investigators are concentrating on miniaturized implantable sensors; any associated electronics may be implanted with the sensor or the signal may be relayed to the outside of the body for processing and read-out.

2.2 Analysis methods

Glucose analysis methods can be divided into two groups: the chemical and enzymatic assays. Fig. 2.2 gives an overview of the different analysis methods. The best known chemical test for glucose involves its reaction with alkaline copper solutions, which readily oxidize the disaccharides (with the exception of sucrose) and the monosaccharides. With the oxidation of the sugar there is simultaneous reduction of copper (III) to insoluble, red copper (II) oxide, which can be determined quantitatively. Numerous variations on this theme have formed the basis for most of the laboratory and home glucose-monitoring methods until the 1960s. Colour changes are determined either spectrophotometrically or visually, and complex autoanalytical equipment has been built to carry out the reaction in clinical laboratories.

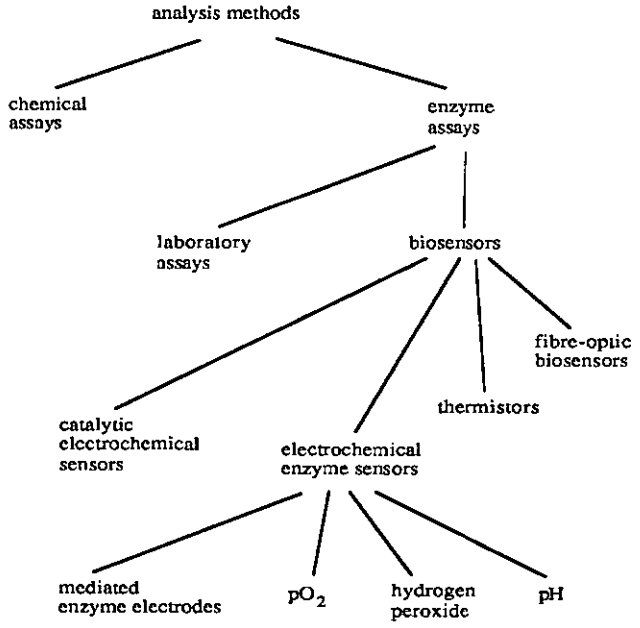

Fig. 2.2: Overview of the glucose analysis methods.

The desire to determine glucose more specifically in clinical samples led to the adoption of enzymatic assay procedures. One standard laboratory assay for glucose involves two enzyme reactions [2]: the first one is the hexokinase (D-hexose-6-phosphotransferase) catalyzed phosphorylation of glucose in the presence of magnesium ions and adenosine triphosphate (ATP).

$$\text{D-glucose} + \text{Mg.ATP} \longrightarrow \text{glucose-6-P} + \text{Mg.ADP} \qquad (2.1)$$

The second enzyme, glucose-6-phosphate dehydrogenase (D-glucose-6-phosphate: $NADP^+$ 1-oxidoreductase) is a stereospecific, nicotinamide adenine dinucleotide phosphate (NADP) dependent dehydrogenase:

$$\text{glucose-6-P} + NADP^+ \longrightarrow \text{Gluconate-6-P} + NADPH + H^+ \qquad (2.2)$$

The formation of NADPH may be followed either directly by ultra-violet spectrophotometry or by coupling to the reduction of a colorimetric reagent such as iodonitrotetrazolium.

An alternative biochemical assay for glucose exploits the following reaction catalyzed by the flavoprotein glucose oxidase (GOD):

$$\text{glucose} + O_2 + H_2O \xrightarrow{GOD} \text{gluconolactone} + H_2O_2 \qquad (2.3)$$

This assay is less specific than the hexokinase-based sequence, but is simpler, cheaper and facilitates a number of approaches to monitoring the reaction; these advantages have led to widespread use of the GOD in clinical analysis and its inclusion in most proposed biosensor configurations. Hydrogen peroxide production may be followed colorimetrically by adding peroxidase and a chromogenic oxygen acceptor:

$$\text{chromogenic oxygen acceptor} + H_2O_2 \longrightarrow \text{chromogen} + O_2 \qquad (2.4)$$

This reaction forms the basis for laboratory analysers and commercially available glucose test strips. The strips consists of dried reagents impregnated into a paper disc mounted on a plastic strip.

2.3 Biosensors

The demands of automation led to the development of biosensors, which can be divided into thermistors, fibre-optic biosensors, catalytic electrochemical sensors and electrochemical enzyme electrodes.

Enzyme thermistors use the fact that most enzymatic reactions are exothermic; the heat generated can be measured and related to the amount of substrate converted. Enzyme thermistors have been constructed to measure glucose concentration using either hexokinase or glucose oxidase and catalase [5]. These devices are closely related to an immobilized enzyme reactor, retaining a flow-through design and incorporating a bulky heat exchanger, so that enzyme thermistors may only be used in bedside artificial pancreas.

An interesting approach of coupling biochemical reactions with optical fibres has been described by Schultz and Sims [6]. Their sensor is based on the detection of fluorescence from a fluorescine-labelled dextran via a single optical fibre. When the dextran is exposed to concanavalin A and glucose a competitive displacement reaction occurs:

$$\begin{aligned} \text{concanavalin A} + \text{glucose} &\rightleftharpoons \text{concanavalin A - glucose} \\ \text{concanavalin A} + \text{labelled dextran} &\rightleftharpoons \text{concanavalin A - labelled dextran} \end{aligned} \qquad (2.5)$$

The amount of free dextran is therefore related to the glucose concentration. A probe has been constructed by enclosing the reactants in a dialysis hollow fibre permeable to glucose. The probe responded non-linearly up to 10 mM glucose with a response time of 10 min [7].

The traditional method of determining pH using indicator dyes may be improved by the use of fibre optics or semiconductor-based optical systems. Fibre optic pH probes have been produced for physiological uses [8] ; they consist of two single-strand optic fibres with a light source and detector at one end and a pH sensitive dye, such as phenol red, at the other. Light from a tungsten source is transmitted down the fibre, through the dye and back along the second fibre to a photomultiplier tube. Immobilization of enzymes such as glucose oxidase in the vicinity of the dye can convert this device to a biosensor.

An optoelectronic sensor using glucose oxidase co-immobilized with bromocresol green on a transparent membrane has been described by Lowe [9]. The membrane is in contact with liquid in a flow cell and the complete arrangement is sandwiched between

a light emitting diode (LED) and a photodiode with an integral amplifier. The output of the photodiode is reported to be directly proportional to glucose concentrations up to 70 mM, but presumably some dilution of the sample is occurring in this configuration. The sensor has a half life time of approximately 7-8 days. Fibre optic devices offer some potential advantages over electrochemical systems; in particular, designs allowing total electrical isolation of the device from the body and sources of electrical noise may be envisaged.

Electrochemical methods can be used either for a direct catalytic oxidation of glucose at a metal electrode or in combination with an enzymatic reaction. The oxidation of glucose at catalytic (e.g. noble metal) electrodes is relatively non-specific and requires complex voltage regimes and data analysis to resolve the glucose concentration in physiological solutions [10-12].

Electrochemical methods in tandem with an enzyme such as glucose oxidase, however, offer the potential of highly specific, simple and accurate sensors for the use in biology and medicine. This configuration forms the basis for the most widely adopted glucose biosensors to date. For this reason, electrochemical enzyme sensors are reviewed separately in the next section.

2.4 Electrochemical enzyme sensors

Electrochemical enzyme sensors for glucose measurement are generally based on the GOD catalyzed oxidation of glucose as described in eq.(2.3). The most obvious approach is to follow changes in the concentration of one of the reactants or products, i.e. oxygen, gluconolactone or hydrogen peroxide by using an electrochemical sensor. Electrochemical devices can be grouped into two categories: the potentiometric and amperometric. Potentiometric sensors are measuring a zero-current potential, as it is done for example in ion-selective electrodes. On the other hand, the potential of amperometric sensors is maintained at a value that allows the reduction or oxidation of substances at an electrode surface. In this case, the resulting current is measured.
In its simplest form an enzyme electrode consists of a thin enzymatic layer held in close proximity to the active surface of a transducer, a suitable reference electrode and a circuit for measuring either the potential difference generated between the two electrodes or the current that flows between them. The relationship is linear for an amperometric electrode and logarithmic for a potentiometric one.
The most direct parameter to monitor, however, would be the amount of reduced glucose oxidase. Direct electron transfer from the prosthetic group of glucose oxidase to an electrode has been proposed using chemically modified graphite electrodes [13] or platinum electrodes [14, 15]. In order to achieve better kinetics of direct electron transfer between the enzyme GOD and electrode material it is important that the transfer is facilitated by promoting proximity between the enzyme active site and the conducting surface of the electrode. Therefore, Foulds and Lowe [16] have concentrated on enzyme immobilization techniques using the entrapement of enzymes in conducting polymer films providing a controlled method of localisation of biologically active molecules to defined areas on electrodes and thus allowing direct electron-transfer from the conducting matrix to the electrode surface. They thus immobilized GOD in a polypyrrole matrix, which was electrochemically deposited on a platinum electrode.
A similiar method has been described by Tamiya and Karube [17]. They used micro gold electrodes covered by a polypyrrole/ GOD matrix, but additionally 1,1'-dimethyl ferrocene has been applied as a mediator of electron transfer between adsorbed GOD and the polypyrrole-modified electrode. Thus prepared enzyme electrodes show a response range between 2.5 and 30 mM glucose.

2.4.1 pO_2 measurement

Oxygen consumption can easily be measured by using a polarographic oxygen electrode. Glucose and oxygen diffuse from a sample into the enzyme layer and the consequent depletion of oxygen at the electrode surface provides a measurement of the glucose concentration.

This Clark-type oxygen electrode is obviously highly susceptible to fluctuations in partial pressure of oxygen. In addition, the signal related to glucose concentration is derived from a reduction of an initially high current; this makes a well-balanced differential measuring device essential for accurate determinations. Despite these inherent limitations some promising results have been obtained. The first definitive paper describing an immobilized enzyme electrode was due to Updike and Hicks [18]. In their device, glucose oxidase was immobilized in a polyacrylamide gel at an amperometric oxygen electrode. A second electrode was included, covered with denatured enzyme, in order to compensate for extraneous fluctuations in oxygen tension and background currents due to species other than glucose. The difference in pO_2 current between these two oxygen cathodes hence became a measure of the glucose concentration.

Notin [19] developed a glucose biosensor where the enzyme was immobilized in a polyacrylamide gel on a cellulose acetate membrane formed on the tip of an oxygen electrode. The sensor gave a linear response over the range 0.2-11 mM glucose and results correlated well with a colorimetric method.

An implantable glucose sensor using an oxygen electrode was first described by Layne [20]. This sensor measured glucose concentration by the difference in the oxygen tension between the enzyme electrode and the reference oxygen electrode, giving a linear response up to 8.3 mM glucose. Kondo [21] developed a miniature glucose sensor using an oxygen electrode with a glucose oxidase membrane covered by a semipermeable membrane. This sensor produced a linear response up to about 11 mM glucose and lost only 10% of its activity during 200 h continuous use in buffer. The sensor had a response time in blood, however, of 10 to 20 min. In vivo experiments were performed using an external arterio-venous shunt and the output of some electrodes showed a reasonable correlation with blood glucose levels. There are other important probes, such as those of Bessman and Schultz [22]. The oxygen had access to the two galvanic electrodes through a polypropylene membrane, the external side of which was fastened to a matrix of nylon cloth. Glucose oxidase was covalently bound to the matrix, at the working electrode, by glutaraldehyde. The whole system was

contained in a plastic disc of 2 cm diameter by 0.25 cm depth. The sensor had a useful in vivo lifetime of four days but a less than optimal sensitivity to glucose, due in part to the low oxygen partial pressure in subcutaneous tissues. Much smaller oxygen electrodes can be designed using photolithography and thick film metallisation [23].
Glucose-oxidising bacteria have been used in place of purified enzyme to produce biosensors for fermentation monitoring. Karube [24] described a glucose sensor consisting of immobilized Pseudomonas fluorescens in a collagen membrane retained at an oxygen electrode. This approach produced a relatively stable sensor which showed no decrease in current output over a two-week period and 150 assays. However, the sensor took 10 min to reach steady state and was relatively non-specific because of the ability of the bacteria to oxidize other substrates. A linear range of 0.01 to 0.1 mM was reported.

2.4.2 pH measurement

In a paper dealing with continuous monitoring of blood chemistry, Clark and Lyons [25] used the term enzyme electrode and proposed the first designs for a glucose biosensor. In this original paper the glucose oxidase was retained by Cuprophane membranes at a glass pH electrode. The increase in hydrogen ion concentration resulting from the glucose oxidase reaction was related to the glucose concentration, the temperature, the initial pH and the buffering capacity of the sample. Nilsson [26] showed that glucose could be determined in this manner down to 1 mM, but the response to glucose was non-linear. The high impedance of potentiometric electrodes makes them particularly susceptible to electrical noise. Moreover, they need an accurate reference potential.
Alternative pH detectors may be incorporated into biosensors. Janata [27] proposed an enzyme-coupled transistor (ENFET) by using a field-effect transistor (FET) to detect the pH change associated with the action of glucose dehydrogenase on β-D-glucose. Similar configurations may be considered for glucose sensors using appropriate enzymes: Katsube [28] constructed recently a FET glucose sensor by fixing the enzyme glucokinase, obtained from a thermophilic bacterium, into a matrix of polypyrrole film. The latter was prepared by an electro-polymerization technique.

2.4.3 H_2O_2 measurement

The most successful glucose biosensors produced to date detect the hydrogen peroxide. The preferred method is the direct electrochemical oxidation of hydrogen peroxide:

$$H_2O_2 \longrightarrow O_2 + 2\,H^+ + 2\,e^- \qquad (2.6)$$

In 1970, Clark patented a device based on this principle which was subsequently successfully commercialised by the Yellow Springs Instrument Company. Glucose oxidase was immobilized between two membranes and the hydrogen peroxide produced measured amperometrically by oxidation on a platinum electrode at +700 mV vs. the saturated calomel electrode (SCE). An outer polycarbonate membrane served to exclude large molecules and to produce a diffusion-limited enzyme electrode, with consequent advantages in the stability and linearity of response. A cellulose acetate membrane separated the enzyme layer from the electrode, thus reducing the access of molecules larger than hydrogen peroxide, such as ascorbic acid, that may undergo oxidation at the anode. A 14:1 dilution step in the instrument ensures that the concentration of potentially interfering substances is reduced to manageable levels and that the oxygen concentration in the sample does not limit the reaction. Guilbault [29] described a similar enzyme electrode consisting of a thin film of glucose oxidase held in place on a platinum electrode by cellophane. Analysis of the kinetic response of the electrode was used to reduce the time of measurement from 1 min to 12 s. The electrodes were relatively stable showing approximately 0.1% change per day for over 10 months at room temperature. High sensitivity is possible with this configuration; glucose has been measured down to 10 nM using amperometric hydrogen peroxide detection with electrochemical interference compensated for by a non-enzymatic electrode [30]. Fogt [31] described an on-line glucose analyser, which is incorporated in a computerised feedback control system for dynamic control of blood glucose (the Biostator).

Potentiometric measurement of glucose concentration is the principle of a sensor developed by Liu [32]. Glucose oxidase and catalase were immobilized in polyacrylamide gel around a platinum screen. This electrode produced a direct potentiometric signal with reference to a standard Ag/ AgCl electrode. The potential difference was linearly related to the logarithm of the concentration of glucose. The reaction mechanism is not entirely clear, but it seems that hydrogen peroxide is the apparent source of the potentiometric signal.

It is important that variation in oxygen tension should not affect the glucose sensor, particularly in the case of in vivo devices where dilution steps are impractical. One approach to the oxygen limitation problem is in situ generation of oxygen by the electrolysis of water, a principle which has been applied by Enfors [33] to produce an oxygen-insensitive glucose probe for fermentation control.

The best reported in vivo results, however, have been obtained by using membranes which restrict the diffusion of glucose while allowing relatively free passage of oxygen, thus ensuring that the glucose oxidase reaction is glucose-limited over a wide range of oxygen concentrations [34-38]. Fischer and Abel [34] described a GOD/ H_2O_2 sensor consisting of a central platinum anode smelted into glas and a silver cathode, which surrounds the anode. Glucose oxidase is immobilized onto sepharose and placed between two hydrophilic cellulose acetate membranes. This sandwich is covered by an additional hydrophobic Teflon membrane, which is mechanically perforated (about 0.1 mm) precisely in front of the anode. This outer hydrophobic membrane is permeable to glucose in the scope of a well-defined perforation only while the oxygen can enter through the entire membrane area. In vivo tests showed reasonable correlation between the sensor output and the plasma glucose reference values with a response time between 90 and 120 s. The linear range for in vitro calibration was up to 40 mM glucose.

The needle-type glucose sensor developed by Shichiri [36-38] is worth of a particular mention since it comes closest to satisfying the requirements for an implantable sensor. The electrodes consist of a fine platinum wire with a bulbous tip, which is coated with glucose oxidase immobilized in a cellulose acetate membrane containing heparin. The bulb of the electrode is further coated with a polyurethane membrane and the remainder of the electrode is encased in a glass tube. An outer tube of silver-plated stainless steel serves as the cathode and reference, and hydrogen peroxide is detected by poising the platinum anode at 600 mV. Even though currents were only in the order of nanoamps, electrical noise did not appear to be a problem. The response was directly proportional to glucose concentration up to 27.7 mM with a response time of 16.2 s (to 90% of the steady state value). Oxygen tensions in the range 25-150 mm Hg did not significantly affect the readings obtained. The output of sensors implanted in the subcutaneous tissue of dogs decreased by 12.8% over a four-day period. Sensors were also used for four days as part of an artificial pancreas to control blood glucose in pancreatomised dogs within the range 5- 9.5 mM. The effect of substances such as ascorbic acid, tyrosine and uric acid, which may also have been oxidized at the anode, were not

discussed; these may, however, have been largely excluded by the cellulose acetate membrane. The same principle, i.e. deposition of polyurethane as outer glucose diffusion limiting membrane, has been used by several other research groups [39-42] and their in vitro and in vivo results are comparable with those found by Shichiri.

Very small glucose sensors can be realized by the use of integrated circuit (IC) fabrication processes. Hence, Murakami [43] built miniaturized glucose sensors consisting of a gold working electrode covered by an immobilized glucose oxidase membrane and a gold auxiliary electrode. A pH sensitive ISFET was applied as reference electrode. The ISFET and both gold electrodes were made on a silicon on sapphire (SOS) wafer and a 1000 Å thick Si_3N_4 layer was used as pH sensitive membrane. The GOD immobilized membranes were deposited on wafer level and a lift off technique was used as patterning process [44].

Sansen developed a planar glucose sensor focussing the attention on the compatibility with standard CMOS processing so that interface electronics (potentiostat) can easily be integrated together with the sensor on the same chip [45]. The counter (auxiliary) and working electrode were made in platinum and the reference electrode was a Ag/ AgCl electrode. The GOD membrane was immobilized on the sensing area of all three electrodes. Recently, Sansen and Lambrechts [46] described a new smart sensor which integrates a planar voltametric structure, a CMOS interface circuit and a temperature sensor all on the same chip (750 µm by 5000 µm). The opamp had a dynamic input range from +1 to -1 V, so that glucose as well as oxygen could be measured. The sensor specific layers are deposited on the wafer after the complete CMOS processing. A silicon nitride passivation layer protects the interface circuit from the analyte. Polysilicon was used as the interconnection material between the electronics and the electrodes.

The combination of thin film and photochemical immobilization techniques is a new approach for the fabrication of miniaturized biosensors. Buxbaum [47] realized miniaturized three-electrode electrochemical cells by evaporating metal layers (Ti/ Pt or Ti/ Pd, Ti/ Ag) on glass substrates isolated with a silicon nitride film. The Pt or Pd surfaces were oxidized electrochemically in diluted aqueous oxidizing solutions. These modified surfaces were then derivated with aminoorganic sililating agents and a bifunctional, redox active and photochemically sensitive reagent was applied to couple the enzyme. Nafion (a fluorinated and sulfonated polymer) was used to protect the enzyme layer and to modify the diffusion characteristics of the electrode.

2.4.4 Electron transfer mediators

According to the previous sections, the amount of glucose present in an analyte solution can be determined by following amperometrically either the rate of oxygen consumption or the rate at which hydrogen peroxide is produced. This current is not always only a function of glucose concentration alone; at higher substrate levels a first limitation due to partial oxygen tension (pO_2) may appear. Secondly, the potentials required to reduce oxygen or oxidize hydrogen peroxide are sufficiently extreme so as to introduce the possibility of interferences.

Glucose oxidase is an FAD (flavin adenine dinucleotide) containing enzyme (see chapter 3). During the catalytic cycle the flavin prosthetic group is first reduced by glucose and then reoxidized by molecular oxygen. The role of oxygen can be replaced by an electron transfer mediator. In this context, a mediator (M) is a low molecular weight redox couple which shuttles electrons from the redox centre of the enzyme to the surface of the indicator electrode. A practical configuration has the mediator in close contact with the electrode surface in such a way that it is able to react with the reduced enzyme and undergoes rapid charge transfer at the electrode surface:

in the membrane: $\text{glucose} + \text{FAD} + H_2O \longrightarrow \text{gluconolactone} + FADH_2$ (2.7)

$$FADH_2 + 2\,M \longrightarrow FAD + 2\,M^- + 2H^+ \quad (2.8)$$

at the electrode: $2\,M^- \longrightarrow 2\,M + 2\,e^-$ (2.9)

The rate at which the reduced mediator is produced is measured amperometrically by oxidation at the electrode.

There are various successful approaches to diverting electrons from their natural electron acceptor (oxygen). Williams [48] developed an enzyme electrode in which oxygen was replaced by benzoquinone in the glucose oxidase catalyzed reaction:

$$\text{glucose} + \text{benzoquinone} + H_2O \longrightarrow \text{gluconic acid} + \text{hydroquinone} \quad (2.10)$$

The hydroquinone produced was measured amperometrically by oxidation on platinum poised at a potential of +400 mV (SCE):

$$\text{hydroquinone} \longrightarrow \text{benzoquinone} + 2\,H^+ + 2\,e^- \quad (2.11)$$

The enzyme was retained at the electrode in a porous gel covered with dialysis membrane. A second non-enzymatic electrode was used to compensate for background currents due to non-specific oxidations. The sensor took 3 to 10 min to reach steady state and gave a linear response up to approximately 5 mM glucose.

Recently, Ikeda [49] described a similar glucose sensor using benzoquinone as cofactor. Glucose oxidase was immobilized on the surface of a p-benzoquinone-carbon paste electrode by coating the enzyme-loaded surface with a nitrocellulose film. Properties of the sensor include the electrocatalytic oxidation of glucose with a linear range up to 15 mM, a response time of about 20 s and insensitivity to variations of oxygen tension in sample solutions.

Other mediators such as 2,6-dichlorophenol indophenol [50] and hexacyanoferrate (III) [51] have been used to couple the glucose oxidase reaction electrochemically, but they are too soluble for use in an immobilized configuration.

The ideal mediator should rapidly accept electrons from the reduced enzyme and exhibit good electrochemistry at a practical electrode. It should be amenable to immobilization, stable in both the reduced and oxidized forms, independent of pH and the reduced state should be unreactive with oxygen. In order to avoid interferences due to the oxidation of extraneous compounds at the electrode, the redox potential of the mediator should be low. Cass [52, 53] has shown that one group of compounds that meet these criteria, ferrocene and its derivates, may be incorporated into enzyme electrodes. Moreover the use of ferrocenes (bis(η^5-cyclopentadienyl)iron) has a number of advantages: they have a wide range of solubilities in different solvents; most are heat-stable; they can be polymerized and they can be used to modify other molecules, including proteins. In addition, and undoubtedly of most importance, substituents can be introduced on either or both of the cyclopentadienyl rings while retaining the properties of a simple one-electron redox couple. Glucose sensors were constructed by covalently attaching glucose oxidase to 1,1'-dimethylferrocene modified carbon foil electrodes. In this configuration, electrochemically generated ferricinium ions act as oxidants for reduced glucose oxidase. Once the ferricinium ion has been reduced ($Fecp_2R^+$ —> $Fecp_2R$) it is reoxidized at the electrode surface. The enzyme catalyzed reaction may be summarized as follows:

$$\text{glucose} + GOD_{ox} \longrightarrow \text{gluconolactone} + GOD_{red} \qquad (2.12)$$

$$GOD_{red} + 2\,Fecp_2R^+ \longrightarrow GOD_{ox} + 2\,Fecp_2R + 2H^+ \qquad (2.13)$$

The ferricinium ion is regenerated at the carbon anode. Depending on the remainder molecule R its potential vs. SCE is between +100 and 450 mV:

$$2\ Fecp_2R \rightleftharpoons 2\ Fecp_2R^+ + 2\ e^- \qquad (2.14)$$

These ferrocene-mediated enzyme electrodes exhibited a broad linear range (up to 30 mM) while retaining a short response time (20 s to 95% of steady state current). Since oxygen is no longer required for the reaction, the electrodes function both aerobically and anaerobically, showing little oxygen interference over the normal physiological range.

Claremont [54] described a potentially implantable glucose sensor based on direct ferrocene-mediated electron transfer between immobilized glucose oxidase and a graphite electrode. Pickup [55] studied the improvement of the stability of ferrocene-based sensors by better retention of the enzyme at the electrode. Electrodes in which the base sensor was platinum and the enzyme was covalently attached to agarose showed the best results. He concluded that both ferrocene-mediated and hydrogen peroxide-detecting amperometric glucose sensors with a high density of covalently-linked enzyme have the best operating stability.

Recently, a pen-type device based on this ferrocene mediated electron transfer has been developed [56]. The device is designed for glucose self-monitoring [57] and is commercialized by ExacTech. It consists of a sensor part, designed as a throw away device and a pen containing the electronics and a digital indicator. The sensor consists of a planar two-electrode cell onto which the enzyme and mediator are immobilized. The device shows a linear range up to 25 mM glucose and the storage life-time of the test stripes is more than two years [58].

2.5 Conclusions

Simple enzyme electrodes lend themselves particularly well to mass production and miniaturization, since they consist essentially only of a protein layer over a suitable conductor. Advances in IC technology [59] are likely to facilitate the rapid application of biosensor technology and, moreover, offer the possibility for the realization of multi-biosensors. New glucose monitoring devices appearing in the near future are likely to be electrochemical, based on either amperometric hydrogen peroxide detection or mediated electron transfer. There is no clear indication that biosensors for in vivo use will achieve lifetimes of more than a few weeks of continuous operation; it is the stability which is still limiting the practical use of enzymatic glucose sensors.
The aim of this work is the development of an implantable glucose sensor with emphasis on its reproducible mass production. Based on the previous results showing the rather limited life time of biosensors it appears that throw-away devices for short-time use are desirable. That is why thin film techniques have been applied to fabricate miniaturized electrochemical enzyme electrodes whose theoretical aspects are treated in more detail in the next chapter.

2.6 References

[1] K.G.M.M. Alberti, A.S. Rowe and A. Dornhorst, Metabolic rhythms in normal and diabetic man, Isr. J. Med. Sci., 11 (1975) 571-580.

[2] A.P.F. Turner and J.C. Pickup, Diabetes Mellitus: Biosensors for Research and Management, Biosensors, 1 (1985) 85-115.

[3] W.F. March, B. Rabinovitch and R.L. Adams, Noninvasive glucose monitoring of the aqueous humour of the eye: part II. Animal studies and the scleral lens, Diabetes Care, 5 (1982) 259-265.

[4] N. Ito, A. Saito, S. Miyamoto, S. Shinohara, T. Kuriyama and J. Kimura, A novel blood glucose monitoring system basedon an ISFET biosensor and its Application to a human 75 g oral glucose tolerance test, Transducers' 89, Digest of Technical Papers, Montreux, Switzerland, 1989, p.302 .

[5] K. Mosbach, C.F. Mandenius and B. Danielsson, New biosensor devices. In: Biotech 83, Omline Publications, Northwood, 1983, pp. 665-678.

[6] J.S. Schultz and G. Sims, Affinity sensors for individual metabolites, Biotechnol. Bioeng. Symp., 9 (1979) 65-71.

[7] J.S. Schultz, S. Mansouri and I.J. Goldstein, Affinity sensor: a new technique for developing implantable sensors for glucose and other metabolites, Diabetes Care, 5 (1982) 245-253.

[8] J.I. Peterson , S.R. Goldstein, R.V. Fitzgerald and P.K. Buckhold, A fibre optic pH probe for physiological use, Anal. Chem., 52 (1980) 864-868.

[9] C.R. Lowe, M.J. Goldfinch and R.J. Lias, Some novel biomedical biosensors. In: Biotech 83, Onlinc Publications, Northwood, pp. 633-641.

[10] H. Lerner, S. Soeldner, C.K. Colton and J. Giner, Measurement of glucose concentration in the presence of coreactants with a platinum electrode, Diabetes Care, 5 (1982) 229-237.

[11] U. Gebhardt, G. Luft, G.J. Richter and F. von Sturm, Development of an implantable electrocatalytic glucose sensor, Bioelectrochemistry and Bioenergetics, 5 (1978) 607-624.

[12] G.J. Richter, G. Luft and U. Gebhardt, Development and present status of an electrocatalytic glucose sensor, Diabetes Care, 5 (1982) 224-228.

[13] R.M. Ianniello, T.J. Lindsay and A.M. Yacynych, Differential pulse voltammetric study of direct electron transfer in glucose oxidase chemically modified graphite electrodes, Anal. Chem., 54 (1982) 1098-1101.

[14] L.B. Wingard, Cofactor modified electrodes for energy transfer. In: Enzyme Engineering, Vol. 5 (Ed. H.H. Weeetal and G.P. Roger), Plenum, New York, 1980, pp. 101-108.

[15] L.B. Wingard, Immobilized enzyme electrodes for glucose determination for the artificial pancreas, Fred. Proc., 42 (1983) 288-291.

[16] N.C. Foulds and C.R. Lowe, Enzyme entrapment in electrically conducting polymers: Immobilization of glucose oxidase in polypyrrole and its application in amperometric glucose sensors, J. Chem. Soc., Faraday Trans.1, 82 (1986) 1259-1264.

[17] E. Tamiya, I. Karube, S. Hattori, M. Suzuki and K. Yokoyama, Micro glucose sensors using electron mediators immobilized on a polypyrrole-modified electrode, Sensors and Actuators, 18 (1989) 297-307.

[18] J.W. Updike and J.P. Hicks, The enzyme electrode, Nature, 214 (1967) 986-988.

[19] M. Notin, R. Guillien and P. Nabet, Le dosage du glucose sanguin a l'aide d'une electrode à enzyme, Ann. Biol. Clin., 30 (1972) 193-197.

[20] E.C. Layne, R.D. Schultz, L.J. Thomas, G. Slama, D.F. Sayler and S.P. Bessman, Continuous extracorporeal monitoring of animal blood using the glucose electrode, Diabetes, 25 (1976) 81-89.

[21] T. Kondo, K. Ito, K. Ohkura and S. Ikeda, A miniature glucose sensor implantable in the blood stream, Diabetes Care, 5 (1982) 218-221.

[22] S.P. Bessman and R.D. Schultz, Sugar electrode sensor for the artificial pancreas, Horm. Metab. Res., 4, 1972, p.413

[23] C.C. Liu, M.R. Neuman, K.L. Montana and M.C. Oberdoerster, Miniature multiple cathode dissolved oxygen sensor for marine science application, Mar. Technol., 16 (1980) 468-472.

[24] I. Karube, S. Mitsuda and S. Suzuki, Glucose sensor using immobilized whole cells of Pseudomonas fluorescens, Eur. J. Appl. Microbiol. Biotechnol., 7 (1979) 343-350.

[25] L.C. Clark and C. Lyons, Electrode system for continuous monitoring in cardiovascular surgery, Ann. NY Acad. Sci., 102 (1962) 29-45.

[26] H. Nilsson, A.C. Akerlund and K. Mosbach, Determination of glucose, urea and penicillin using enzyme-pH electrodes, Biochim. Biophys. Acta, 320 (1973) 529-534.

[27] J. Janata, Chemically sensitive field effect transistor as a potential implantable glucose sensor, Diabetes Care, 5 (1982) 271.

[28] T. Katsube, M. Katoh and S. Kobayashi, Stabilization of an FET glucose sensor with a thermophilic enzyme glucokinase, Transducers' 89, Digest of Technical Papers, Montreux, Switzerland, 1989, p.307 .

[29] G.G. Guilbault and G.J. Lubrano, An enzyme electrode for the amperometric determination of glucose, Anal. Chim. Acta, 64 (1973) 439-455.

[30] D.R. Thevenot, P.R. Coulet, R. Sternberg and D.C. Gautheron, A highly sensitive glucose electrode using glucose oxidase collagen film, Bioelectrochem. Bioenerg., 5 (1978) 548-553.

[31] E.J. Fogt, L.M. Dodd, E.M. Jenning and A.H. Clemens, Development and evaluation of a glucose analyzer for a glucose controlled insulin infusion system (Biostator), Clin. Chem., 24 (1978) 1366-1372.

[32] C.C. Liu, L.B. Wingard, S.K. Wolfson, S.J. Yao, A.L. Drash and J.G. Schiller, Quantitation of glucose concentration using a glucose-catalase electrode by potentiometric measurement, J. Electroanal. Chem. 104 (1979) 19-26.

[33] S.O. Enfors, Oxygen-stabilised enzyme electrode for D-glucose analysis in fermentation broths, Enzyme. Microb. Technol., 3 (1981) 29-32.

[34] U. Fischer and P. Abel, A membrane combination for implantable glucose sensors. Measurements in undiluted biological fluids, Trans. Am. Soc. Artif. Intern. Organs, 28 (1982) 245-248.

[35] L.C. Clark and C.A. Duggan, Implanted electroenzymatic glucose sensors, Diabetes Care, 5 (1982) 174-180.

[36] M. Shichiri, R. Kawamori, Y. Yamasaki, N. Hakui and H. Abel, Wearable artificial endocrine pancreas with needle type glucose sensor, Lancet, ii (1982) 1129- 1131.

[37] M. Shichiri, R. Kawamori, Y. Goriya, Y. Yamasaki, M. Nomura, N. Hakui and H. Abe, Glycaemic control in pancreatectomized dogs with a wearable artificial pancreas, Diabetologia, 24 (1983) 179-184.

[38] M. Shichiri, R. Kawamori, Y Yamasaki, Needle-type glucose sensor, in K. Mosbach (ed.), Methods in Enzymology, Vol. 137, Immobilized enzymes and cells, Academic Press, 1988, p.326.

[39] R. Steinberg, M.B. Barran, L. Gangiotti, D.R. Thévenot, D.S. Bindra, G.S. Wilson, G. Velho, P. Froguel and G. Reach, Study and development of multilayer needle-type enzyme-based glucose microsensors, Biosensors, 4 (1988) 27-40.

[40] G. Velho, Ph. Froguel, D.R. Thévenot and G. Reach, In vivo calibration of a subcutaneous glucose sensor for determination of subcutaneous glucose kinetics, Diab. Nutr. Metab., 1 (1988) 227-233.

[41] S.J. Churchouse, C.M. Battersby, W.H. Mullen and P.M. Vadgama, Needle enzyme electrodes for biological studies, Biosensors, 2 (1986) 325-342.

[42] M.M. El Degheidy, E.S. Wilkins and O. Soudi, Optimization of an implantable coated wire glucose sensor, J. Biomed. Eng., 8 (1986) 121-129.

[43] T. Murakami, S. Nakamoto, J. Kimura, T. Kuriyama and I. Karube, A micro planar amperometric glucose sensor using an ISFET as a reference electrode, Analytical Letters, 19 & 20 (1986) 1973-1986.

[44] S. Nakamoto, N. Ito, T. Kuriyama and J. Kimura, A lift-off method for patterning enzyme-immobilized membranes in multi-biosensors, Sensors and Actuators, 13 (1988) 165-172.

[45] W. Sansen, M. Lambrechts and J. Suls, Fabrication of voltammetric sensors with planar techniques, Digest of Technical Papers, third Int. Conf. Solid-State Sensors and Actuators (Transducers'85), Philadelphia, U.S.A., June 11-14, 1985, pp. 344-347.

[46] W. Sansen, M. Lambrechts, A. Claes, D. de Wachter and L. Callewaert, A smart sensor for voltammetric measurement of oxygen or glucose concentrations, Digest of Technical Papers, 5th Int. Conf. Solid-State Sensors and Actuators (Transducers'89), Montreux, Switzerland, June 25-30, 1989, p. 54.

[47] E. Buxbaum, F. Pittner, T. Schalkhammer, A. Jachimowicz, G. Jobst, F. Olcaytug and G. Urban, New microminiaturized glucose sensors using covalent immobilization techniques, Digest of Technical Papers, 5th Int. Conf. Solid-State Sensors and Actuators (Transducers'89), Montreux, Switzerland, June 25-30, 1989, p.310 .

[48] D.L. Williams, A.R. Doig and A. Korosi, Electrochemical enzymatic analysis of blood glucose and lactate, Anal. Chem., 42 (1970) 118-121.

[49] T. Ikeda, H. Hamada, K. Miki and M. Senda, Glucose oxidase immobilized benzoquinone-carbon paste electrode as a glucose sensor, Agric. Biol. Chem., 49 (1985) 541-543.

[50] W. Mindt, P. Racine and P. Schlaepfer, Sensoren für Lactat und Glucose, Ber. Busenges. Phys. Chem., 77 (1973) 804-808.

[51] J. Mahenc and H. Aussaresses, Electrode à enzyme specifique du glucose basée sur la détection amperométrique de l'hexacyanoferrate (III), C.R. Acad. Sci. Paris, 289 (1979) 357-359.

[52] A.E.G. Cass, G. Davis, G.D. Francis, H.A.O. Hill, W.J. Aston, I.J. Higgins, E.V. Plotkin, L.D.L. Scott and A.P.F. Tuner, Ferrocene-mediated enzyme electrode for amperometric determination of glucose, Anal. Chem., 56 (1984) 667-671.

[53] A.E.G. Cass, G. Davis, G.D. Francis, H.A.O. Hill, W.J. Aston, I.J. Higgins, E.V. Plotkin, L.D.L. Scott and A.P.F. Tuner, Ferricinium ion as an electron acceptor for oxidoredictases, J. Electroanal. Chem., 190 (1985) 117-127.

[54] D.J. Claremont, C.Penton and J.C. Pickup, Potentially-implantable, ferrocene-mediated glucose sensor, J. Biomed. Eng., 8 (1986) 272-274.

[55] J.C. Pickup, G.W. Shaw and D.J. Claremont, Biosensors, (1989) 109.

[56] D.R. Matthews, Pen-sized digital 30-second blood glucose meter, Lancet, April 4 (1987) 778-779.

[57] J. Dudley, Comparative evaluation of accuracy with self-learned blood glucose monitoring, I.D.F. Congress 1988, Abstr. 501.

[58] R.S. Spivey, Patient evaluation of a pen-sized glucose meter, Prac. Diab., 5 (5) (1988) 204-206.

[59] R.S. Pickard, A review of printed circuit microelectrodes and their production, J. Neuro. Met., 1 (1979) 301-318.

III

Theoretical aspects of the glucose electrode

3.0 Summary

This chapter depicts first the structure and reaction scheme of the enzyme glucose oxidase and describes its specificity to the β-D-glucose isomer. The principle of amperometric glucose detection is then detailed. The detection method used in this work is the electrochemical oxidation of hydrogen peroxide formed by the GOD catalyzed oxidation of glucose. In order to understand the behaviour of an enzyme electrode, a basic knowledge of the enzyme kinetics is required. Since the enzyme glucose oxidase obeys the two-substrate reaction mechanism, the substrate (glucose) and cosubstrate (oxygen) concentrations in the sample have to be known for the interpretation of the sensor response. Therefore, the thermodynamic behaviour of dissolved oxygen is briefly reviewed.

3.1 Introduction

The survey of the most common glucose detection methods has shown that the best prospects for in vivo glucose monitoring may be offered by small electrochemical enzyme electrodes implanted at subcutaneous tissue site. Such a biosensor may be realized by placing a membrane containing the immobilized enzyme over a conventional electrochemical cell. Moreover, this simple arrangement allows the use of thin film techniques which offer the potential of the most far-reaching miniaturization.
This chapter describes the working principle of the sensor which is based on the enzymatic oxidation of glucose followed by an electrochemical oxidation of hydrogen peroxide. Further the structure and reaction scheme of the enzyme glucose oxidase and its specificity to the β-D-glucose isomer are detailed.
The general physicochemical phenomena used to describe such an amperometric enzyme electrode are complex, including mass transport through the external medium and within the catalytic membrane, the enzyme reaction and factors that effect its kinetics, and the nature of the electrochemical process by which the product is analyzed. For a better understanding of the amperometric enzyme electrode characteristics the basic enzyme kinetics are reviewed. Since the enzyme glucose oxidase follows the two-substrate reaction scheme, its kinetics depends on both the substrate (glucose) and cosubstrate (oxygen). Thus, for the interpretation of a measured catalytic activity, also the oxygen concentration in the sample has to be considered. Therefore, the thermodynamic behaviour of dissolved oxygen is briefly treated.

3.2 Principle of amperometric glucose detection

An amperometric enzyme electrode is composed of two parts: an electrochemical cell and a membrane part consisting at least in an enzymatic layer. The latter is deposited onto the active surface of an appropriate electrochemical transducer, so that the substrate is made to undergo an enzyme catalyzed reaction that consumes or generates electroactive species. These electroactive species are monitored by the underlying electrochemical sensor, and the measured current is directly proportional to the substrate concentration in the sample. Hence, such a device combines the specificity of an enzyme catalyzed reaction and the sensitivity of an electrochemical sensor.

3.2.1 Species of D-glucose

Glucose is an optically active substance. It is also called dextrose indicating that the rotation of the plane of polarization is clockwise or dextrorotary. This behaviour is taken into account by writing this sugar as D-glucose. There exist two isomeres of D-glucose with different characteristics: α-D-glucose and β-D-glucose. In aqueous solutions both species are in equilibrium with one another by an open aldehydform. Fig. 3.1 shows the structures of the two isomeres α-D-glucose and β-D-glucose.

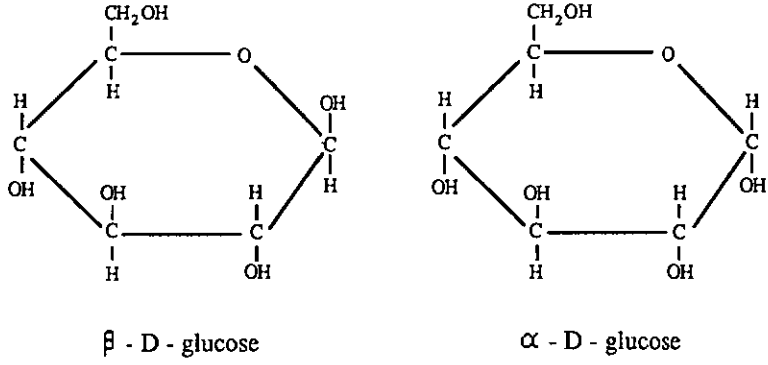

Fig. 3.1: Structure of α -D-glucose and β-D-glucose

3.2.2 Specificity of the enzymatic reaction

Enzymes are high molecular weight biochemical compounds and consist primarly of chains of amino acids (fundamental constituents of proteins) linked together by peptide bonds. One of the properties of enzyme-mediated catalysis is the specificity with which the enzyme acts. Over 2000 enzymes have been isolated and characterized, so that they allow the choice of a specific reaction for species ranging from phosphate and nitrate ions to macromolecules [1].
Without exception, enzymes are members of a class of compounds called proteins, but are distinguished from other proteins by the existence of a geometric area in the structure which facilitates the catalysis. This geometric area, called the active site, can be described as follows [2]:

a) the active site constitutes a small portion of the overall protein structure;
b) the active site is a three-dimensional niche in the protein;
c) the specificity of the enzyme depends on the arrangement of the atoms in the active site;
d) the substrate-enzyme binding process involves a relatively small amount of energy (3-12 kcal/ mole).

The specificity of an enzymatic reaction is, according a postulated mechanism by E. Fischer in 1860, the result of a "lock and key" fit of the enzyme and substrate, that is, stereochemical complementarity.
Some enzymes depend for activity only on their structure, while many others require one or more nonprotein components, called cofactors. A cofactor may be a metal ion or an organic molecule called a coenzyme; some enzymes require both. Cofactors are generally stable to heat, whereas most enzyme proteins lose activity on heating. The catalytically active enzyme-cofactor complex is called the holoenzyme. Its protein portion, which is catalytically inactive by itself, is called an apoenzyme.
Metal ions in cofactors may serve as (a) the primary catalytic center; (b) a bridging group, to bind substrate and enzyme together through formation of a coordination complex; or (c) an agent stabilizing the conformation of the enzyme protein in its catalytically active form. Enzymes requiring metal ions are sometimes called metalloenzymes. In some metalloenzymes the metal component alone already possesses primitive catalytic activity, which is greatly enhanced by the enzyme protein. An example of a metalloenzyme is catalase which contains a ferric tetrapyrrole moiety which catalyzes the decomposition of hydrogen peroxide [2]. Coenzymes, in general, function by accepting or donating groups involved in the catalysis and act therefore as

intermediate carriers of functional groups, of specific atoms, or of electrons that are transferred in the overall enzymatic reaction. Coenzymes are regenerated as part of the enzyme mechanism. When the coenzyme is very tightly bound to the enzyme molecule it is called a prosthetic group. In some cases, however, the coenzyme is only loosely bound and essentially functions as one of the specific substrates of that enzyme.
Of all enzyme properties, it is their high degree of selectivity or even specificity that singles them out as unique analytical reagents. Some enzymes are so specific that they catalyze only a single unique reaction. More frequently, however, enzymes exhibit a *group specificity, catalyzing a number of reactions involving a common functional* group (e.g. amino, phosphate or methyl groups); the rate of reaction of each of these substrates, however, may be different. A third group of enzymes exhibit a wide range of catalytic activity and are relatively nonspecific with respect to the overall substrate structure, but are specific for the type of bond cleaved (linkage specificity) [3]. A final consideration in the use of enzymes is the relatively commonly observed stereospecificity. In the reaction of glucose with oxygen in the presence of glucose oxidase, for example, only the β-form of the D-glucose isomer is oxidized.

3.2.3 Working principle

The working principle of a glucose amperometric enzyme electrode is that the glucose diffuses from the bulk analyte solution through a hydrophilic enzyme membrane where it is oxidized by a GOD-catalyzed process that involves a cosubstrate (O_2) and yields hydrogen peroxide and gluconolactone as products. The components of interest are the hydrogen peroxide species, formed in the whole membrane and allowed to diffuse towards the surface of an electrochemical cell where they are oxidized at a specific potential, thus producing a current depending directly on the bulk glucose concentration.
The enzyme used is GOD (glucose oxidase) which consists of a tightly bound electron transfer moiety (coenzyme) and a protein. The coenzyme FAD (flavin adenine dinucleotide), whose structure is presented in Fig.3.2, is a prosthetic group [4]. The active portion of FAD that takes part in the electron-transfer processes is the isoalloxazine ring. When glucose comes in contact with GOD the flavin moieties are reduced by an addition of two hydrogen atoms to the dimethylisoalloxazine structure. This transfer of a pair of hydrogen atoms yields a reduced form of FAD symbolized as $FADH_2$ whose isoalloxazine ring is shown in Fig.3.3. The latter is then reoxidized by

oxygen yielding hydrogen peroxide. The enzyme is then ready for another cycle. The complete reaction mechanism can be written as follows:

$$\begin{aligned} \text{ß-D-glucose} + \text{GOD/ FAD} + H_2O &\longrightarrow \text{gluconolactone} + \text{GOD/ FADH}_2 \\ \text{FADH}_2 + O_2 &\longrightarrow \text{FAD} + H_2O_2 \end{aligned} \qquad (3.1)$$

To summarize this catalytic cycle where the flavin prosthetic group is first reduced by glucose and then reoxidized by molecular oxygen, we write:

$$\text{ß-D-glucose} + O_2 + H_2O \xrightarrow{\text{GOD}} \text{gluconolactone} + H_2O_2 \qquad (3.2)$$

Since the GOD catalyzed reaction involves two species - the substrate glucose and the cosubstrate O_2 - it is a bisubstrate reaction.

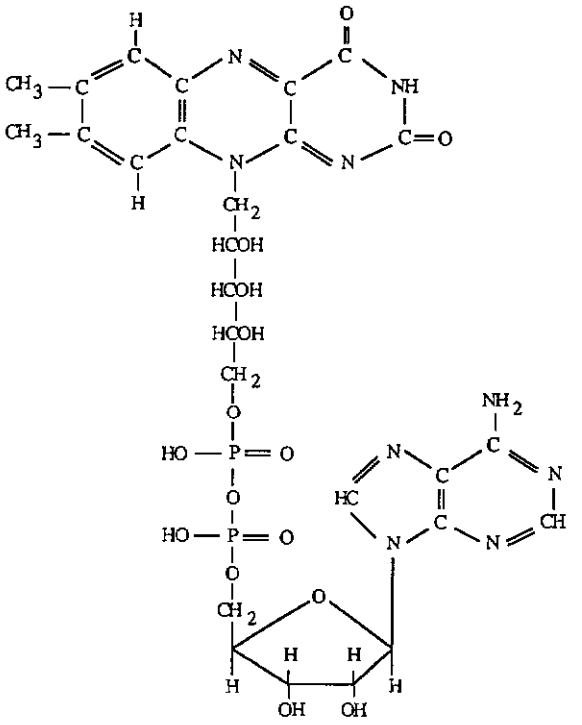

Fig. 3.2: Structure of the FAD-coenzyme

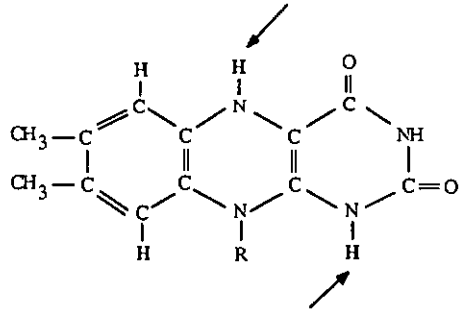

Fig. 3.3: Reduced form of the isoalloxazine ring of the flavin adenine dinucleotide ($FADH_2$). R indicates the remainder of the coenzyme molecule, and the two arrows show the position of the hydrogen atoms which are added to the FAD during the oxidation of glucose.

The products gluconolactone and hydrogen peroxide are formed within the enzymatic membrane and then diffuse either towards the interface between the membrane and the electrochemical sensor or out of the membrane into the bulk analyte solution. The electrochemical sensor used consists of three electrodes (working, auxiliary and reference electrode) and the potential of the working electrode (anode) is maintained at a value that allows the oxidation of hydrogen peroxide at the electrode surface. The potential applied is +700 mV vs. Ag/ AgCl reference electrode so that the following anodic reaction takes place:

$$H_2O_2 \longrightarrow 2\,H^+ + O_2 + 2\,e^- \qquad (3.3)$$

The current generated between the working and counter electrodes is directly related to the glucose concentration in the bulk analyte solution.

The selectivity of the system depends on both the enzyme and the electrochemical detection. The relative reaction rate of glucose oxidase on several closely related carbohydrates is presented in table 3.1 and shows that GOD is highly specific for β-D-glucose [5]. The transducer, on the other hand, is capable of oxidizing other species such as ascorbic acid, uric acid and amino acids which are common components in biological fluids. Obviously, these species may interfere with the glucose measurement if they are allowed to reach the platinum anode. Hence, often a cut-off cellulose acetate membrane is used to restrict their access to the electrode.

Table 3.1: Specificity of glucose oxidase.

substrate	reaction rate relative to β-D-glucose
β-D-glucose	100
2-deoxy-D-glucose	25
D-mannose	1
D-xylose	1
α-D-glucose	0.6
trehalose	0.3
maltose	0.2
D-altrose	0.2
D-galactose	0.1

An additional outer membrane is often necessary in order to restrict the diffusion of glucose while allowing relatively free passage of oxygen, thus ensuring that the enzymatic reaction is glucose limited over a wide range of oxygen concentration. Furthermore, such an additional membrane, e.g. polyurethane, can also prevent the above mentioned interferences as well as electrode poisoning arising from protein adsorption [6].

Finally, the working principle of the complete device is visualized in Fig. 3.4. Glucose and oxygen molecules have to traverse a hydrophobic polyurethane membrane before they diffuse into the hydrophilic enzyme layer where they undergo a bisubstrate reaction. GOD_{ox} means the oxidized and GOD_{red} the reduced form of the enzyme glucose oxidase. One part of the H_2O_2 diffuses then to the electrode surface where it is electrochemically oxidized resulting in a current that is directly proportional to the glucose concentration in the bulk test solution.

In the following section the basic enzyme kinetics is described whereas the last part of this chapter treats the mass transfer effects in hydrophilic enzyme membranes.

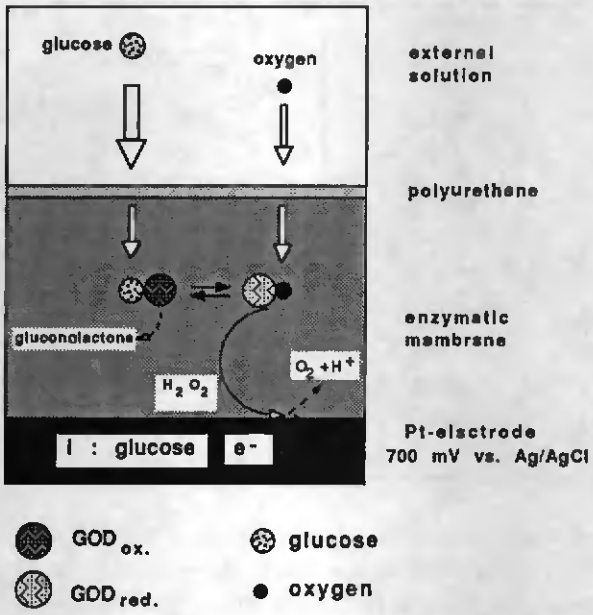

Fig. 3.4: Working principle of an amperometric enzyme based glucose electrode.

3.3 Enzyme kinetics

The determination of the enzyme concentration is usually done by measuring its effect on the rate of an enzymatic reaction. This relationship between the substrate concentration and the reaction velocity is treated by enzyme kinetics. The enzyme activity unit most widely used is the enzyme activity U defined as the amount which causes the transformation of 1μmol of substrate per minute at pH 7 and 25 °C.
As a first step we consider the glucose oxidation as an one-substrate reaction which can be described by the Michaelis-Menten kinetics. This is correct when the reaction mechanism is not limited by the second involved substrate (O_2).

3.3.1 The one-substrate kinetics

The Michaelis-Menten theory reviewed below treats the kinetics of an enzymatic reaction of a non-immobilized enzyme in a solution containing the substrate at the concentration $[S]_0$. This theory assumes that the enzyme E first combines with the substrate S to form an enzyme-substrate complex ES; the latter then breaks down in a second step to form free enzyme and a product P:

$$E + S \underset{k_2}{\overset{k_1}{\rightleftharpoons}} ES \underset{k_4}{\overset{k_3}{\rightleftharpoons}} E + P \,, \qquad (3.4)$$

E = free enzyme
S = free substrate
ES = enzyme-substrate complex

These reactions are assumed to be reversible. Briggs and Haldane [7] derived a rate equation based on the assumption that the concentration change of the enzyme-substrate complex with time is essentially zero almost immediately after the reaction begins. Thus, the concentration of the ES-complex achieves immediately the steady state condition:

$$\frac{d\,[ES]}{dt} = k_1\,[E]\,[S] - k_2\,[ES] - k_3\,[ES] = 0 \qquad (3.5)$$

Since $[E]_0$, the total enzyme concentration, can be written as sum of [E] and [ES] the break down rate of the ES-complex is given as:

$$\frac{d\,[ES]}{dt} = k_1\,[E]_0\,[S] - (k_1[S] + k_2 + k_3)\,[ES] = 0 \qquad (3.6)$$

so that:
$$[ES] = \frac{[E]_0\,[S]}{\frac{(k_2 + k_3)}{k_1} + [S]} \tag{3.7}$$

The rate equation for the formation of product is:

$$v \equiv \frac{d[P]}{dt} = k_3\,[ES] = \frac{k_3\,[E]_0\,[S]}{\frac{k_2 + k_3}{k_1} + [S]} = \frac{k_3\,[E]_0\,[S]}{K_M + [S]}\,, \tag{3.8}$$

where $\frac{d[P]}{dt} = -\frac{d[S]}{dt}$ (conservation of mass) (3.9)

The constant K_M, which replaces the term $(k_2 + k_3)/k_1$, is called the Michaelis-Menten constant. The maximum velocity will be attained when all of the enzyme is in the form of the ES complex ($[E]_0 = [ES]$). If we write a mass balance equation for S, we can see that:

$$[S]_0 = [S] + [ES] \tag{3.10}$$

$[S]_0$ is the initial substrate concentration at the beginning of the reaction. If $[S]_0 \gg [E]_0$, then the concentration of S can be assumed to be equal to $[S]_0$. Thus, to apply the Michaelis-Menten kinetics, $[S]_0$ should be much greater than $[E]_0$. Eq.(3.8) describes the reaction rate of the enzymatic reaction. A graphical presentation of this product formation as a function of the substrate concentration is given in Fig. 3.5.

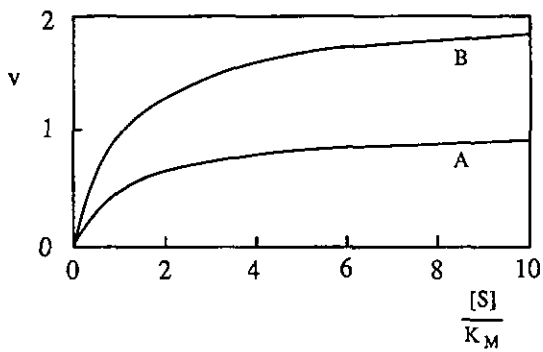

Fig. 3.5: Reaction rate v as a function of $[S]/K_M$ at constant enzyme concentration. Curve B has twice the enzyme concentration of curve A.

If [S] is low with respect to K_M, a linear relation results, and the rate is first order. It should be pointed out that for [S] = 0.1 K_M the deviation of the reaction rate from first-order behaviour is 9%. At high substrate concentrations, the rate is zero order with respect to the substrate concentration, i.e., independent of substrate concentration. If [S] = 10 K_M, the deviation from zero-order conditions is 9%. At very high substrate concentrations, i.e. under saturation, we obtain from eq.(3.8) the maximum reaction rate v_{max}:

$$v_{max} = k_3 [E]_0 \tag{3.11}$$

An important relation results when $v = \frac{v_{max}}{2}$. Using eq.(3.8) again, we get:

$$\frac{v_{max}}{2} = \frac{v_{max} [S]}{K_M + [S]} \tag{3.12}$$

so that $K_M = [S]$ for $v = \frac{v_{max}}{2}$ (3.13)

Thus we see that K_M, the Michaelis-Menten constant, is equal to the substrate concentration at which the reaction velocity is half maximal. K_M for a one-substrate reaction has the dimensions moles per liter and is independent of the enzyme concentration.

In the derivation above, K_M is represented by $(k_2 + k_3)/k_1$, but in some enzymatic reactions k_2 is very large compared with k_3. In this case the rate constant k_3 becomes negligibly small and K_M simplifies to the expression k_2/k_1, where K_M is approximately equal to the dissociation constant of the enzyme-substrate complex:

$$K_s = \frac{[E] [S]}{[ES]} \tag{3.14}$$

Hence, K_M should not be regarded as the dissociation constant of the ES complex unless specific information is available that k_3 is very small compared with k_2.

The values of K_M and v_{max} for any given enzyme following the Michaelis-Menten kinetics can be approximated graphically from a series of simple experiments in which the reaction velocity is measured at different substrate concentrations with a fixed amount of enzyme. Such a calibration curve is usually presented as a graph of v vs. [S]. To evaluate the constants K_M and v_{max}, on the other hand, a linear relation would be more useful. Equation (3.8) can be written in the form:

$$\frac{1}{v} = \frac{K_M}{v_{max}} \cdot \frac{1}{[S]} + \frac{1}{v_{max}} \tag{3.15}$$

A plot of 1/v as a function of 1/[S] will give a straight line with a slope of K_M/v_{max} and an intercept at the 1/v axis of $1/v_{max}$, as it is shown in Fig. 3.6. This double reciprocal graph allows a precise determination of v_{max} and K_M.

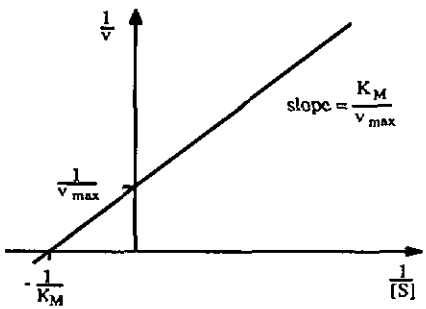

Fig. 3.6: Graph of a Lineweaver-Burke plot

Two other transformations of eq.(3.8) are used on occasion. One is obtained by multiplying eq. (3.15) by $v \cdot v_{max}$ and reshaping the equation, so that

$$v = - K_M \frac{v}{[S]} + v_{max} \qquad (3.16)$$

This presentation is called the Eadie-Hofstee plot which is shown in Fig. 3.7. This plot of v versus v/[S] has a slope of $- K_M$ and an intercept at the v-axis of v_{max}. The major advantage of this method is the more even spacing of the experimental data, that allows a better perception of deviations from the linearity.

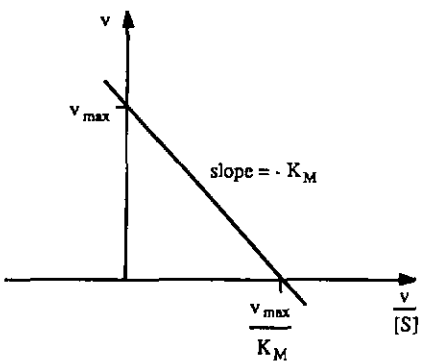

Fig. 3.7: Graph of a Eadie-Hofstee plot

A third presentation of eq. (3.8), proposed by Hanes, is a plot of

$$\frac{[S]}{v} = \frac{1}{v_{max}} \cdot [S] + \frac{K_M}{v_{max}} \qquad (3.17)$$

This equation is obtained by multiplying eq.(3.15) by [S]. The appropriate plot of [S]/v versus [S] has a slope of $1/v_{max}$ and an intercept at the [S]/v -axis of K_M/v_{max}. This Michaelis-Menten reaction scheme describes the simplest case of enzyme reaction, but its application is rather limited in practice.

3.3.2 The two-substrate kinetics

Many enzymes catalyze reactions with two interacting substrates eq.(3.18) and show much more complex kinetics than described by the Michaelis-Menten mechanism.

$$A + B \overset{E}{\rightleftharpoons} P + Q \qquad (3.18)$$

These bisubstrate reactions may have several enzyme-substrate complexes, such as binary complexes EA, EB, EP and EQ, and ternary complexes EAB, EPQ, EAQ and EPB. The determination of K_M and v_{max} for bisubstrate systems is similar to the approach used for one-substrate reactions. The concentration of one substrate, say B, is fixed and the concentration of substrate A is varied to determine its effect on the reaction rate and thus to give the Michaelis-Menten constant for substrate A, namely K_M^A. Three or more fixed concentrations of B are usually employed to obtain an accurate value of K_M^A. Then the experimental arrangement is reversed: the concentration of substrate A is held constant, and the effect of varying the concentration of B is determined to yield K_M^B.

Bisubstrate reactions reduce to the single-substrate case when one of the subtrates is present at a saturating level so that simple Michaelis-Menten kinetics can be applied. Most bisubstrate reactions can be put into one of two classes [8]: single-displacement reactions and double-displacement reactions.

3.3.2.1 Single-displocement reactions

In single-displacement reactions both substrates A and B must be present simultaneously at the enzyme active site to yield a ternary complex EAB in order to proceed the reaction. Single-displacement reactions occur in two forms, random and ordered, which differ in the sequence in which the two substrates bind to the enzyme. In ordered single displacements there is a compulsary sequence of reaction, so that one specific substrate, say A, must be bound first, before the second substrate can be bound:

$$E+A \rightleftharpoons EA+B \rightleftharpoons (EAB \rightleftharpoons EPQ) \rightleftharpoons EP+Q \rightleftharpoons E+P+Q \qquad (3.19)$$

Many dehydrogenases utilizing (NAD^+) as coenzyme catalyze ordered bisubstrate reactions.

In random bisubstrate reactions, either substrate may bind to the enzyme first, indicating that the ternary complex (also called central complex) EAB can be formed equally well in two different ways:

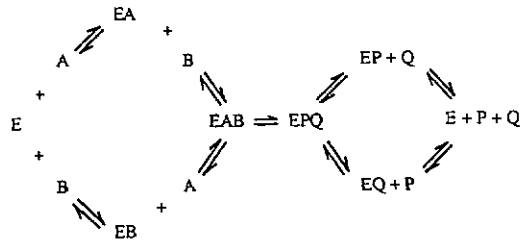

(3.20)

Random single-displacement reactions are catalyzed by many of the phosphotransferases.

The values of K_M^A and K_M^B are most conveniently obtained from double-reciprocal plots. The different types of bisubstrate reactions can often be distinguished by the nature of double-reciprocal plots of 1/v vs. 1/[S] with the other substrate held constant at a fixed concentration. Random single displacements usually give a pattern of intersecting straight lines but are sometimes more complex. Ordered single displacements, on the other hand, give usually converging plots.

3.3.2.2 Double-displacement (ping-pong) reactions

In bisubstrate reactions of the double-displacement type, there is no evidence for the formation of a ternary complex at all. One of the basic mechanisms involves the release of a product molecule during the substrate addition sequence before the entry of the second substrate and the departure of the second product takes place. In such reactions the first substrate reacts with the enzyme to yield a chemically modified form of the latter, which is followed by a second step where the enzyme is transferred in its initial form by the second involved substrate. The reaction scheme of such a double-displacement type, also called ping-pong mechanism, is presented in eq. (3.21).

$$E+A \rightleftharpoons EA \rightleftharpoons E^*P \rightleftharpoons E^*+P+B \rightleftharpoons E^*B+P \rightleftharpoons E^*Q \rightleftharpoons E+Q \quad (3.21)$$

Substrate A combines with free enzyme E to yield the complex EA from which product P departs, leaving the modified enzyme E*. The substrate B then combines with E* to give the complex E*B, which decomposes to yield product Q and free enzyme E. Obviously, the GOD catalyzed reaction described in the previous section corresponds to the ping-pong mechanism.
Double displacements usually yield parallel double-reciprocal plots (Fig.3.8) and therewith can be distinguished from single displacements by kinetic analysis.

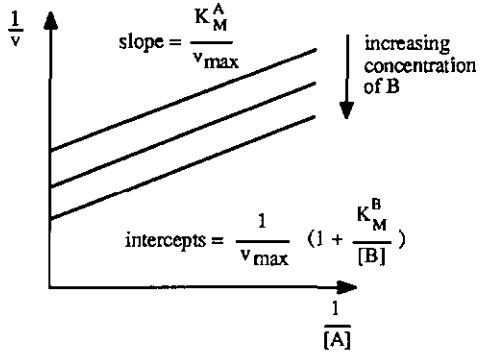

Fig. 3.8: Double-reciprocal plots of (1/ v) vs. (1/ [A]) of a double displacement reaction for different concentrations of substrate B.

The general rate equation for a ping-pong reaction scheme is [8]:

$$v = \frac{v_{max}}{1 + \frac{K_M^A}{[A]} + \frac{K_M^B}{[B]}} \tag{3.22}$$

or in slope-intercept form: $$\frac{1}{v} = \frac{K_M^A}{v_{max}}\left(\frac{1}{[A]}\right) + \left(1 + \frac{K_M^B}{[B]}\right)\left(\frac{1}{v_{max}}\right) \tag{3.23}$$

3.3.3 *Quantitative assay af enzymatic activity*

The amount of an enzyme in a given solution or tissue extract can be assayed quantitatively in terms of the catalytic effect it produces. For this purpose, it is necessary to know:

1.) the overall stoichiometry of the reaction catalyzed
2.) whether the enzyme requires the addition of cofactors such as metal ions or coenzymes
3.) its dependence on substrate and cofactor concentrations (K_M for both substrate and cofactor)
4.) its optimum pH
5.) temperature zone in which it is stable and has high activity

Where possible, enzymes are assayed in test solutions in which the pH is optimum and the substrate concentration is above the saturating level, so that the reaction rate is zero order for substrate. Under these conditions, the reaction rate is proportional to enzyme concentration alone. When enzymes require cofactors, they must also be added in concentrations that exceed saturation so that the true rate-limiting factor in the system is the enzyme concentration.
The two most important parameters affecting enzyme kinetics are briefly treated below, and as an example the typical pH and temperature behaviour of GOD is presented.

3.3.3.1 Effect of temperature

The rate of most enzymatic reactions approximatively doubles for each 10 °C rise in temperature. However, this temperature coefficient varies somewhat for one enzyme to another.

Enzyme-catalyzed reactions often have an optimum temperature. It is a function of a number of parameters such as pH and enzyme concentration. It is not, however, a physicochemical property of the enzyme [9]. The activity-temperature curve is the result of two distinct processes:

a) the usual increase in reaction rate with temperature

and

b) the increasing rate of thermal denaturation of the enzyme above a critical temperature.

Most enzymes are inactivated at temperatures above about 55 to 60 °C, some are quite stable and retain activity at much higher temperature, e.g. enzymes of various species of thermophilic bacteria inhabiting hot springs, which are still active at temperatures exceeding 85 °C.

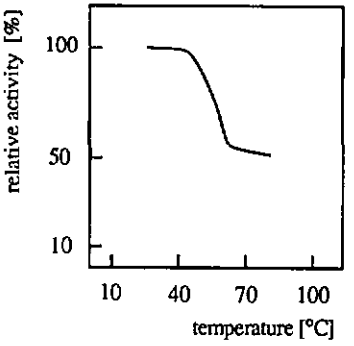

Fig. 3.9: Typical thermal stability of GOD after an incubation of 10 min.

A typical thermal stability curve of GOD (Boehringer) after an incubation of 10 min is presented in Fig. 3.9. The measurements are carried out in a 0.1 M phosphate buffer at pH 7 and at a glucose concentration of 55 mM. Obviously, the GOD activity as function of the temperature shows a thermal stability below 40°C.

3.3.3.2 Effect of pH

Most enzymes have a characteristic pH at which their activity is maximal; above or below this pH the activity declines. The pH-activity relationship of any given enzyme depends on the acid-base behaviour of the enzyme and substrate. Further, the shape of the pH-activity profile usually varies with substrate concentration, since the K_M of most enzymes change with pH. At the extremes of pH, the enzyme may undergo an irreversible denaturation where the activity may not be restored even after readjustment of the pH to the optimum value. Of greater interest is the reversible behaviour exhibited in the general range of the pH optimum. To evaluate such pH-activity curves the enzyme is usually kept saturated with substrate and cosubstrate at all the pH values tested.

A typical pH dependence of GOD (Boehringer) is shown in Fig. 3.10. The sample solution is a 0.1 M phosphate buffer at pH 7 with 55 mM glucose. The pH optimum is at about pH 6.5. The pH stability of this enzyme after an incubation of 10 min in the same test solution is presented in Fig. 3.11 and shows that GOD is stable with pH up to pH 8.

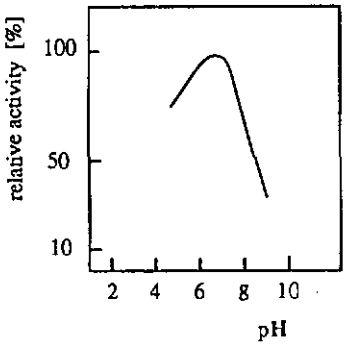

Fig. 3.10: pH dependence

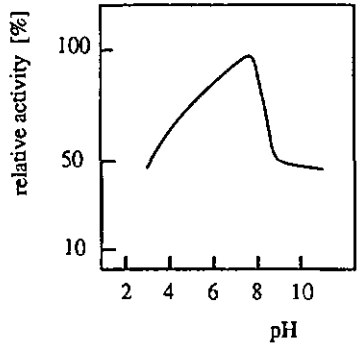

Fig. 3.11: pH stability

It should be noted that after immobilization many of the enzyme characteristics (pH optimum, temperature stability) as well as the kinetic behaviour are modified. Moreover, immobilized enzymes generally exhibit an enhanced stability against different mechanisms of inactivation [10].

3.4 Thermodynamic aspects of dissolved oxygen

The solubility of oxygen in water depends primarly upon three variables: pressure, temperature, and concentration of dissolved salts.

3.4.1 Pressure dependence

The solubility of a gas, at constant temperature, can be described by Henry's law [11]:

$$p = k\,C \tag{3.24}$$

where p is the partial pressure and C the concentration of gas dissolved in a solution. Henry's law in this form is valid for many gases, including oxygen, at low partial pressures (up to 1 atm or more). According eq.(3.24), the concentration of gas dissolved in the solution is proportional to the partial pressure of the gas above the solution. The partial pressure of any gas in a mixture of gases is that pressure that the gas would exert if it occupied the entire volume by itself.

A second assumption for Henry's law in this form is that the mole fraction of the solute becomes proportional to the concentration. For a component i, the mole fraction x_i of this component is defined as the ratio of the number of moles of component i to the total number of moles present. Thus, for a solution containing N_A moles of solvent A, N_B moles of solute B, and N_C moles of solute C, the mole fraction x_B of B is given by:

$$x_B = \frac{N_B}{N_A+N_B+N_C} \tag{3.25}$$

And, of course: $$x_A + x_B + x_C = 1 \tag{3.26}$$

From eq.(3.25) we see that in a very dilute solution the mole fraction of a solute becomes proportional to its concentration.

For oxygen at a partial pressure of 760 torr the concentration of gas dissolved in water is 41.05 mg/l at 25 °C, which corresponds to a mole fraction of oxygen of about $2*10^{-5}$. Thus the solution is very diluted and eq.(3.24) holds. Using the above indicated value for T = 25 °C the constant k in eq.(3.24) can be calculated to be 18.5 torr*l/mg. For dry air which contains 20.95 % of oxygen, thus having an oxygen partial pressure of 159 torr (if the total pressure is 760 torr), the concentration of dissolved oxygen at T = 25 °C can be calculated to be 8.6 mg/l.

3.4.2 Temperature dependence

It is well known that, in general, when the temperature of a gaseous solution is raised the gas is driven off until complete degassing occurs at the boiling point of the solvent. The exact determination of oxygen solubility in water as function of the temperature has occupied a considerable number of workers for over half a century. A critical review of the values obtained by chemical and physical methods, together with suggested "improved" values, is given by Montgomery et al.[12]. Battino and Clever [13] presented all the values obtained by eleven groups of workers up until 1965. These values are not given in the form of solubility in mg/l but as the Bunsen absorption coefficient, α. The value of α is the volume of gas, reduced to 0 °C and 760 torr, which at the given temperature is dissolved in one volume of solvent. The mean value of α at each temperature is reproduced in table 3.2.

Table 3.2: Variation of oxygen solubility with temperature at a total pressure of 760 torr (units: Bunsen coefficient x 10^3).

T [°C]	0	10	20	25	30	35	40	50
mean values	49.0	38.1	31.0	28.4	26.3	24.6	23.2	20.9

The variation of the solubility of a solute with temperature can be derived from thermodynamics [13]. The resulting relation is:

$$\left[\frac{\partial \ln \left(\overline{x_g} / x_g \right)}{\partial T}\right]_P = - \frac{\Delta H}{R T^2} \qquad (3.27)$$

where x_g is the mole fraction of the gaseous constituent in solution;
$\overline{x_g}$ is the mole fraction of the gas in the vapor above the solution;
T is the temperature in °C;
R is the gas constant (8.314 J K^{-1} mol^{-1});
ΔH is the heat of solution in kJ mol^{-1} at a given temperature and pressure;
P is the total pressure above the solution.

This equation strictly holds only for solutions which behave ideally (i.e. where all molecular interactions are the same), but it is a good approximation to the observed behavior for many dilute solutions.

In the special case where the partial pressure of the gas, and hence its mole fraction in the vapor phase, $\overline{x_g}$, remains constant, eq.(3.27) becomes:

$$\left[\frac{\partial \ln x_g}{\partial T}\right]_{P,p_g} = \frac{\Delta H}{R T^2} \qquad (3.28)$$

where p_g denotes a constant partial pressure of the gas. This condition is approximated at a total constant pressure if the vapor pressure of the solvent is negligible in comparison with the gas pressure at all temperatures. Effectively this means that the solvent must be fairly nonvolatile.

The data in table 3.2 can be described by eq.(3.28). For this purpose the variation of the heat of solution, ΔH, with temperature is expressed in the form of a power series:

$$\Delta H = A' + B' T + C' T^2 + \ldots \qquad (3.29)$$

As a first approximation all terms beyond the linear one are neglected:

$$\Delta H = A' + B' T \qquad (3.30)$$

The substitution of ΔH in eq.(3.28), together with α for x_g, and integration gives an equation of the form:

$$\ln 10^3 \alpha = \frac{A}{T} + B \ln T + C \qquad (3.31)$$

where A, B, and C are constants. For oxygen dissolved in water we find by fitting eq.(3.31) to the mean values of α in table 3.2 that:

$$A = 8.55 \times 10^3 , \; B = 2.38 \times 10 , \; C = -1.61 \times 10^2. \qquad (3.32)$$

It should be noted that the integration of eq.(3.28) with α instead of x_g is under the condition of constant partial pressure, which by definition is 760 torr. Also, since α is defined without reference to the total pressure this can be chosen to be constant, so that eq.(3.31) is a thermodynamically accurate way of representing the variation of α with the temperature. We could express $\ln x_g$ in the same form as eq.(3.31) but this would never be strictly thermodynamically correct since p_g does not stay constant.

A second form of equation to describe the variation of α with temperature is obtained by fitting a general power series to the mean values in table 3.2.:

$$10^3 \alpha = a + b T + c T^2 + d T^3 + e T^4 + \ldots \qquad (3.33)$$

where T is the temperature in °C. The coefficients of this power series for oxygen solubility as a function of temperature are:

$$a = 49,\ b = -1.335,\ c = 2.759 \times 10^{-2},\quad d = -3.235 \times 10^{-4},\ e = 1.614 \times 10^{-6} \tag{3.34}$$

Values calculated from eqs.(3.31) and (3.33) for the same temperature agree to within ± 0.5 %.

The Bunsen absorption coefficient, while being useful to allow all measurements to be referred to common conditions, is not a very practical measure. Values of α have therefore to be converted to mg/l. If it is assumed that oxygen behaves as an ideal gas, then, under the condition of 0 °C and 760 torr, one mole of oxygen (32 g) occupies 22.414 liters. Thus the solubility, S_1, in g/cm^3, corresponding to the volume represented by α is:

$$S_1 = \frac{32\ \alpha}{22.414 \times 10^3}\ \text{g cm}^{-3} \tag{3.35}$$

This is for a partial pressure of oxygen of 760 torr. If, however, the total pressure is 760 torr then there will be a contribution to this pressure from the vapor pressure of the water.

From eq.(3.24) we see that the solubility, S_2, corrected for this contribution of the water vapor pressure, p_1, to the total pressure is:

$$S_2 = S_1 \times \frac{760 - p_1}{760} = \frac{32\ \alpha}{22.414 \times 10^3} \times \frac{760 - p_1}{760}\ \text{g cm}^{-3} \tag{3.36}$$

Finally, this oxygen solubility is for oxygen saturated water since there is no other gas contributing to the total pressure. Often the oxygen solubility, S, in air saturated water is required. Dry air consists of 20.95 % oxygen and so:

$$S = S_2 \times \frac{20.95}{100} = \frac{32\ \alpha}{22.414 \times 10^3} \times \frac{760 - p_1}{760} \times \frac{20.95}{100}\ \text{g cm}^{-3}$$
$$= 3.936 \times 10^{-7}\ \alpha\ (760 - p_1)\ \text{g cm}^{-3} \tag{3.37}$$

At 25 °C, $\alpha = 28.43 \times 10^{-3}$ and $p_1 = 23.76$ torr, we get:

$$S = 8.24 \times 10^{-6}\ \text{g cm}^{-3} = 8.24\ \text{mg/l}$$

3.4.3 Combined dependence an temperature and pressure

The oxygen solubility at any other barometric pressure than the above used 760 torr value can be obtained by using the dependence of the solubility on the oxygen partial pressure. If the solubility is S at a barometric pressure of 760 torr, i.e. a partial dry air pressure of (760 - p_1) torr, then the solubility S', at any other total pressure, P_T, i.e. a partial pressure of dry air of (P_T - p_1) torr, is given by:

$$S' = S \frac{P_T - p_1}{760 - p_1} \text{ mg/l} \qquad (3.38)$$

The variation of water vapor pressure with temperature is represented over a short temperature range by [15]:

$$\ln p_1 = -\frac{\Delta H_v}{R\,T} + \text{constant} \qquad (3.39)$$

where ΔH_v is the heat of vaporization, R is the gas constant, and T is the thermodynamic temperature. The constant contains the reference temperature and pressure. Once these have been fixed and knowing ΔH_v , the vapor pressure at any temperature can be determined. Table 3.3 gives values of water vapor pressure at various temperatures[16]:

Table 3.3: Variation of water vapor pressure with temperature.

T [°C]	0	10	20	25	30	37	40	50
p_1 [torr]	4.6	9.2	17.5	23.8	31.8	47.1	55.3	92.5

Combining eqs.(3.37) and (3.38) gives a more general expression for oxygen solubility in terms of the Bunsen absorption coefficient and total pressure:

$$S' = 3.936 \times 10^{-4}\, \alpha\, (P_T - p_1) \text{ mg/l} \qquad (3.40)$$

It has to be pointed out that a change of about 10 torr in the barometric pressure leads to a variation of 0.1 mg/l in the dissolved oxygen concentration. This shows the need of careful measurement of ambient atmospheric conditions.

3.4.4 Dependence on salt concentration

The solubility of oxygen in water as a function of temperature and salt concentration shows at any fixed salt concentration the expected decrease of solubility as the temperature increases. But in addition there is a decrease in the oxygen solubility, at a constant temperature, with increased salt concentration. This phenomenon is known as the salting-out effect.

Let S and S_e represent the solubility of the gas in pure water and in the electrolyte solution, respectively. It can be verified on a theoretical basis [14] that ln (S/S_e) varies approximately in a linear fashion with the ionic strength of the electrolyte, that is:

$$\ln \frac{S}{S_e} = k_s I \tag{3.41}$$

where k_s is known as salting coefficient. The ionic strength is given by:

$$I = 0.5 \sum_i C_i z_i^2 \tag{3.42}$$

where C_i is the concentration of ion i, z_i is its charge and the summation is taken over all ions, both positive and negative, in solution. So, for example, a 1M solution of $Fe_2(SO_4)_3$ has an ionic strength given by $I = 0.5\,[2\,(3)^2 + 3\,(2)^2] = 15$.

According to section 5.3, the solution usually applied for sensor testing is composed of 115 mM NaCl, 2.5 mM KCl, 5 mM K_2HPO_4 and 0.5 KH_2PO_4. The ionic strength of this Krebs physiological solution expressed in units of g/l can be calculated to be:

$$I_{Krebs} = 0.5\,[6.72\ (1+1) + 0.186\ (1+1) + 0.871\ (2+1+9) + 0.068\ (1+2+9)]\ g/l$$
$$= 12.54\ g/l \tag{3.43}$$

The value of the constant k_s depends on the electrolytic species added and also varies with the nature of the nonelectrolytic ones. In aqueous solutions k_s is positive in most cases. Thus, $S > S_e$, i.e. the solubility of a nonelectrolyte is lower in a salt solution than in pure water.

When an electrolyte is uni-univalent (e.g. NaCl), then the ionic strength and molarity (g / liter of solution) are identical, and we obtain:

$$\ln \frac{S}{S_e} = k_s C_e \tag{3.44}$$

where C_e is the electrolyte concentration. For solutions containing a mixture of electrolytes, even when they are univalent, the concentration C_e in eq.(3.44) has to be replaced by the ionic strength.

For the derivation of equation (3.41) any interaction of the nonelectrolyte gas with itself is ignored. This is justified for oxygen at the low solubilities we are considering. For gases of high solubility an additional term has to be introduced into eq.(3.41) to take account of such interactions [13].

3.4.5 Dependence an temperature, pressure and salt concentration

Fox [17] proposed an extension of eq.(3.33) of the form:

$$10^3 \alpha = a + b\,T + c\,T^2 + d\,T^3 + e\,T^4 - I\,(p + q\,T + r\,T^2 + s\,T^3 + t\,T^4) \qquad (3.45)$$

The coefficients a to e are those of eq.(3.34) and p to t are new constants. These latter constants are obtained by fitting the power series to experimental data. The values are [11]:

$$p = 0.5516,\ q = -1.759 \times 10^{-2},\ r = 2.253 \times 10^{-4},$$
$$s = -2.654 \times 10^{-7},\ t = 5.362 \times 10^{-8} \qquad (3.46)$$

To obtain an oxygen solubility from the absorption coefficient the same procedure as described previously is used.
Oxygen solubilities for different temperatures, pressures and salt concentrations have been calculated and tables are presented in appendix A.

3.5 Conclusions

In this chapter the amperometric glucose detection principle has been detailed. It is based on the enzymatic oxidation of glucose followed by the electrochemical oxidation of hydrogen peroxide. Hence, the amperometric enzyme electrode is composed of an electrochemical cell and a membrane part consisting at least in an enzymatic layer. The selectivity of such a system depends on both the enzymatic reaction and the electrochemical detection. As shown, the glucose oxidase catalyzes highly specifically reactions of the β-D-glucose isomer. The second element of the sensor, the electrochemical transducer, is capable of oxidizing other species than glucose. To restrict their influence sometimes an inferior cut-off cellulose acetate membrane is applied. An additional outer polyurethane membrane is often necessary in order to restrict the diffusion of glucose while allowing relatively free passage of oxygen, thus ensuring that the enzymatic reaction is glucose limited over a wide range of oxygen concentration. Furthermore, such an outer membrane can also prevent interferences as well as electrode poisoning arising from protein adsorption.

For a better understanding of the amperometric enzyme electrode characteristics, the one- and two-substrate enzyme kinetics have been described. Since GOD follows the two-substrate kinetics, also the cosubstrate concentration of the sample solution has to be considered for the interpretation of the sensor response. Therefore, the thermodynamic behaviour of dissolved oxygen has been treated in detail and tables are presented in appendix A.

The enzyme kinetics discussed in this chapter is valable for free enzymes in solution. When the enzyme is immobilized, its kinetics is changed. This is subject of the next chapter.

3.6 References

[1] T.E. Barman, Enzyme Handbook, Vol. 1-2, Suppl.1, Springer Verlag, New York, 1974.

[2] P.W. Carr and L.D. Bowers, Immobilized Enzymes in Analytical and Clinical Chemistry, in P.J. Elving, J.D. Winefordner and I.M. Kolthoff (eds.), Chemical Analysis, Vol. 56,John Wiley & Sons, New York, 1980, Ch. 1.

[3] H.A. Mottola, Enzymes as Analytical Reagents: Substrate Determinations with soluble and with immobilized enzyme preparations, Analyst, 112 (1987) 719-727.

[4] A.P.F. Turner, I. Karube and G.S. Wilson, Biosensors: Fundamentals and Applications, Oxford University Press, New York, 1987, Ch. 15.

[5] P.W. Carr and L.D. Bowers, Immobilized Enzymes in Analytical and Clinical Chemistry, in P.J. Elving, J.D. Winefordner and I.M. Kolthoff (eds.), Chemical Analysis, Vol. 56, John Wiley & Sons, New York, 1980, Ch. 3, p. 62.

[6] G. Sittampalam and G.S. Wilson, Anal. Chem., 55 (1983) 1608.

[7] G.E. Briggs and J.B.S. Haldane, Biochem. J., 19 (1925) 338.

[8] A.L. Lehninger, Biochemistry, Worth Publishers, INC.,1975, Ch. 8.

[9] P.W. Carr and L.D. Bowers, Immobilized Enzymes in Analytical and Clinical Chemistry, in P.J. Elving, J.D. Winefordner and I.M. Kolthoff (eds.), Chemical Analysis, Vol. 56, John Wiley & Sons, New York, 1980, Ch. 2.

[10] A.M. Klibanov, Enzyme stabilization by immobilization, Analytical Chemistry, 93 (1979) 1.

[11] M.L. Hitchman, Measurement of dissolved oxygen, John Wiley & Sons, Inc. and Orbisphere Laboratories, Div. of Orbisphere Corporation, Geneva, Switzerland, 1978, Ch.1.

[12] H.A.C. Montgomery, N.S. Thom and A. Cockburn, Determination of dissolved oxygen by the Winkler method and the solubility of oxygen in pure water and sea water, J. Appl. Chem., 14 (1964) 280.

[13] R. Battino and H.L. Clever, The solubility of gases in liquids, Chem. Revs., 66 (1966) 395.

[14] K.S. Pitzer and L. Brewer, Thermodynamics, McGraw-Hill, New York, 1961.

[15] S. Glasstone, Thermodynamics for Chemists, D. Van Nostrand Company, New Jersey, 1947, p.228.

[16] Handbook of Chemistry and Physics, 51st ed., The Chemical Rubber Co., Cleveland, 1970, p. D143.

[17] C.J.J. Fox, On the coefficients of absorption of nitrogen and oxygen in distilled water and sea water and of atmospheric carbon dioxide in sea water, Trans. Farad. Soc., 5 (1909) 68.

IV
Immobilized enzymes

4.0 Summary

A large number of immobilization procedures allows in principle the fixation of any biologically active macromolecule, e.g. enzymes. Most of them result in an improved enzyme stability. Unfortunately, this advantage is often coupled with an important loss of enzyme activity. Presently, there is no way to predict the results that will be obtained with a particular technique. Hence, the immobilization of an enzyme aimed at a specific application still requires an empirical trial and error approach.
The properties of these immobilized enzymes are quite variable and depend on the immobilization method employed. Thus, also the kinetic properties usually are changed. This modified enzyme behavior can be explained by different effects resulting in the distinction between the intrinsic, inherent and effective reaction rates, allowing thus a theoretical treatment of immobilized enzyme kinetics.

4.1 Introduction

Enzymes and other biological agents immobilized on or within solid insoluble matrices are used as highly specific reagents, which often possess improved characteristics. As described in the previous chapters, immobilized enzymes in conjunction with a detector have led to the development of highly specific electrode systems.

The immobilization of an enzyme presents several advantages such as, frequently, an increase in the stability of the enzyme. Thus, on the contrary to an enzyme in solution, an immobilized enzyme matrix, prepared with the same amount of enzyme, can be used repetitively to perform a multitude of analyses. In addition, longer predictable half-lifes of those enzyme preparations allow the immobilized enzymes to become part of the analytical instrumentation.

In any enzyme immobilization, two of the major considerations are the maintenance of enzyme activity and the stability of the final preparation. Several types of stability can be distinguished: thermal, storage, and operational. In many cases, the thermal stability of an enzyme is increased after the immobilization, so that the enzyme-support conjugate withstands higher temperature before denaturation occurs. Storage stability is the ability of the preparation to retain its activity under some specified storage conditions and gives some idea of the shelf life of this reagent. The most important stability parameter is the operational one. The operational stability of the preparation is not only a function of the enzyme, but also a function of the carrier durability, inhibitor concentrations in the analyte solution (in particular irreversible inhibitors), deactivation of the enzyme by their products, etc. An example where the product is harmful to the enzyme activity is glucose oxidase. Its reaction product, H_2O_2, has been found to deactivate the enzyme [1].

The activity of an immobilized enzyme is calculated as the ratio of the determined activity of an amount of insolubilized enzyme (in U/ mg) to the same amount of initial active solution. It takes into account both the chemical yield of the immobilization and the specific activity of the immobilized enzyme.

The effects of enzyme immobilization, resulting most often in a loss of enzyme activity, are discussed in the next section where the major immobilization methods are briefly reviewed. A rather complete listing of enzymes which have been immobilized can be found in Zaborsky's book [2]. Further considerations are the kinetic properties of insolubilized enzymes which, generally, are changed compared with free enzymes in aqueous solutions. The underlying effects leading to this modified kinetic behaviour are treated in detail in section 4.3.

4.2 Methods of enzyme immobilization

This section treats the chemical and physical aspects of enzyme immobilization, i.e., the description of the most commonly methods used.
A first basic classification can be made by the distinction of physical and chemical methods. Physical methods include any methods which do not involve the formation of covalent bonds. Chemical methods involve the formation of at least one covalent bond between the enzyme and a functionalized insoluble carrier, or between two protein roolecules. The main difference between the two types of methods is the firmness of the enzyme-matrix conjugate.
A more common classification of the methods available for the immobilization of enzymes and other biologically active proteins is:

1.) Physical adsorption at a solid surface

2.) Entrapment, by occlusion within cross-linked gels or by encapsulation within microcapsules, hollow fibers, liposomes, and fibers

3.) Cross-linking by bi- or multifunctional reagents, often in combination with adsorption or entrapment within a structure of defined geometry

4.) Covalent binding to a reactive insoluble support, via functional groups nonessential for the biological activity of the protein.

A schematic visualization of this classification is given in figure 4.1. Because of the large field of applications of immobilized enzymes, only the basic considerations are treated in this section. Specific examples and detailed immobilization procedures can be found in the litterature [3].

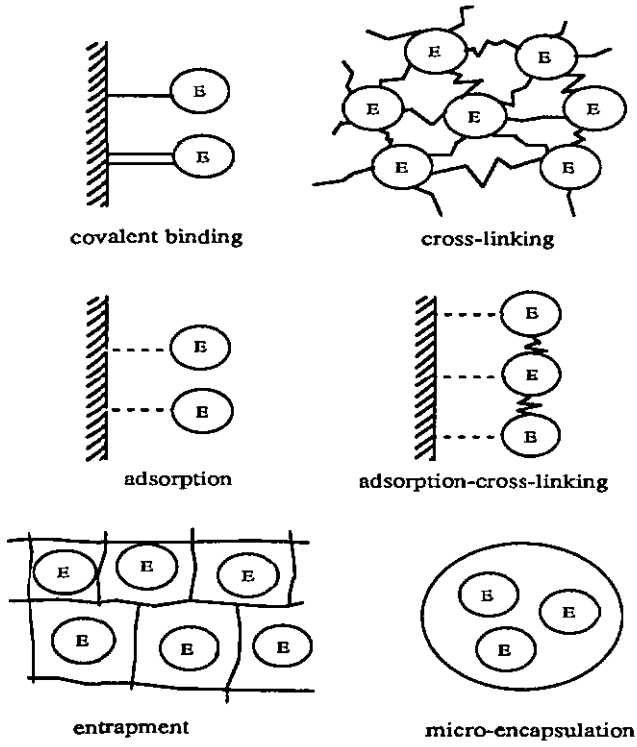

Fig. 4.1: Methods of enzyme immobilization

4.2.1 Adsorption

Historically the earliest method of protein immobilization - adsorption - is also the easiest way of preparing solid-supported enzyme conjugates [3]. Adsorption of an enzyme can be achieved by simply bringing an enzyme solution in contact with the adsorbent surface for some time after which the excess enzyme is washed off.

Substances such as alumina, charcoal, clay, cellulose, kaolinite, collodion, silica gel, glass, hydroxyapatite, collagen, and controlled-porosity glasses and ceramics are known to adsorb enzymes [4, 5]. Further adsorbent substances are anion and cation exchange resins and a variety of phenolic resins.

Binding forces between protein and support are due to hydrogen bonds, ionic bonds ,

Van der Waal's forces, and the formation of electron transition complexes. Unfortunately these binding forces, except the last named, are in most cases relatively weak and, consequently, are susceptible to change in pH, temperature and ionic strength.

The advantages in using adsorption to fix an enzyme to a carrier arise from its simplicity, the wide variety of adsorbents which can be used, and the reusability of the adsorbent. The simplicity, compared with other immobilization methods, results from the fact that usually no reagents and only a minimum of activation steps are required. The nature of the interactions is such that a high level of activity is retained by the preparation.

The major difficulties in using adsorbed enzymes are the empirical process required in optimizing the system and the reversibility of the adsorption process. The "leakage" of the enzyme due to the reversible binding may be a serious problem but can be solved by cross linking the adsorbed proteins with bifunctional reagents, such as bisdiazobenzidine-2,2'-disulfonic acid or glutaraldehyde.

In a number of cases adsorption of reaction products or enzyme inhibitors has been found resulting in partial or total inactivation of the enzyme. It should be noted that structural similarity between carrier and enzyme generally improve the adsorption. Moreover, enzymes adsorbed on specific "affinity supports" have been reported to retain their catalytic activity [6].

The optimal values of pH, temperature, and ionic strength to use with a given support and enzyme system must be empirically determined to achieve good activity and stability. It has been found that in many cases, maximal adsorption occurs near the isoelectric point of the protein.

4.2.2 Entrapment

All entrapment methods are based on the occlusion of an enzyme within a constraining structure tight enough to prevent the diffusion of the protein into the surrounding medium, while still allowing penetration of substrate.

If a polymeric gel is prepared in a solution containing an enzyme, the enzyme becomes trapped within the forming gel matrix. The obvious advantage of such methods is their generality, since the enzyme molecule itself does not participate directly in the formation of the water-insoluble constraining structure and, thus, is trapped within a three dimensional lattice. The generality of the occlusion techniques is limited by the

fact that they are suitable mainly for enzymes that utilize substrates of molecular weights low enough to diffuse trough the matrix.

The most popular matrices for entrapment technique include polyacrylamide, silicone rubber, polyvinyl alcohol, starch, and silica gel. By far the most widely used entrapment technique is the occlusion of an enzyme within cross-linked polyacrylamide gels. The method is based on the polymerization of acrylamide in the presence of varying amounts of N,N'-methylene bis(acrylamide) as cross-linker, in an aqueous medium containing the dissolved enzyme. The pore size of the gel and its mechanical properties are determined by the total and relative concentrations of acrylamide and N,N'-methylene bis(acrylamide). The resulting polymeric gel can be mechanically dispersed into particles of defined size and stored in suspension or in the form of lyophilized powders [7-9]. The acrylamide-gel entrapment technique suffers from one intrinsic drawback: the continuous loss of enzyme. It is particularly pronounced with proteins of relatively low molecular weight. This leakage has been attributed to local variations in permeability, arising from the broad distribution of pore sizes encountered in cross-linked gels of the polyacrylamide type. This serious practical disadvantage can be only partially overcome by optimizing the composition of the gel, i.e., concentration and degree of crosslinking.

An other approach of enzyme entrapment is the inclusion of whole droplets of enzyme solution within semipermeable nylon microcapsules [10, 11]. Microencapsulation is usually achieved by dispersing an aqueous enzyme solution containing 1,6-diaminohexane (hexamethylenediamine) into a solution of hexanedioic acid dichloride (adipoyl chloride) in an organic solvent immiscible with water (e.g. chloroform, carbon tetrachloride, toluene). The diamine and acid dichloride polymerize upon contact at the water-organic solvent interface, forming a thin polyamide (nylon-6,6) membrane around aqueous droplets of enzyme solution. The stability of microencapsulated enzymes has been found to be similar in most cases to that of the corresponding free enzymes in solution. Enhancement of stability could be obtained in several cases by encapsulating enzymes in the presence of an inert protein, followed by cross-linking with glutaraldehyde.

Enzymes immobilized by entrapment techniques exhibit large diffusional barriers to the transport of substrate and product leading to diffusion-limited kinetics, particularly with high molecular weight substrates. Hence, the occlusion methods are best suited for enzyme systems that work on low-molecular-weight substrates.

4.2.3 Crass-linking by bi- or multifunctional reagents

Enzyme immobilization can be obtained by chemical aggregation with bifunctional or multifunctional reagents. When acting on a homogeneous solution of proteins, bifunctional reagents can either react with identical functional groups of the same molecule, resulting in an intramolecular cross-link, or with those in different molecules, resulting in a cross-linked aggregate of molecules. The control of such reactions is rather difficult in terms of aggregate size and mechanical properties [2]. Additionally, bi- or multifunctional reagents can bind the enzyme to solid supports: one of the molecule's functional groups forms a covalent link with the support; the other functional group can then be used to bind the enzyme [12].

Of the considerable number of cross-linking agents described in the literature [3], only two have found widespread use for enzyme immobilization: bisdiazobenzidine-2,2'-disulfonic acid and glutaraldehyde. The latter (see Fig.4.2) is by far the most commonly used cross-linking agent and has been employed for the fixation of histochemical preparations, for cross-linking enzymes adsorbed on solid supports, for co-cross-linking enzymes with an inert protein in the presence or in the absence of a solid support or filler and for the cross-linking of enzymes enclosed in microcapsules as well as for the chemical modification of materials such as aminoethyl cellulose, partially hydrolyzed nylon and other polymeric supports containing primary amino groups.

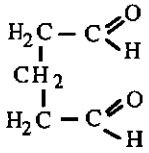

Fig. 4.2: Sructure of the bifunctional reagent glutaraldehyde.

The insolubilization of enzymes through the coupling reaction with bifunctional reagents is dependent on the concentration of the protein and reagent, the pH and ionic strength of the solution, the temperature, and the time of reaction. It should be pointed out, that the reaction of multifunctional reagents with an enzyme must not necessarily result in the formation of only intra- or intermolecular cross-links. It may involve only one part of the functional group of the reagent; the other part of the molecule can be left unmodified or may be transformed into a nonreactive group through the action of solvent molecules. Thus, depending on the conditions used, the reaction can result in modified but still water-soluble monomers, dimers, trimers, or oligomers, or in water-insoluble polymers. This behavior is schematically represented in Fig.4.3.

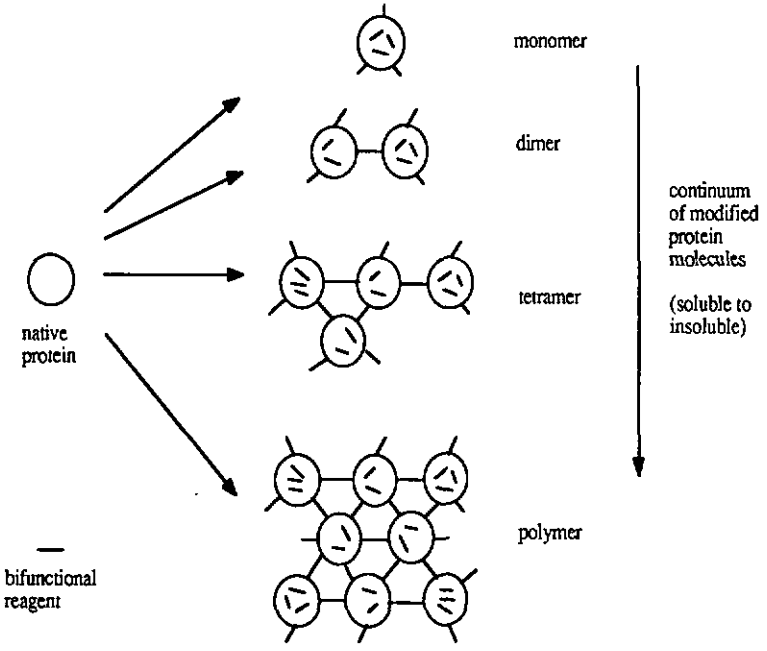

Fig. 4.3: Schematic representation of the reaction of a protein with a bifunctional reagent.

The application of a bi- or multifunctional reagent, such as glutaraldehyde, to solutions of low proteic concentrations give rise initially to water-soluble oligomers. When applied to more concentrated solutions, aggregation rapidly gives rise to high molecular weight, water-insoluble polymers [13]. The nature of the protein also has an influence on its insolubilization. The linkages formed between proteins and glutaraldehyde are irreversible and survive extremes of pH and temperature.

In order to insolubilize low concentrations of an enzyme, it is often necessary to increase the overall protein concentration by adding an inert carrier-protein, such as bovine serum albumin, to the enzyme solution. When glutaraldehyde is added, cross-linking between the enzyme and the inert protein is observed. If the concentration of the auxiliary protein is high enough, it can be considered as the insoluble supporting matrix of the enzyme. When the bovine serum albumin is employed at concentrations higher than 50 mg/ ml, it is easily insolubilized at any pH between 5 and 7.

Direct aggregation by glutaraldehyde (without a carrier-protein) often results in poor

activity yield. The reasons for such an important loss of activity are:

a) excess of cross-linking agent which acts on amino groups located at (or close to) the active site;

b) the production of compact pseudocrystalline structures that multiply steric hindrances;

c) excess cross-links, which hinder the conformational adaption of the enzyme to the substrate and result in an inactivation of the enzyme.

Insolubilization of enzymes by aggregation with an inert protein (co-cross-linking) permits sufficiently high protein concentrations for immobilization, while reducing the above-mentioned constraints. Fig.4.4. gives a schematic representation of co-cross-linking enzymes with albumin using glutaraldehyde as bifunctional reagent.

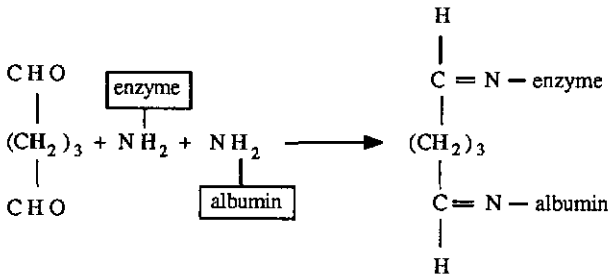

Fig. 4.4: Schematic representation of co-cross-linking enzymes with albumin using glutaraldeghyde as bifunctional reagent.

The optimal ratio of glutaraldehyde to protein concentration is usually in the range of 10% (w/w) [13]. With low concentrations of glutaraldehyde (0.25%), no insolubilization occurs even with concentrated protein solutions. With increasing glutaraldehyde concentrations, the enzyme is partly insolubilized. The ratio of immobilized activity to total activity increases with increasing glutaraldehyde concentrations, up to a maximum. In the concentration range of 0.3 to 1%, activity of the insoluble phase remains nearly constant. With higher glutaraldehyde concentrations, more rapid insolubilization and tighter material are obtained. When the concentration of the cross-linking agent increases above this optimum range, the activity of the immobilized enzyme decreases. Two factors cooperate in a negative way: the increase of diffusional resistances and the denaturation of the enzyme due to the multiplication of cross-links. The optimum range, usually, varies with different

enzymes and operating conditions. Thus, the determination of the optimal conditions for retention of activity is a trial and error procedure. In general however, most immobilization procedures using bi- or multifunctional reagents cause an important loss of enzyme activity ; often residual activity of immobilized enzymes relative to free forms of only 10% or less have be obtained.

4.2.4 Covalent bonding

Covalent bonds should be formed between nonessential amino acid residues of the enzyme and reactive groups attached to the surface of a solid carrier. Unfortunately, the compositional and structural complexity of proteins has not allowed, except in a very limited number of cases, the application of general rules by means of which the method best suited for a specific task could be predicted. There are several methods of preparing covalent conjugates, but the most popular techniques involve the reaction of an aqueous solution of enzyme with an activated, functionalized water-insoluble support or the copolymerization of an enzyme with a reactive monomer.

Covalent bonding reactions should exhibit, under ideal conditions, relatively high specificity toward one type of functional groups on the protein and minimal side reactions with other functional groups or with the aqueous medium [14-16]. Use is made of nucleophilic functional groups present in amino acid side chains of proteins for coupling. These are as diverse as amino, carboxylic acid, hydroxyl, phenolic, imidazole, and thiol groups. Coupling preferably takes place at low temperature and low ionic strength. Often coupling is done in the presence of the enzyme substrate to protect its active site.

The choice of an appropriate coupling procedure for the immobilization of a given enzyme depends on the amino acid composition, the amino acids involved in the active site, the effects of specific chemical modifications on activity, the protection of the active site region by specific chemical agents or inhibitors, as well as the three-dimensional structure of the enzyme [5]. The most common covalent coupling reactions involve amino groups, carboxyls, or the aromatic rings of tyrosine and histidine [3]. The use of sulfhydryl groups is increasing in popularity due to the ease with which the coupling can be reversed [4].

There are essentially three steps in an immobilization scheme: activation of the support, enzyme coupling, and removal of loosly bound enzyme. The activation of the support is an important aspect of the process. Thus, the degree of activation has a significant effect on the recovery of enzyme activity. In addition, it is in general easier to control

the covalent bonding by varying the concentration of the activation reagent than by manipulating reagents during the coupling step.

Covalent bonding has the great advantage that, during use, the release of enzyme from the optimum support matrix chosen (e.g. for porosity, non-biodegradability, etc.) is improbable. A further advantage of this method is that often an increase in enzyme stability results.

A further parameter of enzyme immobilization by covalent bonding is the determination of the support material which plays a significant role since its interaction with the enzyme may have an influence on stability and kinetics. Carriers are chosen by their capacity to bind proteins, their properties of solubility, functional groups, mechanical and chemical stability, surface area, swelling, the ease of activation, and hydrophobic or hydrophilic nature. Essentially, three types of carriers are employed: inorganics (e.g., porous silica glass, alumina, and metal oxides), natural polymers (e.g., cellulose, agarose, sepharose, and dextran), and synthetic polymers (e.g., nylon, polystyrene, polyacrylamide, and silicon rubber). More complete lists of support media can be found in the litterature [4].

The capacity of the carrier to bind protein is an important parameter since relatively high activity per unit volume of support is advantageous for the linearity and the limit of detection of methods using immobilized enzymes. The binding capacity is a function of the number of binding sites which can be activated.

On a trial-and-error basis it has been established that with most supports rich in hydrophobic groups (e.g., aromatic residues) preparations of low protein content and low enzymatic activity are obtained; moreover, such preparations often exhibit low stability presumably due to denaturation effects analogous to those caused by organic solvents. Supports rich in hydrophilic groups bind on the average considerably larger amounts of protein; in such preparations the bound enzyme retains a higher proportion of its activity and usually exhibits higher stability.

Several of the common support materials, e.g., cross-linked polyacrylamide, cross-linked dextrans, or cross-linked copolymers of maleic, acrylic, and methacrylic acids are hydrophilic and thus possess desirable characteristics in terms of the improved stability they might confer on the bound protein. Their mechanical strength, however, is rather poor. Removal of solvent by drying or by exposure to high pressures results in the collapse of the swollen three-dimensional networks and to changes in porosity. Rigid dense particles, e.g., quartz, glass, nylon, or microcrystalline cellulose, would not suffer from such drawbacks; their protein-binding capacity, on the other hand, will be low owing to the relatively small surface area. Rigid, preformed macroporous matrices, e.g., porous "silica-rich" alkali-borosilicate glasses do not collapse or

change in porosity under normal conditions. Their protein-binding capacity and permeability to substrate would be lower as compared to those of highly swollen gels, but considerably higher relative to rigid, dense particles.

The emergence of an "ideal" support of universal applicability cannot, however, be anticipated due to the compositional and structural diversity of proteins. Hence the immobilization of an enzyme aimed at a specific application still requires an empirical, essentially trial and error approach, because the available information is inadequate due to the widely variable conditions under which immobilized enzyme preparations have been tested and characterized [3].

4.3 Effects of immobilization on enzyme kinetics

When an enzymatic reaction takes place in a well stirred homogeneous solution, the concentration of all species is uniform throughout the system. With bound enzymes, however, the enzyme activity can be influenced by changes of the three-dimensional enzyme structure, by different concentrations of species between the immediate vicinity of the bond enzyme and those in the bulk solution, and by different kinetic properties due to diffusion resistances. Therby, the solution in contact with the solid phase constitutes the macroenvironment, whereas the enzyme molecule and its immediate vicinity is known as microenvironment.
In the following discussion, we assume that the enzyme is uniformly distributed on a surface or in a porous medium. Under such conditions, the changes in the enzymatic behavior due to immobilization can be classified as follows:

1.) Conformational and steric effects

2.) Microenvironmental effects:
   a) Partitioning effects
   b) Intrinsic catalytic effects

3.) Mass-transfer effects

A clear separation of these factors is usually very difficult in practice because, in most cases, the structure of the enzyme, the way of attachment, and the matrix properties are not known sufficiently well. Nevertheless, the distinction between these different effects is necessary for a theoretical treatment of enzyme kinetics and can be very useful in the design of enzyme electrodes and the interpretation of sensor responses.

4.3.1 Conformotional and steric effects

Conformational and steric effects are changes in the enzyme or in its immediate vicinity that arise directly from the attachment of the enzyme molecule to the carrier. These can manifest themselves in conformational changes in the protein structure and/ or in restrictions on the accessibility of the active sites (steric hindrances) [3]. These two effects are illustrated schematically in Fig.4.5.

The properties of the active sites of an enzyme molecule depend strongly on the three-dimensional structure of the protein molecule. Thus, when an enzyme is adsorbed or covalently bound to a solid support, this interaction likely results in a modification of the enzyme conformation (e.g., covalent bonds can stretch the whole molecule). Steric hindrances, on the other hand, are caused by the shielding effect of the matrix, which renders certain parts of the enzyme molecule less accessible to the substrate or cosubstrate.

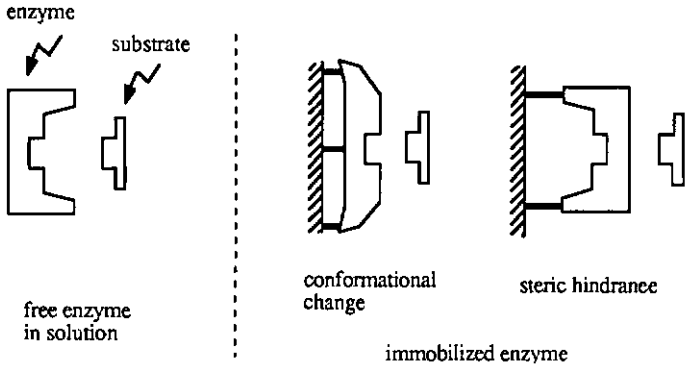

Fig. 4.5: Schematic illustration of conformational changes and steric hindrances.

Conformational changes and matrix interactions can modify not only the catalytic activity, but also the selectivity and stability of the bound enzyme with respect to the free enzyme in solution. In many cases the stability of the enzyme is increased by immobilization [2] because of the stabilization of the protein structure, the prevention of autolysis, or simply because the immobilized enzyme is less accessible to denaturing agents and microbial attack.

4.3.2 Microenvironmental effects

Partitioning effects may arise from electrostatic or hydrophobic interactions (solubility) between the matrix and low-molecular-weight species present in the medium, leading to an unequal distribution of these species between the micro- and macroenvironment, i.e., to different concentrations of substrate, cosubstrate, product, hydrogen and hydroxyl ions, etc., in the domain of the immobilized enzyme.

Partitioning of the various species between the bulk of solution and the enzyme matrix can be described using a partition coefficient K_i which is defined by:

$$K_i = \frac{[C_i]_m}{[C_i]_b} \tag{4.1}$$

where K_i is the partition or solubility coefficient for species C_i between bulk solution and matrix;

$[C_i]_m$ is the concentration (solubility) of species i within the matrix;

$[C_i]_b$ is the bulk concentration (solubility) of species i (i.e., concentration of species i in the fluid surrounding the matrix).

Figure 4.6 illustrates possible concentration profiles for the substrate, cosubstrate and product for the case of partition without diffusional resistances. The partition of the species between the matrix and the liquid phase due to electrostatic, hydrophilic, or hydrophobic interactions results in a steep concentration change at the interface.

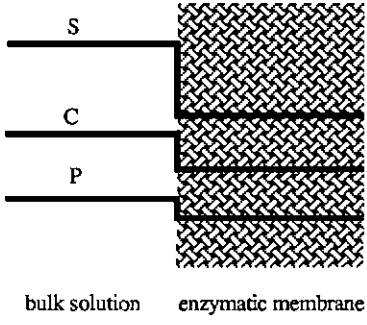

Fig. 4.6: Schematic illustration of the concentration profiles of the substrate S, cosubstrate C, and the product P in the enzyme matrix and in the surrounding solution in the presence of partition effects alone.

Intrinsic catalytic effects are due to the perturbation of the catalytic pathway of the enzymatic reaction and, thus, reflect events arising from the fact that interactions between enzyme, substrate and cosubstrate occur in a different microenvironment when an enzyme is immobilized. Due to the low diffusivities of species in the enzyme matrix and the high catalytic activity of enzymes often concentration gradients are established in the surroundings of the bound enzyme so that the concentrations may differ between the micro- and the macroenvironment.

4.3.3 Mass-transfer effects

When an enzyme is bound to a carrier, the substrate and cosubstrate diffuse from the bulk solution to the catalytic sites, and the products of the reaction usually diffuse back to the bulk solution. Such processes can involve both diffusion and convection. An immobilized enzyme functioning under conditions of diffusional restrictions hence is exposed, even in the steady state, to local concentrations of substrate, cosubstrate and product different from those in the bulk solution. This is reflected in the values of the kinetic parameters usually employed to characterize enzymatic reactions.
In the case of diffusional resistances, the concentration differences in the system are caused by the respective depletion and accumulation of the substrate, cosubstrate, and product as a result of the chemical reaction. The extent of depletion and accumulation of species in the matrix usually depends on their size. Large molecules have a relatively small diffusivity in the porous medium so that they usually encounter significant diffusional resistances. The molecular weight and diffusivity in aqueous solution are shown for certain biological substances in table 4.1. As expected from these data, the decrease in enzyme activity due to immobilization has been found to be greater with high- than with low-molecular-weight substrates [17, 18]. When the substrate molecules are larger than the pore size of the medium containing the enzyme, the substrate cannot diffuse to the catalytic sites and no reaction can take place even if the enzyme is fully active.

Table 4.1: Dependence of diffusion coefficient on molecular weight in water at 20°C.

species	MW	diffusion coefficient $[10^{-6}\,cm^2/s]$
glucose	180	6.7
sucrose	342	4.5
ribonuclease	13 683	1.1
serum albumin	66 500	0.6

4.3.4 Intrinsic, inherent, and effective rates

In view of the above effects, in the case of immobilized enzymes, where the apparent kinetic behavior can be controlled by both microenvironmental and mass-transfer effects, it is useful to distinguish between intrinsic, inherent, and effective rates of reaction. Each is characterized by different values of the kinetic parameters. The relationship between these overall rates is schematically illustrated in Fig. 4.7. The different reaction rates are defined as follows:

1.) The true kinetic behavior of a bound enzyme is characterized by the intrinsic kinetic parameters. Thus, the intrinsic kinetic behavior of an enzyme matrix can be observed in the macroenvironment only if the concentration of the substrate, cosubstrate, and product is the same in both the micro- and macroenvironment. The intrinsic kinetic parameters of an immobilized enzyme are not necessarily the same as those of the free enzyme in solution because conformational changes, matrix interactions, and steric effects can change the intrinsic kinetics of an enzyme upon immobilization.

2.) The inherent rate of reaction is defined as the rate that would be observed in the absence of any diffusional limitations, i.e., if the transport of species between the enzymatic micro- and macroenvironment is infinitely fast. In practice, the inherent enzyme activity can be observed with thin membranes, with low enzyme activity, and with sufficient stirring of the bulk solution.

3.) The effective rate of reaction and the effective kinetic parameters for bound enzymes are observed when diffusional limitations occur in the presence or in the absence of partition effects. Values can be determined from the overall rate as measured under usual experimental conditions.

Because of the relatively slow transport of biochemical substances, diffusional resistances most often affect the activity of immobilized enzyme systems and, therefore, are treated in more detail in the next section.

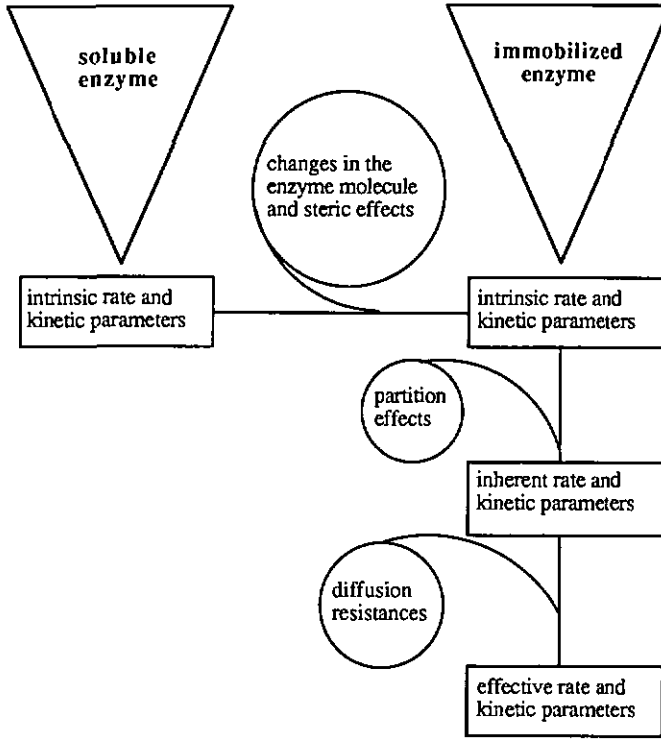

Fig. 4.7: Schematic illustration of the different rates and kinetic parameters and their interrelation.

4.4 External and internal diffusion

The transport of substrate and cosubstrate from the bulk analyte to the active sites of an immobilized enzyme as well as the reverse transport of the product away from the enzyme molecules can be divided into two modes: external and internal transport. External transport is the mass-transfer between the bulk solution and the outer surface of the enzyme matrix and is based on diffusion and convection. The internal transport, on the other hand, is based on diffusion only and ensures mass-transfer inside the catalytic matrix. The main difference between external and internal mass transport is, however, that the latter proceeds simultaneously with the chemical reaction, whereas external diffusion occurs in series with the actual catalytic reaction step process.
When the mass transport of substrate is slower than the rate of its transformation by the enzyme, the observed reaction rate would be lower than expected for a given amount of enzyme in solution, since not all enzyme molecules would be in contact with substrate at a concentration level identical with that of the bulk solution [19]. This phenomenon can be expressed quantitatively by the effectiveness factor η, defined as the ratio of the actual reaction rate v' to the rate v which one would obtain if no mass-transfer limitations were present and hence all enzyme molecules were exposed to the same substrate concentration as that in the bulk solution. This relationship is expressed by

$$v' = \eta\, v \tag{4.2}$$

For an enzymatic reaction following Michaelis-Menten kinetics, v is given by eq.(3.8). Hence, in the presence of diffusional limitations, the reaction rate obeys no longer the Michaelis-Menten kinetics. Moreover, the conventional methods of treating data of enzyme kinetics, whereby the characteristic rate parameters v_{max} and K_m are deduced from the slopes and intercepts of the appropriate linear plots, give misleading results. This can easily be seen by introducing the effectiveness factor η from eq.(4.2) into the Michaelis-Menten expression (3.8):

$$v' = \eta \left(\frac{v_{max}\,[S]}{K_M + [S]} \right) \tag{4.3}$$

and rewriting the latter in the common linear form of eq.(3.15):

$$\frac{1}{v'} = \frac{K_M}{\eta\, v_{max}} \cdot \frac{1}{[S]} + \frac{1}{\eta\, v_{max}} \tag{4.4}$$

Eq.(4.4) need not represent a straight line because η is a function of the substrate concentration.

In the case of external diffusional limitations, the chemical reaction occurs after the substrate has reached the catalyst's surface. The depletion of substrate across the boundary layer can in many cases be approximated by a linear gradient. Moreover, partial cancellation of external diffusional limitations can be effected by increasing the rate of stirring of the sample solution. With internal transport limitations the diffusion process occurs simultaneously with the chemical reaction, so that the two events are coupled in the mathematical sense and would normally give rise to nonlinear substrate concentration gradients within the enzymatic membrane.
In the following the effects of the external and internal diffusional resistances on a solid-phase enzyme reaction are discussed. The treatment is carried out by using planar geometries (flat surfaces and membranes). Hence, mass transport can be considered as an one-dimensional problem.

4.4.1 External diffusion

When an enzyme is attached to a fluid-impervious solid surface, the rate of flow of substrate J_s from the bulk solution to the catalytically active surface can be described according to the 1st Fick's law by the product of a transport coefficient and the corresponding driving force which is the concentration difference between the surface and the bulk:

$$J_s = \frac{D_s}{\delta} ([S_b] - [S_s]) = h_s ([S_b] - [S_s]) \qquad (4.5)$$

$[S_b]$ is the bulk and $[S_s]$ the surface concentration of substrate, D_s is the diffusion coefficient for substrate, δ the thickness of the boundary layer and h_s the transport coefficient for substrate. δ represents the so-called Nernst (unstirred) layer. The flow of product J_p away from the surface can be similarly expressed by:

$$J_p = \frac{D_p}{\delta} ([P_b] - [P_s]) = h_p ([P_b] - [P_s]) \qquad (4.6)$$

where D_p is the diffusion coefficient for product P. In a surface reaction the flow of substrate to the catalytic surface and its transformation by an enzyme reaction take place consecutively . At steady state, the two processes proceed at the same rate. When the enzyme reaction obeys Michaelis-Menten kinetics, we get from eq.(3.8) and eq.(4.5):

$$J_s = v' \qquad (4.7)$$

$$h_s ([S_b] - [S_s]) = \frac{v_{max} [S_s]}{K_M + [S_s]} \qquad (4.8)$$

In the particular case where the overall reaction obeys first-order kinetics (K_M » [S]), eq.(4.8) can be written as:

$$h_s ([S_b] - [S_s]) = \frac{v_{max}}{K_M} \cdot [S_s] \qquad (4.9)$$

Hence the effective substrate concentration at the catalytic surface can be obtained from eq.(4.9):

$$[S_s] = \frac{h_s [S_b]}{h_s + \frac{v_{max}}{K_M}} \qquad (4.10)$$

Thus the effective first-order reaction rate v' in case of K_M » [S] can be written as:

$$v' = \frac{v_{max}}{K_M} \cdot [S_s] = \frac{v_{max}}{K_M} \cdot \frac{[S_b]\, h_s}{h_s + \frac{v_{max}}{K_M}} \qquad (4.11)$$

According to Faraday's law the corresponding current response is [20]:

$$i = n F A v' \qquad (4.12)$$

In the particular cases of high and low transport coefficients we get:

$$h_s » \frac{v_{max}}{K_M}: \qquad v_{kin} \equiv v' = \frac{v_{max}}{K_M} \cdot [S_b] \qquad (4.13)$$

$$h_s « \frac{v_{max}}{K_M}: \qquad v_{dif} \equiv v' = [S_b]\, h_s \qquad (4.14)$$

At high values of h_s mass transport is much faster than the enzymatic reaction, and the overall reaction is controlled by the enzyme kinetics (v_{kin}). Conversely, at low values of h_s the enzymatic reaction proceeds much faster than mass transport, and the reaction is diffusion controlled (v_{dif}). At intermediate transport coefficients h_s either v_{dif} or v_{kin} will play predominant roles, depending on their relative magnitudes.

At the limit of sufficiently high substrate concentrations, when $[S_s]$ » K_M and the reaction is zero order with respect to substrate, v' will always be equal to v_{max}, the inherent saturation value of the enzymatic reaction. The values of the apparent Michaelis constant, defined as the substrate concentration which gives a reaction velocity corresponding to one-half of v_{max} will, however , be considerably higher when diffusional limitations are present [21]. The behaviour of the enzyme kinetic and diffusion controlled reactions as well as the reaction rate of an intermediate h_s are visualized in Fig.4.8.

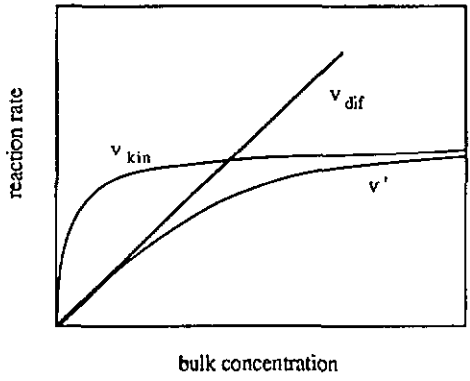

Fig. 4.8: *Schematic plot of overall reaction rates as a function of bulk substrate concentration.*

According to eq.(4.11) the relation v'/v_{max} for first-order reaction can be expressed as:

$$\frac{v'}{v_{max}} = \frac{\frac{[S_b]}{K_M}}{1 + \frac{v_{max}}{K_M h_s}} \qquad (4.15)$$

Further, a dimensionless substrate modulus μ can be defined: $\mu \equiv \frac{v_{max}}{K_M h_s}$

so that: $$\frac{v'}{v_{max}} = \frac{[S_b]}{K_M} \cdot \frac{1}{1 + \mu} \qquad (4.16)$$

μ is a physical constant for a given system. Eq.(4.16) shows that the dependence of v'/v_{max} is a linear relation of $[S_b]/K_M$, but demonstrates also the general importance of external diffusion limitations on the observed reaction rates.

4.4.2 Internal diffusion

The functioning of an enzyme membrane involves two simultaneous phenomena: enzyme catalyzed reaction and metabolite (substrate, cosubstrate and product) transport. Thus, the rate of catalytic reaction per unit volume element of immobilized enzyme decreases with increasing distance (in depth) from the surface of the immobilized enzyme due to substrate consumption in the course of its diffusion through the catalytically active medium. In parallel, the formation of product leads to the generation of product concentration gradients.

If edge diffusion is prevented, the concentration of any substance is constant over any plane parallel to the elecrode. Thus the concentration can vary only normal to its surface. In this one dimensional problem, the origin of the homogeneous membrane of thickness d is taken at the membrane-solution interface. S_b is the substrate concentration in the bulk solution, S(x,t) the substrate and P(x,t) the product concentration at a given location x in the membrane at time t. To render the mathematical formulas dimensionless the substrate and product concentrations are normalized, resulting in the fractional substrate, f_s, and product concentration, f_p:

$$f_s(x,t) = \frac{[S(x,t)]}{S_b} , \qquad f_p(x,t) = \frac{[P(x,t)]}{S_b} \tag{4.17}$$

At steady state, the diffusion can be described by the 1st Fick's law. The metabolite transformation causes a flux of substrates and products. If the enzyme kinetics follows the Michaelis-Menten mechanism, it is:

$$J_s(x) = - D_s \frac{f_s(x)}{\partial x} = \frac{v_{max}\, f_s(x)}{K_M + f_s(x)} \tag{4.18}$$

Taking account the conservation of mass: $$- \frac{\partial f_s}{\partial t} = \frac{\partial f_p}{\partial t} , \tag{4.19}$$

we get: $$J_p(x) = - D_p \frac{f_p(x)}{\partial x} = - \frac{v_{max}\, f_s(x)}{K_M + f_s(x)} \tag{4.20}$$

D_S is the diffusion coefficient for substrate and D_p for product. To calculate the time dependent diffusion and thus taking into account the metabolite concentration changes with time, the 2nd Fick's law has to be applied:

$$\frac{df_s(x,t)}{dt} = D_s \frac{d^2 f_s(x,t)}{dx^2} = \frac{v_{max}\, f_s(x,t)}{K_M + f_s(x,t)} \tag{4.21}$$

and

$$\frac{df_p(x,t)}{dt} = D_p \frac{d^2 f_p(x,t)}{dx^2} = - \frac{v_{max}\, f_s(x,t)}{K_M + f_s(x,t)} \tag{4.22}$$

Eqs.(4.21) and (4.22) are the differential equations describing the linear diffusion of substrate through an enzymatic membrane taking into account the appropriate substrate loss and product formation calculated with the Michaelis-Menten kinetics. To solve these differential equations, we need the boundary conditions.

With amperometric electrodes the electroactive species is consumed rapidly at the electrode surface, with the result that the concentration at the membrane-electrode interface is maintained at zero:

$$f_p(x,t) = 0 \qquad \text{at} \qquad x = d \tag{4.23}$$

The substrate, on the other hand, is assumed to be electroinactive. Thus, there is no flux of substrate at the electrode-membrane interface:

$$\frac{df_s(x,t)}{dx} = 0 \qquad \text{at} \qquad x = d \tag{4.24}$$

A concentration gradient may exist in the solution immediately adjacent to the membrane (Nernst's diffusion layer). This gradient depends strongly on the stirring conditions and is often neglected. This results in a fractional substrate concentration equal to 1 at the membrane-solution interface:

$$f_s(x,t) = 1 \qquad \text{at} \qquad x = 0 \tag{4.25}$$

The flux of product out of the membrane is often neglected, because the initial product concentration is zero and stirring serves also to dilute the product concentration at the membrane-solution interface:

$$f_p(x,t) = 0 \qquad \text{at} \qquad x = 0 \tag{4.26}$$

Similar differential equations as eqs.(4.21) and (4.22) are deduced in chapter 6 and are then applied to modelize the amperometric two-substrate enzyme electrode. Thereby, the here discussed boundary conditions are still valid but are completed by those of the cosubstrate.

4.5 Conclusions

The description of the most commonly used enzyme immobilization methods has shown that, in principle, any biologically active macromolecule can be insolubilized and fixed on a solid support, in a gel or in a porous matrix. The different immobilization techniques can be grouped in adsorption, entrapment, cross-linking by bi- or multifunctional reagents and covalent bonding to reactive supports. Moreover, the combination of different methods is possible. The activity, the pH optimum, the Michaelis-Menten constant K_M and the stability of the immobilized enzyme are usuallly changed compared with those of the soluble species depending on the particular enzyme, the support material, and the type of enzyme-support interaction. Unfortunately, there is no way to predict the resulting behavior of immobilized enzymes, so that the optimum parameters must be determined empirically by trial and error procedures. There are, however, logical approaches to immobilization based on a knowledge of enzyme and active-site structure, and an understanding of the coupling chemistry.

In contrary to a well stirred homogeneous enzyme solution, where the concentration of all species is uniform throughout the system, bound enzymes show modified kinetics due to structural changes upon immobilization, interactions between the matrix and the substrate and/ or cosubstrate resulting in concentration nonuniformities in the enzyme matrix, as well as the presence of diffusional resistances. The different effects leading to such a changed behavior have been discussed in order to allow a theoretical treatment of immobilized enzyme kinetics which is necessary for the understanding of enzyme electrode design and the interpretation of sensor responses. Since biological substances show a relatively low diffusibility, diffusional resistances often affect the activity of immobilized enzyme systems. Therefore, both external and internal diffusion have been treated mathematically for planar enzyme electrode design resulting in a distinction of two operational modes: the diffusion controlled and the catalytic reaction controlled mode.

As an example of immobilization techniques the insolubilization and fixation of the enzyme glucose oxidase (co-cross-linking GOD with albumin by a bifunctional reagent) is detailed in the next chapter. A profound treatment of the combination of enzyme kinetics with internal metabolite diffusion is given in chapter 6 where the appropriate differential equations are deduced and applied to modelize the current response of an amperometric enzyme electrode.

4.6 References

[1] S. Krishnaswamg and J.R. Kittrell, Biotechnol. Bioeng., 20 (1978) 821.

[2] O.R. Zaborsky, Immobilized Enzymes, CRC Press, Cleveland, Ohio, 1973.

[3] L.B. Wingard, E. Katchalski-Katzir and L. Goldstein, Immobilized enzyme principles, in Applied biochemistry and bioengineering, Vol. 1, Academic Press, New York, 1976.

[4] P.W. Carr and L.D. Bowers, Immobilized enzymes in analytical and clinical chemistry, Fundamentals and applications, in P.J. Elving and J.D. Winefordner (eds.), Chemical Analysis, Vol. 56, John Wiley & Sons, New York, 1980, Ch. 4.

[5] A.P.F. Turner, I. Karube and G.S. Wilson, Biosensors: Fundamentals and Applications, Oxford University Press, New York, 1987, Ch. 6.

[6] R.A. Messing, Enzymologia, 38 (1970) 370.

[7] P. Bernfeld, R.E. Bieber, and P.C. McDonnell, Arch. Biochem. Biophys., 127 (1968) 779.

[8] G.P. Hicks and S.J. Updike, Anal. Chem., 38 (1966) 726.

[9] K. Mosbach and B.Mattiasson, Acta Chem. Scan., 24 (1970) 2093.

[10] T.M.S. Chang, Artificial cells, Thomas, Springfield, Illinoise, 1972.

[11] T.M.S. Chang, in Insolubilized enzymes, eds. M. Salmona, C. Saronio and S. Garattini, Raven, New York, p. 15.

[12] A.C. Johansson and K. Mosbach, Biochim. Biophys. Acta, 370 (1974) 339.

[13] K. Mosbach, Immobilized enzymes, in S.P. Colowick and O. Kaplan (eds.), Methods in enzymology, Vol. XLIV, Ch. 20, Academic Press, New York, 1976.

[14] P.D. Boyer, Enzyme structure and control, in The enzymes, 3rd Ed., Vol. 1, Academic Press, New York, 1970.

[15] G.E. Means and R.E. Feeney, Chemical modification of proteins, Holden-Day, San Francisco, California, 1971.

[16] C.H.W. Hirs and S.N. Timasheff, Enzyme structures, Part B, in Methods in Enzymology, Vol.25, Academic Press, New York, 1972.

[17] K. Mosbach and R. Mosbach, Acta Chem. Scand., 20 (1966) 2807-2810.

[18] H.I. Silman, M. Albu-Weissenberg and E. Katchalski, Biopolymers, 4 (1966) 441-448.

[19] K. Mosbach, Immobilized enzymes, in S.P. Colowick and O. Kaplan (eds.), Methods in enzymology, Vol. XLIV, Academic Press, New York, 1976, Section VI, Ch. 29.

[20] A.J. Bard and L.R. Faulkner, Electrochemical Methods, John Wiley & Sons, New York, 1980, Ch. 1.

[21] C. Horvath and J.M. Engasser, Biotechnol. Bioeng., 16 (1974) 909.

V

Fabrication and characterization of a planar amperometric glucose sensor

5.0 Summary

A planar electrochemical microcell is fabricated using standard planar processing. The electrochemical behaviour of this device consisting of two Pt electrodes (working and counter electrode) and one Ag/AgCl reference electrode is studied in order to draw a parallel between some technological parameters of thin film processing and the electrode surface properties. An immobilized glucose oxidase membrane is then manually deposited and the amount of H_2O_2 produced is measured. In order to render the sensor response less dependent on pO_2 an additional outer polyurethane membrane is dip-coated. The overall dimensions of the device are 0.8 mm x 3 mm. The sensor is then characterized in a modified Krebs solution and tested in vivo, subcutaneously implanted in rats.

Thin enzyme membranes can also be deposited on wafer level and patterned by the IC-compatible lift-off technique. Thus obtained membranes are well defined and have a good uniformity of membrane thickness. The linear response range of such prepared membranes, however, is rather low.

5.1 Introduction

A glucose sensor is a transducer that converts glucose concentration into an easily measurable current. Its fabrication and characterization is subject of this chapter. It is layed out as miniaturized amperometric glucose sensor designed for the use in analytical chemistry as well as for bioprocess control and biomedical applications. In this latter field sensor miniaturization plays an important role, especially when enzyme electrodes have to be used in vivo.

Until recently, such sensors have been realized with thin metallic wires. The optimization of these wire electrodes resulted in needle-type electrodes with diameters of less than 1 mm [1]. An important disadvantage of this technique is the difficult mass production. This problem can be solved using microfabrication technology, in particular metal evaporation and patterning on silicon substrates, resulting in planar sensors [2, 3]. In this case, the silicon wafer only serves as flat substrate and can, in principle, be substituted by a glass plate.

The amperometric glucose sensor can be divided into two parts: the electrochemical cell and the membrane part. The electrochemical cell consists of planar metallic electrodes deposited on a passivated silicon substrate. Biological modification of the electrode surface is done by immobilization of an enzyme onto the transducer surface [4].

The stability and the life-time of an enzymatic sensor depend on the solid-state part as well as on the enzymatic membrane. The first part of this chapter is intended to characterize the solid-state electrochemical microcell so that before it is completed by a membrane its electrochemical behaviour is known. In the following, the fabrication of the membrane part consisting of a manually deposited enzyme layer and the dip-coated glucose diffusion limiting polyurethane membrane is detailed. The thus completed glucose enzyme electrode is then characterized in vitro, i.e., in a modified Krebs physiological solution.

In order to obtain precisely patterned membranes with good uniformity of membrane thickness, the IC-compatible lift-off technique has been applied for patterning enzymatic membranes on wafer level [3, 5]. The final devices are tested for the determination of glucose and the responses of different glucose electrodes are compared. This technique can only be used for the fabrication of thin membranes of about 1-2 µm thickness [6] which are not suitable for in vivo testing. On the other hand, they can be used for flow injection analysis (FIA) with predilution of the sample.

This chapter, finally, is completed by an in vivo characterization of glucose sensors consisting of manually deposited enzyme membranes and dip-coated polyurethane films. Implanted in subcutaneous tissue of rats, they are used to monitor glucose levels during various glucose physiological tests (IVGTT, IP, clamp).

5.2 Fabrication and characterization of a planar electrochemical cell

This section describes the fabrication and characterization of a planar electrochemical microcell. It consists of two platinum electrodes (counter and working electrode) and one Ag/ AgCl reference electrode, which are deposited as thin films on a Si/ SiO_2/ Al_2O_3 substrate. To improve their adhesion on oxide films, generally, an intermediary layer (Cr or Ti) is required. Care has to be taken to characterize such electrodes [7], because first of all no mechanical cleaning can be carried out and second a contamination of the metal by interdiffusion of atoms from the adhesion layer, which may influence adsorption/ desorption processes, can occur.

5.2.1 Thin film technologies

In silicon planar technology, circuits are built on the surface of a silicon wafer in a succession of process steps. Each step begins with coating the wafer surface with a radiation-sensitive material called a resist. A pattern is done in this material by shining ultraviolet light onto it through a mask containing the desired pattern. In positive-type resists, the exposed region is made soluble, whereas in negative resists, the exposed region remains insoluble. This process is known as photolithography. There are two principle methods of applying this photolithographic technique:

1.) Applying the photolithography on a previous deposited layer (insulator, metal film) so that the pattern of the resist can be repeated in this layer by etching away the undesirable area.

2.) Applying the photolithography previous to the deposition of a metallic layer or a polymeric membrane followed by lifting off the undesired film area by dissoluting the unexposed resist.

A survey of the principle resist processes is given in Fig.5.1 showing the negative and positive resist definition. Positive resists develop in the exposed region and usually remain soluble in acetone for lift-off. Negative resists remain in the exposed region but are insoluble in acetone and not suitable for lift-off. For etching, however, both positive and negative resists are used.

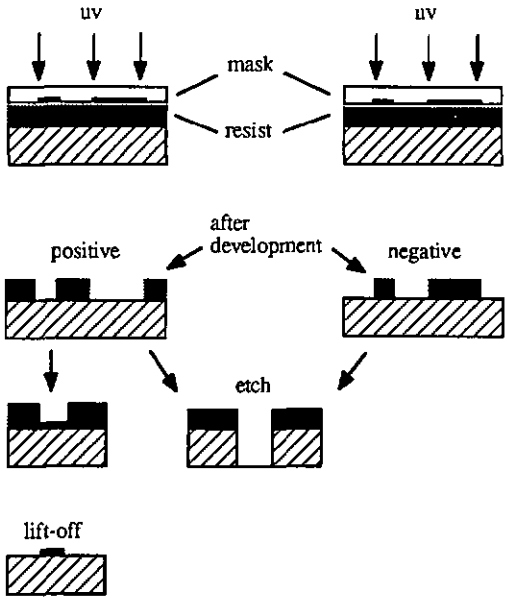

Fig. 5.1: Resist processes and their principle use in thin film technologies.

By using etching processes, oxides or metals are first deposited on the whole wafer. The areas that have to stay are protected by a photoresist layer. This resist film is previously patterned by photolithography and, thus, acts as etching mask. Applying then an appropriate etch solution, the undesired part of the metal or insulator layer is removed selectively. Hence, the etching technique comprises four principal processes:

1.) Evaporation of metal layers, oxidation of Si or deposition of other insulating layers by chemical vapor deposition (CVD), etc.

2.) Photolithography, i.e., deposition of a photoresist layer followed by its patterning

3.) Selective etching of unwanted metal

4.) Removing the photoresist by applying a stripping procedure.

By applying the lift-off technique the process sequence is changed, i.e., the photoresist is first deposited and patterned. A metal layer, a polymeric membrane or an insulating

layer is then deposited on top of the resist and patterned by dissolving the underlying resist. Thus, this technique comprises only three processes:

1.) Deposition and patterning of a resist film

2.) Evaporation of a thin metallic film, deposition of an insulating layer or application of a polymeric membrane

3.) The material that has to be removed is on top of the resist and, thus, is lifted off during resist stripping.

The lift-off technique has the advantage that it saves one process step. Additionally and often more important is that it requires no etch selectivity between substrate and material to be removed. However, there is the problem of adhesion which, hereby, is much more pronounced due to the strong mechanical stress between the material on the substrate which has to stay and the material on top of the resist which is removed.
Etch processes suffer not only of the required selectivity, but sometimes also of an appropriate etching solution. Hence, some metals such as platinum are very difficult to etch. For this reason, the lift-off technique has been chosen for the fabrication of the electrochemical cell described in this chapter.

5.2.2 Lift-off process

This section describes the lift-off procedure used for patterning the platinum and silver electrodes. The typical process steps involved are illustrated in Fig.5.2 and are treated in more detail in the following. A more complete description of semiconductor lithography can be found in the literature [8].
The cleaning and dehydration of the wafer surface, generally, is followed by applying a priming procedure in order to improve the adhesion of photoresist on oxide layers. The wafer is then placed on a spinner and held by a vacuum. Using a pipette, a certain amount of positive resist is deposited. By rotating the wafer, the photosensitive liquid is leveled and spun off by centrifugal forces. In order to remove the solvents contained in the resist, the film is mildly baked. The prepolymerized resist is then exposed to uv-light. After the development where the exposed part is removed, the film is hard baked to improve its mechanical and chemical resistance. Further, the metal layer is evaporated and patterned by dissolving the unexposed resist.

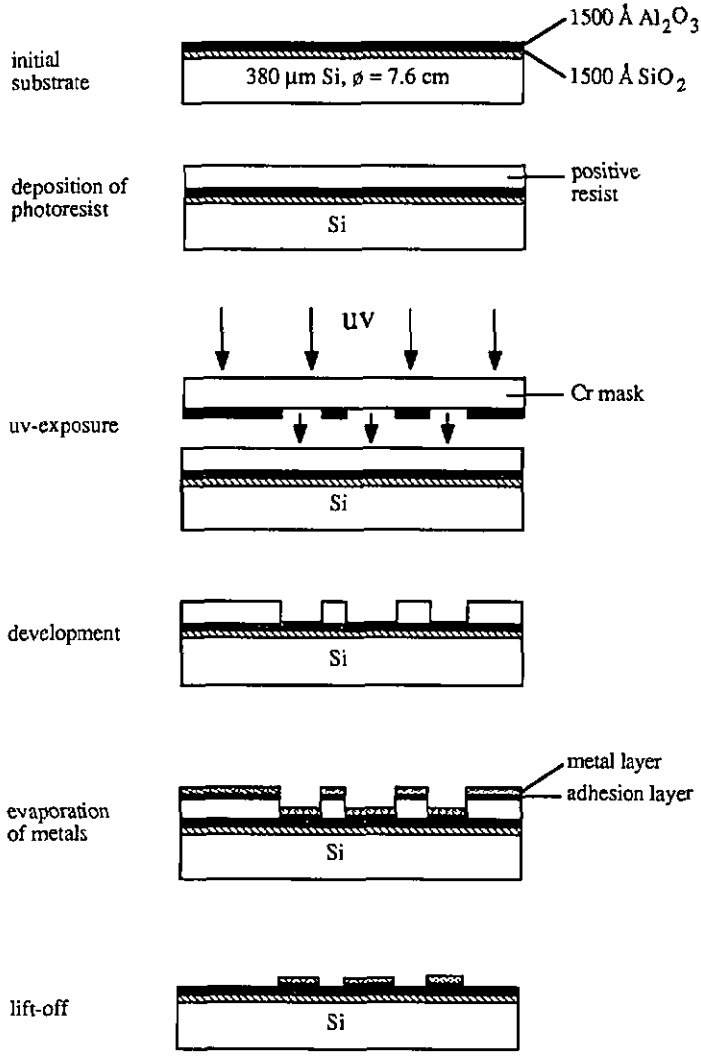

Fig. 5.2: Typical process steps involved in a lift-off procedure.

5.2.2.1 Substrate

The substrate used is generally a three inch silicon wafer with two passivating layers (1500 Å SiO_2, 1500 Å Al_2O_3 or Si_3N_4). Ideally, the photolithography should be carried out immediately after the deposition of Al_2O_3 or Si_3N_4. If the wafers are stored longer than one day or if there is another reason why the wafers are dirty, they have to be cleaned by immersion in acids (e.g., fuming HNO_3) for organic contamination removal. All cleaning procedures are finished by rinsing the wafers with deionized water. The clean wafers are then dehydrated by baking them at the maximum temperature the device allows at this stage of fabrication. Usually, a minimum dehydration bake at 200 °C during 30 minutes is recommended. This removal of water is often followed by a deposition of an adhesion promoter such as hexamethyldisilazane (HMDS). The application of this silane on the surface of oxides just prior to resist coating improves subsequent resist adhesion. The priming is applied in cold vapor phase and produces an interfacial bonding layer for the photoresist and, additionally, removes any residual moisture held at the surface. The automatic settings of the silanization apparatus used are: 3 min purging in N_2, 15 min in HMDS and again 5 min in N_2.

5.2.2.2 Resist coating

Most of the photoresists are two-component formulations made of a polymer base and a photosensitizer, i.e., they are a mixture of film-forming polymers, photoactive compounds (PAC), solvents and other additives. The general resist requirements affect thickness, topography, thermal stability, profile control, resolution, adhesion, film defects, wet etch resistance, plasma and RIE resistances. Except for the photosensitivity and the spectral response, all of the properties of a resist are derived from the polymer component. The required resist thickness depends on the application. The lift-off process, e.g., requires mostly a thicker resist layer than an etching process. For this reason, there are several photoresists with different viscosity on the market. Besides resist types, thicknesses depend also on spin speeds during the coating procedure.

All resists used are from Shipley. Microposit S-1400-27 is applied for Pt-patterning and Microposit 1350 J for Ag. The amount required for one coating is about 1 ml per wafer (3 inch). Their coating thicknesses as a function of spin speed are shown in Fig.5.3.

All photoresist coatings are done using a Convac ST 145 spinner. This instrument has six parameters which are divided into two part: cycle-step one and cycle-step two. Each part includes three variables: ramp, time and spin speed in rpm, i.e., rotation per minute. Typical spinner speeds are between 3000 and 5000 rpm.
Each deposition is followed by softbaking the resist coating. Typical prebake temperatures are between 80 °C and 90 °C so that, after 30 - 40 minutes, the majority of solvent is removed. Under-baking leads to an increased loss of unexposed photoresist and decreased adhesion.

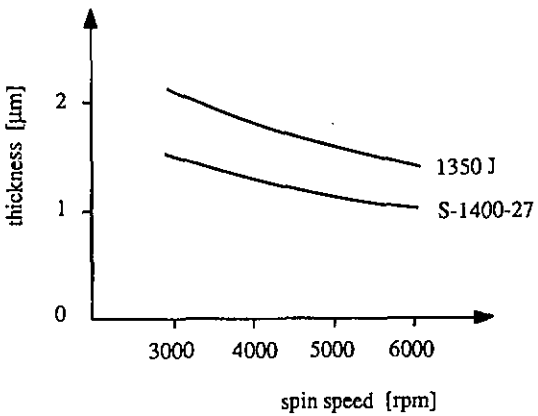

Fig. 5.3: Resist thickness vs. spin speed.

5.2.2.3 Exposure

Photoresists are very sensitive in the UV-region, but insensitive to long waves of the optic spectrum. For this reason all work can be done in a yellow room. Thus, when the softbaked resist system is exposed to ultraviolet light, the PAC undergoes a photochemical reaction which alters its molecular structure and changes its solubility. Typically, photoresists are exposed in the 340 to 450 nanometer range. In the case of positive resist, nitrogen is liberated during exposure. It is important that water molecules are present in the resist film during exposure for the mechanism to proceed properly. Insufficient relative humidity causes decreased light sensitivity. The proper working condition is at least 35 % relative humidity. In our laboratory, a humidity of 40 % is guaranteed by air conditioning.

Often there is a need for several photolithographic steps which requires a very exact alignment. For this reason each mask contains alignment marks for overlaying one circuit pattern level precisely on top of the previous layer. Thus, the selective uv-exposure of the resist is performed under microscope (Karl Süss maskaligner). The appropriate mask, which is usually a chromium oxide pattern, has the same structure as the metallic layer we want to obtain. The chromium oxide pattern is deposited on a glass plate and is opaque for uv-light. The required energy of the uv-light depends on the resist employed. To calculate the exposure time, the lamp intensity of the mask aligner has to be measured. During exposure, the wafer is in contact with the mask.

5.2.2.4 Chlorobenzene soak

A first requirement for a successful lift-off is a high ratio of resist to metal thickness, thus ensuring that the metal deposit does not become a continuous film. A second consideration is the resist profile. Generally, three different profiles are distinguished (see Fig. 5.4): overcut, vertical and undercut. The formation of profiles depends first of all on the applied dose of uv-exposure.

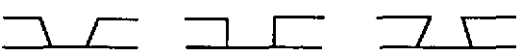

Fig.5.4: Major resist profiles.

If the profile is undercut (see Fig.5.5), metal wing formation may occur and cause poor edge definition and subsequent problems with thin membranes. Additionally, problems may result during lift-off when parts of the protruding feet break and then are redeposited on the wafer surface. Hence, in order to facilitate the lift-off and to obtain good line width control, an overcut profile with a smaller opening at the top than at the bottom is necessary to prevent step coverage. To enhance the formation of this profile, additionally, a chlorobenzene soak can be applied.

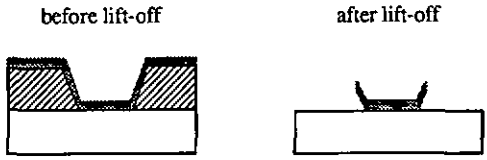

Fig. 5.5: Schematic illustration of microcrack at the top of the metal layer.

When exposed resist films are soaked in chlorobenzene, low molecular weight components are partially removed resulting in a hardening of the top of the resist layer. Thus, the top layer becomes less soluble during development, resulting in an overhang profile. Moreover, the diffusion of chlorobenzene into the resist results in a swollen top layer (see Fig.5.6). The depth of penetration depends on soak time and solvent content after prebake. The whole soaking process is controlled by the prebake, the soak time, the time of uv-exposure and the development.

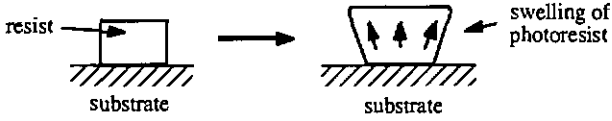

Fig.5.6: Swelling of photoresist during soaking in chlorobenzene.

An overhang of the resist step induced by chlorobenzene treatment is required in order to minimize the microcrack at the top of deposited substrate, but is not always sufficient to achieve a sharp metal step. Thus, even when the top of resist is overcut but the rest of profile is undercut protruding feet may form (see Fig.5.7).

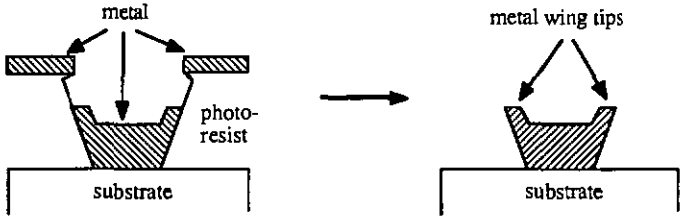

Fig. 5.7: Formation of metal wing tips in lift-off due to resist foot.

A further consideration is the outgassing which may arise during metal deposition (see Fig.5.8). Hence, fluctuations of the vacuum pressure are evidence for resist outgassing from such components as N_2 from the sensitizer, the phenol in the resin of the resist, trapped water and other solvents. Outgassing from walls of resist acts as a streaming source to divert the depositing metal into forming pyramidal profiles. To minimize outgassing, careful bake conditions as well as low metal deposition temperatures are required.

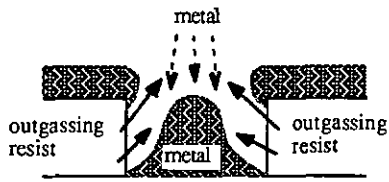

Fig. 5.8: Outgassing resist at elevated temperatures and electron bombardement during e-beam metal deposition distorting angle of metal deposition.

Because the top opening of the resist serves as the metal deposition mask, e-gun metal evaporation should be done at an angle nearly normal to the wafer surface. Thus, rotating of the wafer during deposition, as often applied to smooth the deposited layer, cannot be used.

5.2.2.5 Development

Excessive delay between exposure and development brings a reduction of image fidelity known as latent image decay. Photoresist coatings should be subjected to no more than 4 hours delay between exposure and development.

The dissolution rate of the exposed resist by the developer is up to a hundred times faster than that of the unexposed resist. Increased developer temperature will also increase development rate. It is recommended that developers are used between 20 °C and 25 °C. The here used resist types, usually, are developed in a AZ 351 developer (150 ml AZ 351, 750 ml H_2O) for about 60 seconds. Finally, the wafers are washed in disolled water.

To prevent outgassing during metal deposition the resist is postbaked and thus allowed to completely polymerize. In order to enhance the effect of chlorobenzene soak the prebake is done at the lower limit of recommended temperatures. Thus, to avoid a too

violent removing of solvents during postbake which would result in a rough resist surface, the wafers are postbaked in two steps: first, at a temperature of 85 °C for 20 minutes and second at 120 °C for 20 minutes.

5.2.2.6 Metal deposition and lift-off

Metal deposition can be done by physical vapor deposition (PVD), galvanic deposition or chemical vapor deposition (CVD). Any deposition procedures consists of three steps:

a) Transition from a condensed phase to the vapor phase
b) Transport of the vapors between source and substrate
c) Condensation of vapors followed by film nucleation and growth

PVD processes have the advantage that all three steps can be controlled independently. Three PVD techniques are known [9] : evaporation, ion plating and sputtering:

Evaporation:
Vapors are produced from a material located in a source which is heated by direct resistance, radiation, eddy currents, electron beam, laser beam or arc discharge. Such evaporation processes are carried out in vacuum so that the evaporated atoms undergo an essential collisionless transport prior to condensation on the substrate. Thereby, the substrate is usually at ground potential, i.e., not biased.

Ion-plating:
The material is vaporized similar to the evaporation process but it passes through a gaseous glow discharge on its way to the substrate, thus ionizing the vaporized atoms. The glow discharge is produced in a gas chamber (e.g., argon) by biasing the substrate to a high negative potential (-2 to -5 kV). Thus, the substrate is bombarded by high-energy gas ions which results often in a better adhesion of the deposited film and lower impurity content.

Sputtering:
Positive gas ions (usually argon ions) are produced in a glow discharge. They are used to bombard the target material (cathode), dislodging groups of atoms which pass into the vapor phase and deposit onto the substrate. Sputtering is an inefficient way to induce a solid-to-vapor transition but, due to a continuously cleaned surface (ion bombardement), a better adhesion results compared to evaporated layers.

All metal films used for the fabrication of the electrochemical cell are e-gun evaporated. This technique is based on the evaporation of electron beam heated metal and is performed under high vacuum conditions (typically 10^{-5} to 10^{-6} torr). The source material is placed in a multi-crucible so that thin film multilayers of different metals such as Ti/ Pt or Ti/ Ag can be deposited.

Thus deposited metal films suffer often from residual mechanical stresses which may influence the adhesion behaviour. They may arise from imperfections built in during growth. Their appearance can, in principle, be reduced by increasing the deposition temperature of the substrate. Applying lift-off technique, this method is useless because the photoresist does not support temperatures above 120 °C. An other reason is due to the different thermal expansion coefficients of the substrate and the deposited layer. This may be solved by depositing an intermediary layer with a graded expansion coefficient. The linear expansion coefficients of silicon [10], alumina [11], nitride [12], glass [11] and metals [10] used for the electrochemical cell are given in table 5.1.

Table 5.1: Expansion coefficients of several materials used for the planar electrochemical cell.

material	coefficient of linear expansion (x 10^{-6} / °C)
platinum	9
silver	19
titanium	8.5
chromium	6
silicon	3
alumina	6
nitride	4
glass	9

The positive photoresist is then dissolved in acetone (stripping) and, thus, the metal on top of the resist is removed. As a result only the metal situated on the exposed part of the wafer surface will remain. Negative resists have to be stripped in fuming nitric acid or specific solutions (resist remover).

During metal lift-off, the frequent filtering and changes of the lift-off tank are necessary to prevent polymer and metal redeposition. Sometimes, heating of the lift-off solvent is necessary to facilitate its permeation. If the solvent does no dissolve the lift-

off layer, ultrasonic agitation is often used to assist removal of the undesired metal. Thereby, care has to be taken because adhesion failure may occur.

5.2.3 Mask sets

One of the first step in the realization of a planar sensor is the design of the sensor layout which defines the electrode geometry. The layout is strongly linked with the processing sequence because, generally, each step requires a different mask. Further, critical dimensions, e.g. size of the electrodes and the distances between them, are defined by processing limitations. The different masks used for the fabrication of our standard planar electrochemical cell are presented in Fig. 5.9.

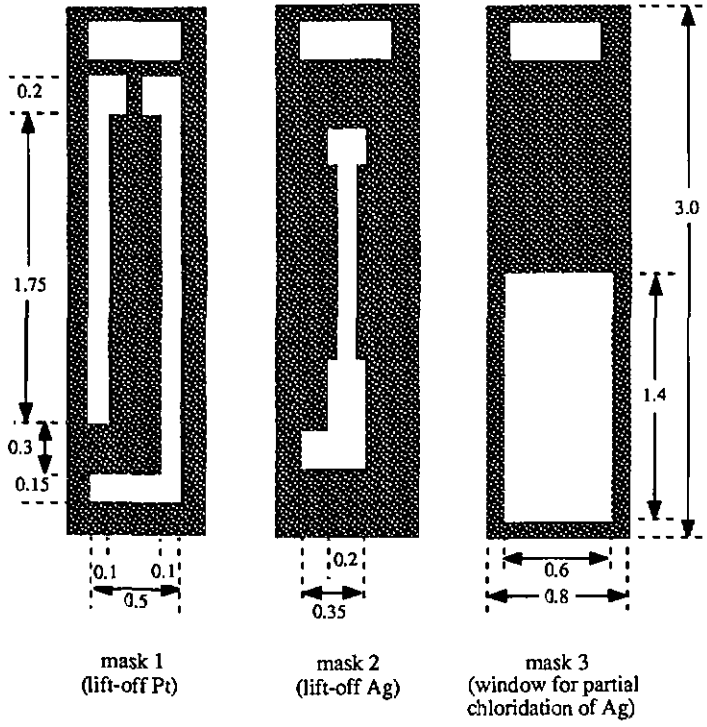

Fig. 5.9: Mask layout SGL200 of the standard three electrode cell (dimensions in mm).

Such a sensor layout is usually done on an intuitive basis. Since biomedical applications are envisaged, the geometries should be as small as possible, especially in width, allowing thus the assembly in a catheter. On the other hand, the response of an amperometric sensor (i.e. current) is proportional to the area of the working electrode. Additionally, small electrodes show a large noise to signal ratio. Hence, narrow but long electrodes are preferable. An other consideration is the ratio, r_A, between working and counter electrode area, A_W and A_C respectively, which should be small to prevent current limitations at the counter electrode. Also, a too close spacing between the electrodes has to be avoided to prevent migration of AgCl. In order to facilitate the encapsulation of the bonding wires, the distance between the electrochemical active electrode surface and the bonding pads should be sufficiently large. All these parameters have been taken into account for the above presented mask design.

The first mask defines the Pt-electrodes and the second the Ag-electrode. The working electrode area exposed to the analyte solution is 0.085 mm^2 and that of the counter electrode 0.19 mm^2. Thus, the ratio r_A is about 0.45. In order to facilitate the wire bonding, the area of the bonding pads is 0.2 x 0.2 mm^2. 150 µm on each side of the chip are provided for an easy encapsulation. The electrode spacing is 50 µm and the overall chip dimensions are 0.8 mm x 3 mm x 0.38 mm (one wafer contains 1071 cells). The third mask serves as window for the partial chemical chloridation of the silver electrode. It could have been chosen much smaller, but such a large window over all three electrodes can also be used for lift-off of on-wafer deposited membranes (see section 5.4).

In order to optimize the sensor miniaturization, an other layout has been developed. Due to encapsulation, the most limiting point for further miniaturization are the chip sides. This problem can be solved using glass wafers. Their use offers several advantages such as no passivating layers and no encapsulation of the chip sides are required. On the other hand, they possess a serious drawback: large glass disks are rather delicate to mechanical stresses, especially during dicing. Thus, the density of cell structures on the wafer has to be reduced. On the other hand, the absence of sides' encapsulation allows to obtain smaller width of the final chip (see Fig. 5.10) which is especially favourable for in vivo applications. In order to use the same working facilities in the production line as for silicon wafers, three inch glass wafers are preferred. They are obtained from Schott & Schleiffer and are 0.15 mm thick.

The layout shown in Fig. 5.10 contains 286 electrochemical cells per wafer. The working electrode area exposed to the solution is 0.08 mm^2 and that of the counter electrode 0.1 mm^2. Due to the smaller design, the bonding pads measure 0.2 mm x 0.1 mm, still allowing a fast and easy bonding procedure.

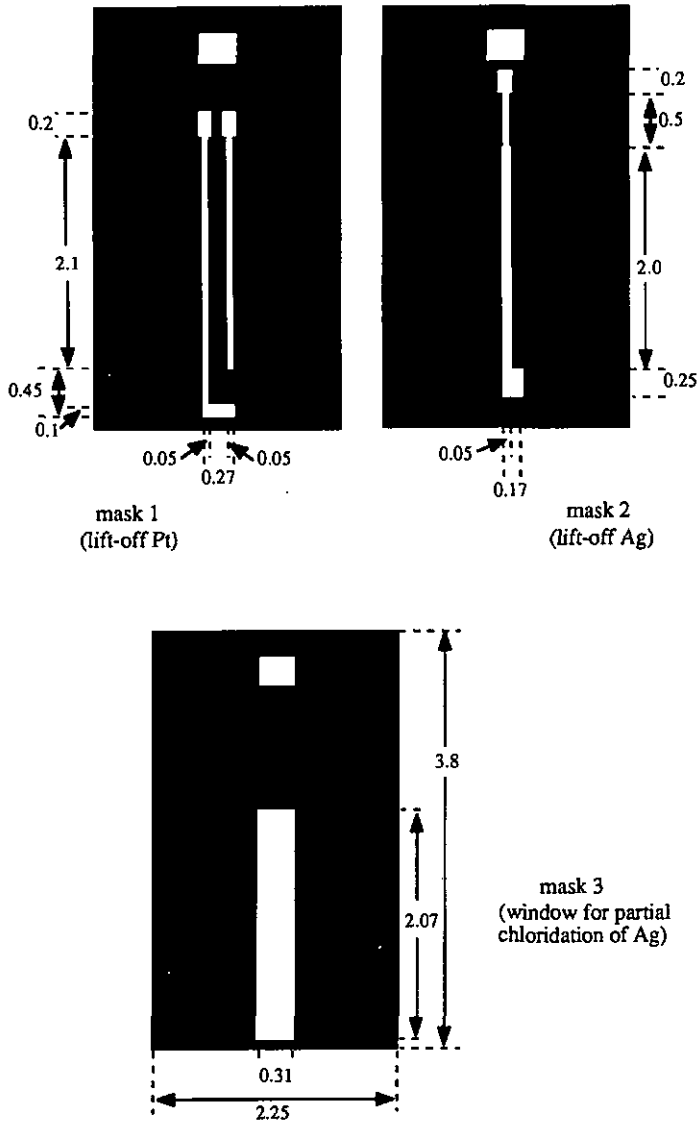

Fig. 5.10: Mask layout SGL600 (dimensions in mm).

The smallest distance between the electrodes is still 50 μm. The larger spacing between the different cells, compared with the standard layout, allows the choise of the chip width. After dicing the wafer, the minimum glass chip width is about 0.45 mm. When this layout is applied to silicon wafers, the minimum width is 0.5 mm. In this case, after dicing, about 0.1 mm is left for encapsulation on each side.

5.2.4 *Process steps for the realization of the electrochemical cell*

The layout of the standard electrochemical cell is schematically presented in Fig.5.11 whereas Fig. 5.12 illustrates its complete fabrication procedure. The substrate used is n-type, (100) oriented silicon, 75 mm in diameter and has a resistivity of 15-35 Ωcm. After a standard cleaning procedure, the wafer is thermally oxidized at 1100 °C in a dry oxygen atmosphere during 80 minutes. The thickness of the SiO_2 film is about 1500 Å as determined by ellipsometry. This high quality SiO_2 film acts as a first isolation layer between the electrodes and between the electrodes and the bulk. The use of SiO_2 alone shows several deficiencies such as poor chemical stability, permeability to alkali ions (causing electrical conduction between the electrodes) and susceptibility to breakdown because of the poor electric field strength of the hydrated oxide [13]. To improve the life-time of the device an additional inorganic film such as Si_3N_4 [14] or Al_2O_3 [15] has to be deposited on top of the SiO_2 to form an ion-barrier film. Its thickness is about the same as that of SiO_2.

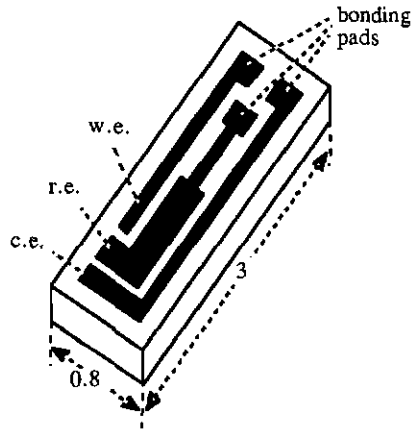

Fig. 5.11: Schematic layout of the standard electrochemical cell.

Such passivating layers can be deposited by chemical vapour deposition (CVD) where the constituents of the vapor phase react to form a solid state film on the substrate. Silicon nitride films are deposited at low pressures (LPCVD) by a silane (SiH_4)-ammonia (NH_3) reaction which occurs at temperatures of 900-1000 °C.

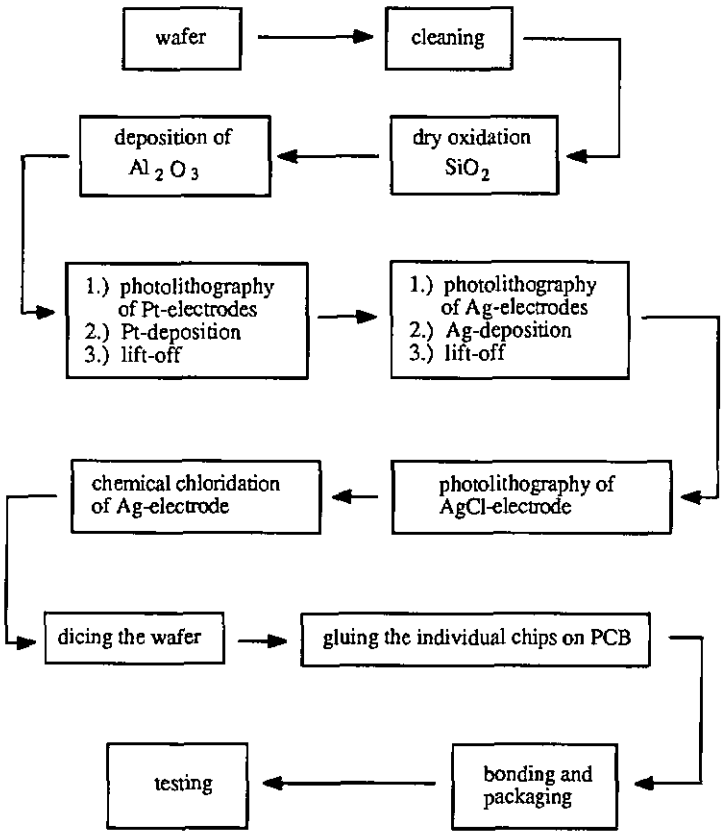

Fig. 5.12: Schematic description of process steps.

All metals are electron-gun evaporated at a substrate temperature of 25°C and then patterned by the lift-off process. The evaporation rate for Ti is 10 Å/s, for Cr 50 Å/s and that for Ag is 100 Å/s. For Pt a standard evaporation rate of 10 Å/s is used. Electrodes fabricated in this way are very smooth as shown in Fig. 5.14, where a SEM-photo of the Pt-surface is presented.

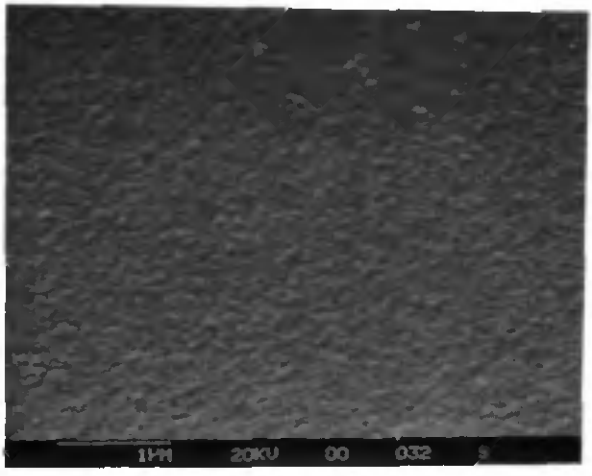

Fig. 5.14: SEM photo of the Pt surface (evaporation rate: 30 Å/s).

This standard planar processing is used twice to fabricate two Pt and one Ag electrode. The Ti and Cr adhesion layers have a thickness of 500 Å and the Pt and Ag layers measure 1500 Å and 1 μm respectively. Partial chloridation of the Ag layer is performed chemically on wafer level in a 25 mM $FeCl_3$ solution [18]. A SEM-photo of the chloridized silver electrode is presented in Fig. 5.15. The SEM-photo shows the Si bulk with the two passivating layers (SiO_2, Al_2O_3) and the Ag/AgCl-electrode with the Ti-adhesion layer. The thin AgCl layer is only weakly visible on top of the electrode. The photo also shows that the lift-off process produces straight and very smooth electrode sides.

Alumina can be deposited by chemical vapor deposition at atmospheric pressure (APCVD) [16]:

$$2\,NO + 2\,H_2 \xrightleftharpoons{T > 700\,^{\circ}C} N_2 + 2\,H_2O \qquad (5.1)$$

$$2\,AlBr_3 + 3\,H_2O \rightleftharpoons Al_2O_3 + 6\,HBr \qquad (5.2)$$

Thus, the complete reaction is:

$$4\,AlBr_3 + 6\,NO + 6\,H_2 \rightleftharpoons 2\,Al_2O_3 + 3\,N_2 + 12\,HBr \qquad (5.3)$$

Since reaction (5.1) occurs only at temperatures greater than 700 °C, the gases can be mixed at low temperatures before they get in the reaction chamber.

The thin film electrodes (Pt and Ag) are fabricated using the lift-off technique as described in section 5.2.2. The sequence of photolithographic steps is visualized in Fig. 5.13. The overcut resist profile is achieved by a chlorobenzene soak of 5 minutes just after the ultraviolet light exposure [17]. Shipley Microposit S 1400-27 (1.2 μm) is used for the Pt-patterning and Microposit 1350 J (2.2 μm) for the silver.

Noble metals such as platinum and silver, i.e., metals which do not easily form an oxide, show a rather poor adhesion on oxide layers. Thus, intermediary layers such as chromium or titanium are required and are deposited in one pump down process just prior to the Pt or Ag deposition.

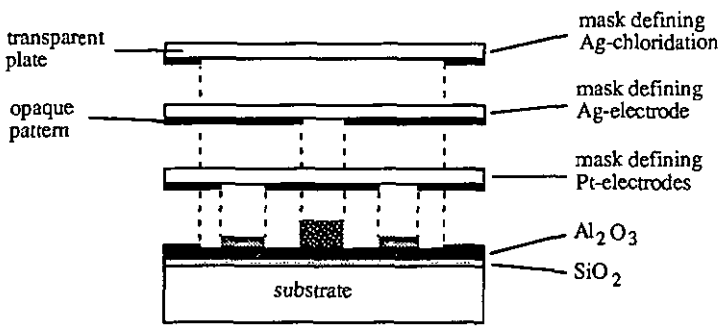

Fig. 5.13: Photolithography steps.

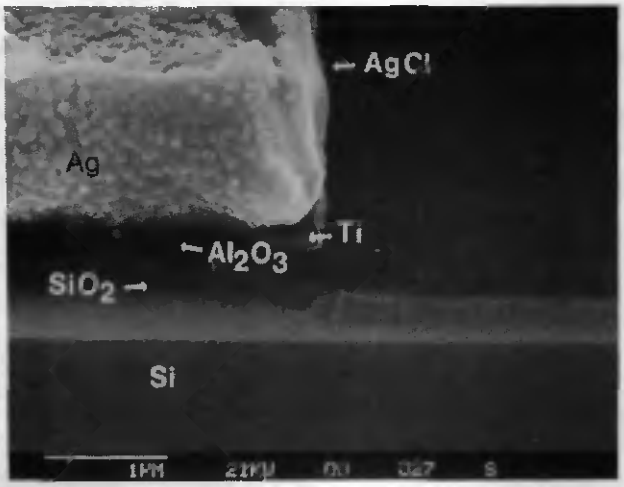

Fig. 5.15: SEM photo of the chloridized Ag electrode (cross-section).

5.2.5 Packaging

After dicing the wafer, the individual sensor chips are mounted on a printed circuit board, bonded and encapsulated with an araldite-type epoxy. This encapsulation, called packaging, is a decisive procedure in the fabrication of chemical sensors and is required because the chemical part of the sensor has to be exposed to the environment whereas the electronic part has to be completely protected. If the device is not well isolated, parasitic electrochemical processes occur which destabilize the device response and cause further breakdown of the encapsulation.

Packaging is generally situated on two levels. The first one is the passivation layer which is deposited on wafer level and provides the electrical isolation of the electrodes. Additionally, in the case of planar sensors, it prevents leakage currents between high impedance points, i.e.,between electrodes. The second one is the encapsulation which protects the interconnections between the sensor and the printed circuit board (PCB). The PCB acts as sensor support and therewith as interconnection between the sensor and the external electronics. A further goal of the encapsulation is the exclusion of interferences from the analyte environment, i.e. the isolation of the sensor part which is not protected by the passivation layer and which should not be exposed to the analyte solution such as, for example, the side of the sensor chip. The packaging by

encapsulation is difficult to automate so that, in general, it is still done manually. Hence, the packaging of electrochemical sensors is often the most time-consuming procedure of the whole sensor fabrication.
The most critical point in any encapsulation is the zone where the three different materials come together (sensor surface, analyte solution and the encapsulant). This point is the most critical one in terms of the adhesion of the encapsulant to the sensor surface. Usually, it is at this point where a packaging starts to deteriorate.

5.2.5.1 Packaging on PCB

The easist way of packaging a miniaturized electrochemical sensor is done by mounting the sensor on a PCB (see Fig. 5.16) followed by an encapsulation with a non-conductive araldite-type epoxy. The procedure is as follows:

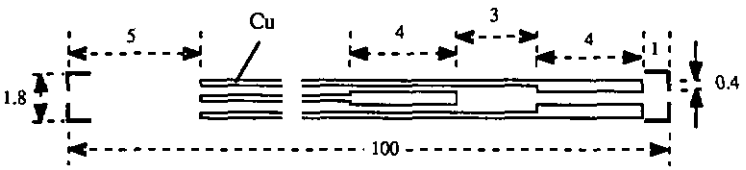

Fig. 5.16: Scheme of the standard printed circuit board.

1.) Gluing the sensor chip on the aboved presented PCB.

2.) The two components (the resin and the hardener) of the araldite-type epoxy are well mixed and then left to prepolymerize during one hour at room temperature. When the mixture is prepared carefully only a few air bubbles are formed, so that no deaeration is required. The prepolymerization is an important step in order to prevent the flow of non-polymerized epoxy over the whole sensor surface.

3.) The sides of the chip are encapsulated. Moreover, a thin wall of epoxy is deposited (see Fig.5.17) in order to prevent the flow of encapsulant during step 5.

A photograph of a bonded and encapsulated planar three electrode cell is presented in Fig. 5.19. In order to connect encapsulated electrochemical cells with the potentiostat, wires are soldered onto the Cu-lines of the PCB. If the encapsulation is done carefully, the packaging of cells immersed in phosphate buffer or in physiological solution holds for at least one month. The electrochemical characterization of the solid-state part is performed at this stage.

Fig. 5.19: Photo of the bonded and encapsulated electrochemical cell. The width is 0.8 mm and the length is 3mm.

5.2.5.2 *Catheter type packaging*

When sensors are used for biomedical applications, a catheter type packaging is recommended in order to render them biocompatible. As the chip dimensions are too small to solder connecting wires directly onto the bonding pads, they have first to be mounted onto printed circuit boards. In order to render a certain flexibility of the catheter tip, the support (see Fig. 5.20) should be shorter than the standard PCB.

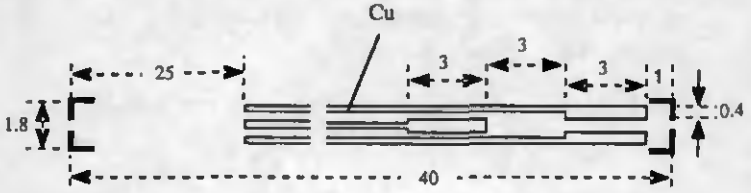

Fig. 5.20: Schema of the PCB used for catheter type packaging.

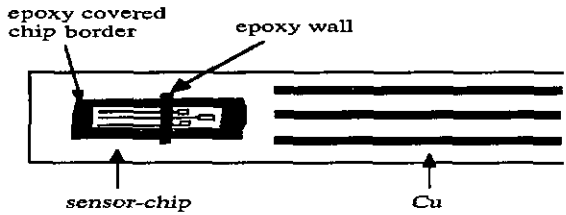

Fig. 5.17: Encapsulation of the chip sides and deposition of a thin wall of epoxy.

The thus encapsulated sensor is again left to prepolymerize during one hour at room temperature. The epoxy is then hardened during 15 minutes at 100 °C. This second prepolymerization prevents the readily flowing of epoxy during the polymerization step in the oven. It should be noted that epoxies become fluid first when they are heated (before polymerization starts).

4.) Bonding by Al wires (diameter: 45 µm), i.e., interconnecting the electrodes on the chip with the copper lines on the PCB (see Fig. 5.18).

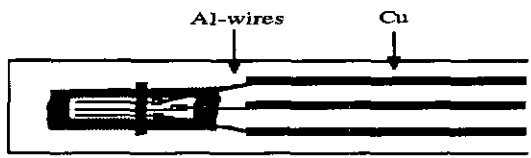

Fig. 5.18: Encapsulated chip after bonding.

5.) Encapsulation of the bonding wires with freshly prepared epoxy. The encapsulant is left to polymerize during two hours at room temperature before it is hardened during 15 min at 100 °C.

6.) Covering the remaining unencapsulated part of the PCB with epoxy (Cu-lines, both sides of the PCB).

The Cu-lines of this layout measures 0.2 mm, the spacing between them is 0.4 mm, the outer soldering pads are 3 mm x 0.4 mm and the inner one measures 3 mm x 0.6 mm. The encapsulation procedure is the same as described in section 5.2.5.1. The long connecting wires soldered onto the Cu-lines of the PCB and one part of the encapsulated support are then put into a silastic medical grade tube (inner diameter: 1.98 mm; outer diameter: 3.18 mm) so that only the chip containing part of the PCB protrudes.

A photograph of a catheter type packaged electrochemical microcell for in vivo applications is presented in Fig. 5.21. The photo shows in the background a diced silicon wafer with the three-electrode cells containing the two Pt-electrodes and the chloridized Ag/ AgCl reference electrode (dark). Further, the photo shows on the left, an in house made catheter-type encasulated cell and on the right, a chip packaged by an industrial manufacturer (PPG Hellige, Holland).

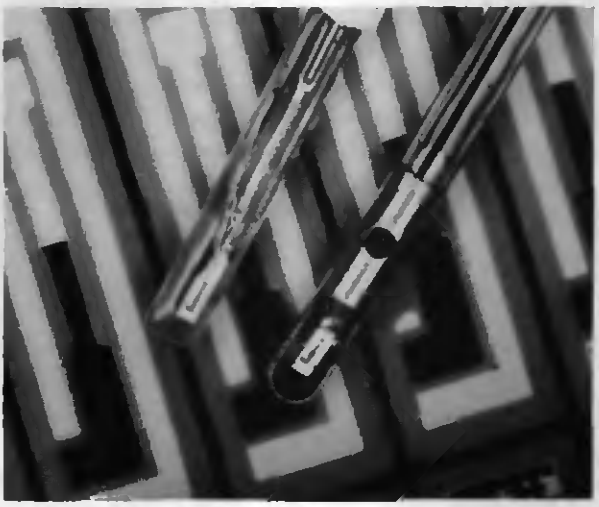

Fig. 5.21: Catheter type packaged electrochemical cell.

5.2.6 Electrachemical evaluation of thin film electrodes

Since all electrochemical measurements are extremely sensitive to the surface properties of electrodes, their control is important in order to avoid stability and reproducibility problems of the cell. A very convient method for the study of noble thin film metal electrodes is the cyclic voltammetry, as the voltammograms of bulk materials are well-known [19]. Such an electrochemical characterization is carried out in order to draw a parallel between some technological parameters of thin film processing and the electrode surface properties. This allows us first to establish the process of thin film electrochemical cell fabrication and second to achieve a reasonable reproducibility of all electrochemical parameters tested.

The stability and life-time of the reference electrode depend strongly on the adhesion of AgCl on thin film Ag [20], which is correlated with the transformation ratio of Ag to AgCl [21]. The best results are obtained with a conversion ratio of about 10-30 % of the silver layer. When the ratio is higher than 50 % a loss of adhesion occurs.

In Fig. 5.22 the voltammogram of bulk Pt in 0.5 M H_2SO_4/ N_2 is presented. In this figure peaks H_c correspond to the formation of adsorbed hydrogen whereas at peaks H_a the desorption of hydrogen occurs. Plateau O_a represents the formation of platinum oxide and in region O_c the reduction of the oxide layer occurs. Point 1 and 2 show the onset of bulk hydrogen respectively oxygen evolution.

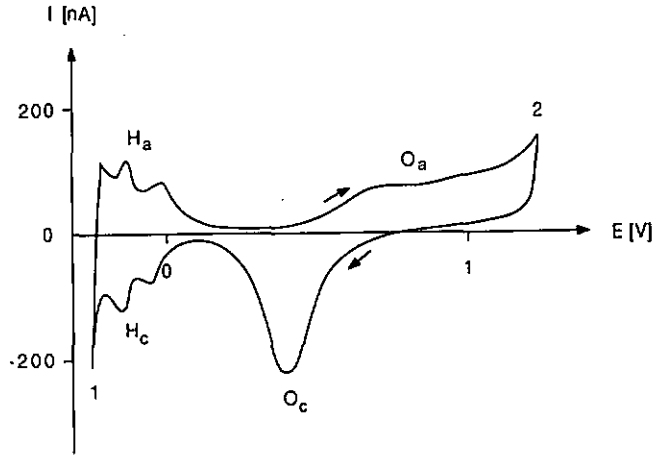

Fig. 5.22: Voltammogram of bulk Pt electrode in 0.5 M H_2SO_4/ N_2. Potentials vs. SCE.

The shape of the voltammograms, the position, the presence or absence of different peaks give indications on the condition of the electrode surface. The shape, number, and size of the peaks for adsorbed hydrogen depend for example on the crystal faces of exposed platinum, the electrode pretreatment and solution impurities. Many substances can adsorb onto a platinum electrode [22] and inhibit for example the hydrogen electrode reaction as e.g. after the formation of an adsorbed oxygen layer.
Fig. 5.23 shows two voltammograms of the thin film Pt electrode corresponding to (a) as prepared and (b) electrochemically pretreated electrode respectively. The latter has been subject to a sequence of potential steps where oxide films are formed and then reduced and desorption of impurities occurs: 1.3 V, 1 V, -0.2 V and 0.2 V vs. SCE (30 s per step) [23, 24]. The voltammogram (a) shows only minor differences from that of the bulk Pt electrode (Fig. 5.23) and consequently the thin film Pt surface can be considered clean enough for most of practical uses.

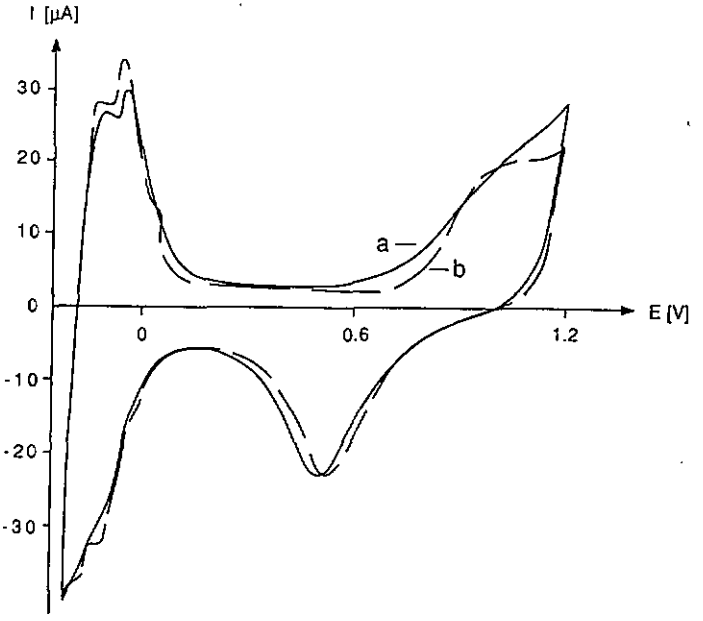

Fig. 5.23: Voltammograms (scan rate: 50 mV/s) of the thin-film Pt electrode corresponding to (a) as-prepared and (b) electrochemically pretreated electrodes (steps of 30 s at 1.3 V, 1 V, -0.2 V and 0.2 V). Solution: 0.5 M H_2SO_4/ N_2. Potentials vs. SCE.

The pretreated electrode shows a virtually identical voltammogram to that of the bulk Pt and thus, under stringent requirements on the surface cleanliness (e.g. study of the electrochemical reactions mechanism) the pretreatment should be carried out. It has to be mentionned that, usually, the bulk Pt electrodes are also electrochemically pretreated.

Stability and reproducibility problems of the electrochemical cell can also arise from the use of adhesion layers. Depending on the metal used for this intermediary layer and the fabrication procedure, when thermal treatments are used, an interdiffusion of atoms from this layer to the electrode surface can occur. Thus, the use of a Cr adhesion layer results in a contamination of the Pt surface: a comparison of the voltammogram of thin film Pt (Fig. 5.23), thin film Cr (fig. 5.25) and the contaminated Pt electrode (Fig. 5.24) shows, that the resulting curve is that of Cr superposed on that of clean Pt. This is especially evident in the H adsorption/ desorption region which corresponds to that of Pt, but in the oxidation/ reduction range of Pt, the Cr peaks are superposed.

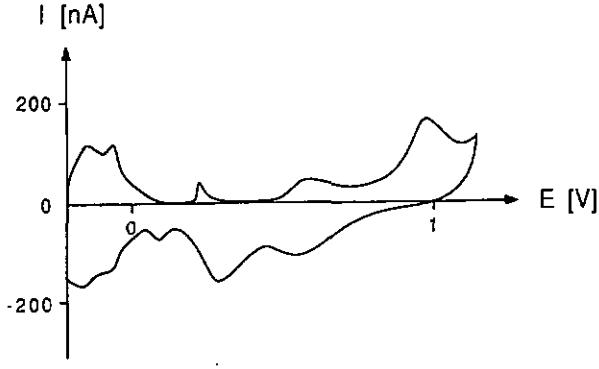

Fig. 5.24: Voltammogram of the Cr-contaminated thin-film Pt electrode in 0.5 M H_2SO_4/ N_2. Potentials vs. SCE.

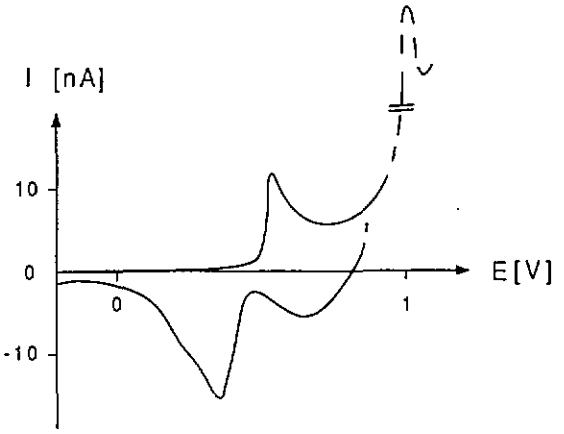

Fig. 5.25: Voltammogram of thin-film Cr electrode in 0.5 M H_2SO_4. Potentials vs. SCE.

The electrochemical reaction rate (current) is a function of the real surface area of the electrode and of its potential (19). The latter depends on the stability of the reference electrode potential and the former on the thin film deposition conditions (substrate temperature, rate of evaporation). The real surface area of Pt and the roughness factor (f_r = real area/ geometrical area) can be obtained from potential sweep techniques (25). The current-potential curve for a platinum-electrode in a H_2SO_4 solution shows peaks for the formation and oxidation of both adsorbed hydrogen and adsorbed oxygen. The hydrogen adsorption method is the best available method for determining real surface area. It is generally assumed that each platinum atom at the surface adsorbs one hydrogen atom and that monolayer coverage is obtained at about 0 V. The conversion of the adsorption charge to real area is complicated by the variation of surface site density with the crystallographic orientation of the surface and hence requires a knowledge of the crystal faces exposed. In addition there is the problem of defining which atoms constitute surface atoms and can be involved in chemisorption reactions. Because H is the smallest adsorbant, the charge-measurement in the hydrogen region represents the maximum surface area available. This "H-surface" may not be completely accessible to larger species.

The charge per real cm^2, associated with the adsorption of a monolayer of hydrogen on the low-index planes, is 208 μC for the (100) plane, 241 μC for the (111), and 147 or 295 μC for the (110), depending on the definition of coordination atoms as "surface atoms" (25). Generally an arbitrary value of 210 μC/ cm^2 is employed for

polycristalline surfaces. When this value is used, one real cm^2 is defined as 1.3×10^{15} surface platinum atoms.

The surface roughness for three different Pt-films has been tested using evaporation rates of 1 Å/s, 10 Å/s and 30 Å/s. By means of scanning electron microscopy no difference in the grain size and structure could be found. To confirm this result, voltammetry has been used to compare the roughness factors f_r of these different Pt-films (Fig. 5.26). The minimum current that follows the second cathodic H peak is used as end-point for the charge integration. Carrying out this calculations for each Pt-film, values of f_r between 2 and 3 are obtained. No correlation between f_r and the deposition conditions could be found which is in agreement with the SEM observations. Those values are very small compared to usual values found for polished Pt-wires and show that we have a smooth surface.

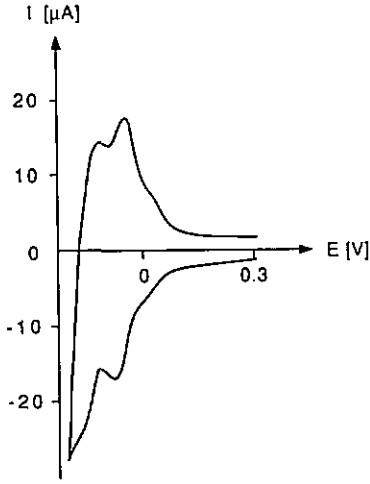

Fig. 5.26: H adsorption/ desorption region (scan rate: 25 mV/s) of thin-film Pt electrode for roughness factor determination; $f_r = 2.6$. Potentials vs. SCE.

This section has shown that thin-film technology is a suitable method for realizing planar electrochemical devices by reproducible mass fabrication. However, the control of thin-film surface properties has to be included in the fabrication procedure to ascertain that no Pt contamination occurs. The next section describes the use of this electrochemical microcell as part of an enzymatic glucose sensor.

5.3 Completion of the electrochemical cell with a membrane part

In this section the solid-state electrochemical sensor is combined with an immobilized glucose oxidase membrane to yield a glucose electrode. The enzymatic membrane is deposited on the whole sensing part of the three electrode system by chemically co-crosslinking glucose oxidase and bovine serum albumin using glutaraldehyde. The characterization of the enzyme electrodes is performed at this stage .
To render the glucose response less dependent on dissolved oxygen concentration, an additional polyurethane membrane is deposited by dip-coating and the complete device is then tested for the determination of glucose.

5.3.1 Enzymatic membrane

The enzyme is insolubilized and immobilized by chemical co-cross-linking GOD with an inert protein (bovine serum albumin) by a bifunctional reagent (glutardialdehyde) [26]. By crosslinking, the enzyme molecules are bound mutualy with a bifunctional reagent, whereas by co-cross-linking also inactive molecules (carrier proteins) are inclosed in the polymer network (see Fig. 5.27). For this intermolecular co-cross-linking, the two aldehyde groups react with the two amino groups of the enzyme and the carrier protein to form the immobilized enzyme.

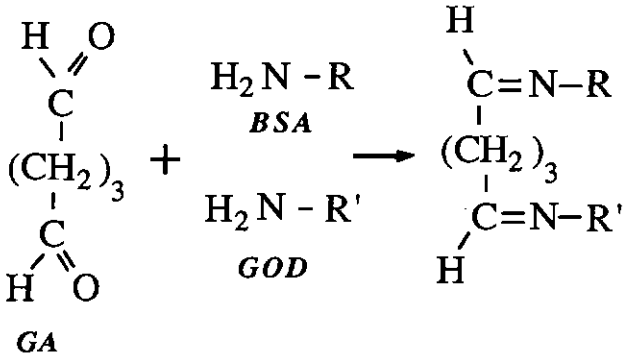

Fig. 5.27: Reaction scheme of chemical co-cross-linking GOD with albumin by glutaraldehyde.

The density, the swelling behaviour and the mechanical stability of the resulting membrane depend strongly on the relative ratios of involved components. A typical procedure for application of the membrane is as follows. Glucose oxidase (50 mg/ml) and bovine serum albumin (80 mg/ml) solutions are mixed together and then 0.1 ml of 2.5% glutaraldehyde are added. After homogenization, 5-10 µl of this mixture are deposited on the transducer surface and left to polymerize for three hours at room temperature. The resulting enzymatic layer has a good adhesion and also a good swelling behaviour. The thickness of thus-prepared enzymatic membranes has been measured under microscope and was about 30 µm with a rather good reproducibility.
All chemicals are obtained from Fluka. Glucose oxidase (from Aspergillus niger, 250 U/mg) as well as bovine serum albumin (fraction V) are obtained from Calbiochem. All reagents employed are of analytical grade. The sensor characteristics are tested in Krebs physiological solution containing 115 mM NaCl, 2.5 mM KCl, 5 mM K_2HPO_4 and 0.5 mM KH_2PO_4 (pH 7.4). No prehydration treatment is carried out before measurements. The temperature of the sample cell (25 ml) is set to 37 °C. When not in use the devices are stored at 4 °C in 10 mM phosphate buffer.
All electrochemical measurements are performed in the three electrode mode [27] using an IBM Voltammetric Analyzer or an in-house potentiostat. For glucose testing the applied working potential for H_2O_2 measurements is 700 mV vs. Ag / AgCl reference electrode. The configuration of the measurement set-up is shown in Fig. 5.28.

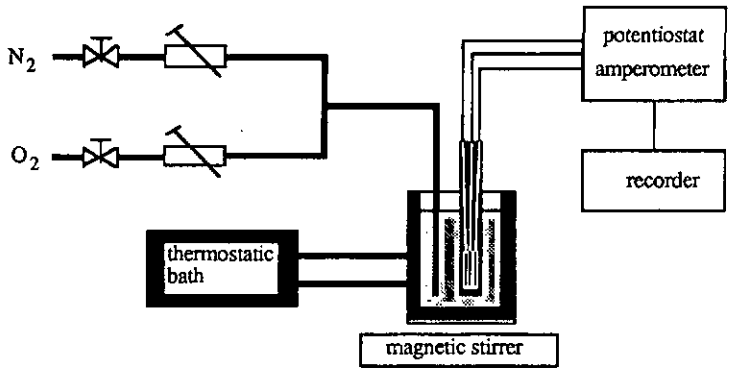

Fig. 5.28: Configuration of the measurement set-up.

Following stabilization of the sensor in the test solution (about 5 minutes), aliquots of a stock solution of 1 M glucose are added and the sensor current output recorded. The background current is always about 1 nA and remains stable during the use. The as-prepared electrodes exhibit initially lower glucose sensitivity and it takes about one day to obtain a stabilized response. A possible explanation for this initial response evolution is the hydration of the enzymatic layer. The stabilized response is linear up to 8 mM glucose and the corresponding sensitivity is 25 ± 3 nA/mM (sample size n = 30). The response time $t_{90\%}$ is about 30 s. After deposition of the enzyme membrane, sensor sensitivity variations are of ± 10%, with 90 % of the devices being within specifications.

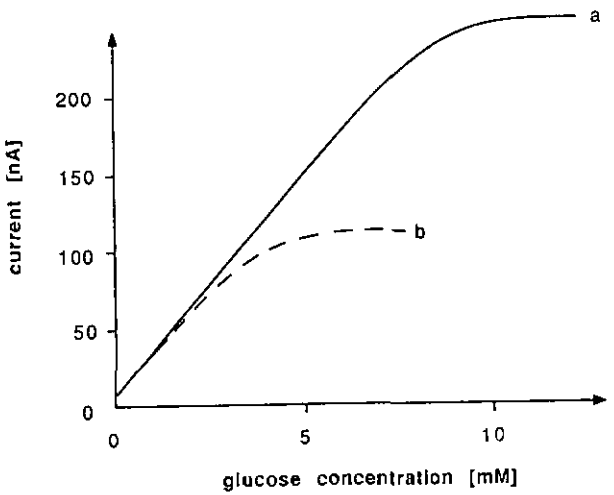

Fig. 5.29: Effect of dissolved oxygen concentration on the glucose calibration curve in a Krebs solution (pH 7.5) saturated with (a) air and (b) 5 % O_2.

The operational stability of the sensor is defined as the time period during which the sensitivity is constant, thus allowing the use of a single-point calibration method. It has been found to be two weeks for a sampling frequency of two calibration curves a day. Obviously, the stability of the sensor depends on the manner in which it is measured. When the sensor is tested daily for several hours at high glucose concentrations, its

operational stability decreases to a few days. This seems to suggest that, in our case, the sensor lifetime and stability are more critically limited by the glucose oxidase deactivation by H_2O_2 [28] than by its leakage from the membrane. This is also confirmed by the storage stability, which is about one month in 10 mM phosphate buffer at 4 °C. The corresponding loss of sensitivity has been estimated to be 5 % per week.

Glucose response tests have also been carried out using very small (25 µl) sample volumes deposited as a drop on the sensor surface. The only observed difference is the response decrease after about one minute due to the depletion of reactants at the interface.

The dependence of the sensor response on dissolved oxygen concentration should be minimized if the sensor is to be usable under variable O_2 tensions. As is clearly shown in Fig. 5.29, this is not the case with this device, for which the response changed drastically on going from air to 5% O_2 saturated solutions.

5.3.2 Polyurethane membrane

Since the glucose sensor should be usable under variable O_2 pressures (biological fluids) the device dependency on the cosubstrate (O_2 concentration) has to be minimized, e.g. by coating the sensor with a polyurethane membrane. In the presence of this hydrophobic membrane, the system becomes diffusion limited, with several concomitant effects on its response in addition to that of decreased O_2 influence. The extension of the linear response range up to 40 mM glucose is thus accompanied by a loss in sensitivity and also longer response times.

The deposition of reproducible polyurethane membranes is one of the most critical part of the sensor fabrication. This hydrophobic glucose diffusion-limiting membrane is formed by dipping the sensor in a polyurethane solution. This solution consists of 4-6 % (w/v) polyurethane obtained from Japan Erastran Inc., dissolved in 1/9 (v/v) mixture of dimethylformamide (DMF) and tetrahydrofuran (THF). The solutions are stored at 4 °C and not used for more than one week because polyurethanes are liable to have hydrolysis reactions and THF easily evaporates. Before their use they are stirred at room temperature for about 15 minutes.

The dip-coating, generally, is done by hand and the excess of polyurethane solution at the end of the sensor is removed by skimming over a filter paper. The solvents are then allowed to evaporate during one hour in air. The sensors are stored in a 10 mM phosphate buffer at 4 °C.

A polymer concentration of 6 % is, in general, the upper limit for membrane fabricaöon by dip-coating. At higher concentrations impermeable, dense membranes are formed. The maximum solubility of polyurethane at room temperature is about 16 % in THF and about 10 % in DMF. Further, it should be pointed out that the support on which the polyurethane is deposited has an influence on the membrane formed, e.g. the polyurethane membranes deposited onto hydrophobic glass are different in size and form of the pores compared to those deposited onto hydrophilic enzyme membranes. Another consideration is the inter-mixing of water with the solvents. Thereby, it should be noted that membranes formed with water containing solutions become inhomogeneous, e.g. after mixing 6 % water to THF the solution separates in two phases. When the percentage of water is lower than 1 %, however, there is no visible influence.

The complete sensor consists of the planar electrochemical microcell, the enzyme layer and the polyurethane membrane. A cross-section of the complete device is shown in Fig. 5.30.

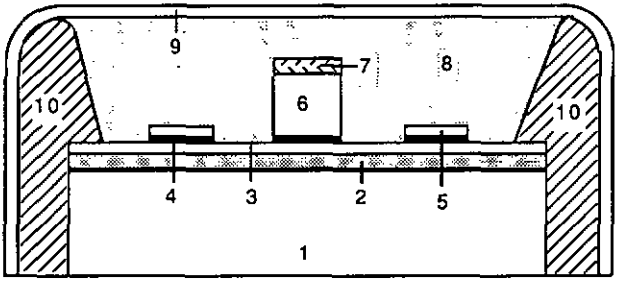

Fig. 5.30: Schematic diagram of the glucose sensor. (1) Silicon substrate, (2) SiO_2, (3) Al_2O_3, (4) Ti, (5) Pt, (6) Ag, (7) AgCl, (8) enzyme membrane, (9) polyurethane membrane, (10) epoxy encapsulant.

After the evaporation of the solvents, the resulting polyurethane membrane is transparent and dense. Since this dense polyurethane is hydrophobic, only dissolved oxygen can pass. Hence, to allow the diffusion of glucose, some small pores are necessary. A typical response, shown in Fig. 5.31, is linear up to 40 mM glucose with a sensitivity of 1-2.5 nA/ mM in a stirred Krebs solution saturated with different percentages of oxygen down to 2 %. If there are too many pores in the polyurethane membrane the glucose transport is not enough limited and, thus, an oxygen dependence of the sensor response is still, but to a lesser extent, observed.

A SEM (scanning electron microscopy) study has shown that the polyurethane membranes have an average thickness of about 5 µm with a good reproducibility. The thickness of these membranes depend on the concentration (viscosity) of the polyurethane solution. Since the diffusion of glucose requires also the diffusion of water (both are hydrophilic), it is important that the polyurethane films are not too thick due to their hydrophobic behavior (capillary forces). Otherwise, if the pores are too long, the diffusion of glucose would be lacking except external pressure is applied.

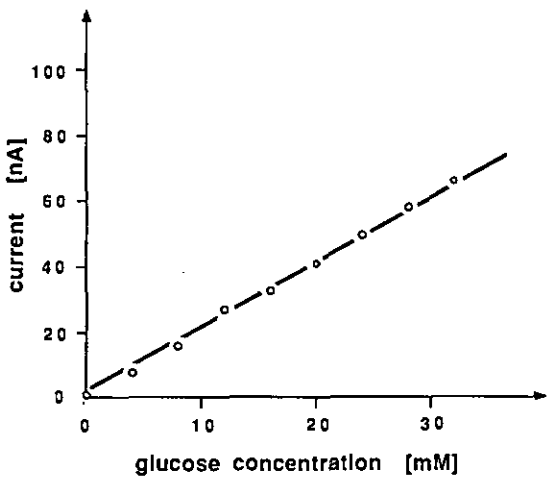

Fig. 5.32: Glucose calibration curve of the sensor covered by an outer polyurethane membrane in a Krebs solution saturated with 5 % O_2. The sensitivity is 2.02 ± 0.15 nA/mM glucose. The Correlation coefficient is r = 0.999 and the standard deviation of the sensitivity (using two consecutive points) is s.d. = 0.396 nA/mM.

This way of depositing the polyurethane membrane is rather irreproducible, so that, most of the time, they are completely dense or possess too many pores. Only about 20% of such fabricated sensors have a sensitivity of 1-2.5 nA/mM after the first dip-coating. Stripping the polyurethane membranes presenting an unacceptably low or high upper limit of the linearity and repeating the dip coating procedure allowed finally a yield of 70 % of sensors being within specifications. The sensitivity of 2.02 ± 0.15 nA/mM (n=20) remains constant during the operational stability of the sensor, which has been more than one week for extensively tested devices (two calibration curves a day and response drift measurements).

The response time, $t_{90\%}$, is 180 s at low (less than 15 mM) and 400 s at high glucose concentrations. Usually current values at two minutes are used for calibration curves. A typical glucose response curve to a stepwise addition of a 1 M glucose stock solution and the response drift are presented in Fig. 5.32. At 20 mM glucose the response drift is about 5% per hour. This drift depends strongly on the membrane characteristics and on the glucose concentration. The response time as well as the sensor current output are independent of external stirring.

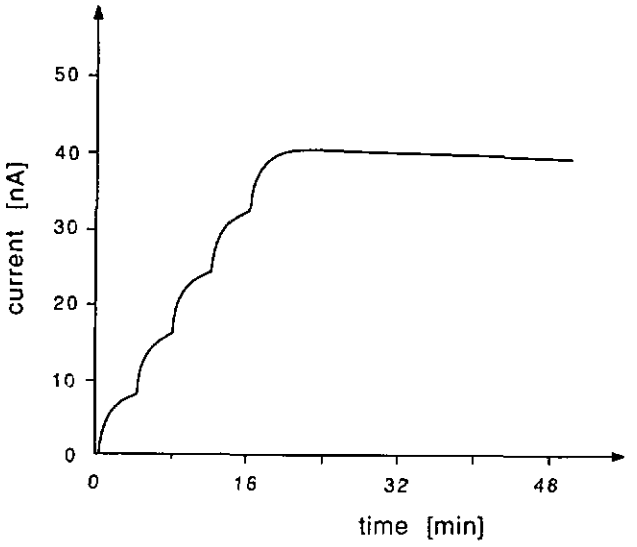

Fig. 5.33: Typical glucose response curve. Stepwise addition of glucose up to 20 mM and the response drift in a Krebs solution saturated with 5% O_2.

The temperature coefficient depends on the glucose concentration and is at 20 mM glucose about 5% / °C over the temperature range of 30-41 °C. Another important characteristic is the hysteresis of the sensor response. It is almost always exhibited by membrane covered devices, especially when they are used at very high and low concentrations alternately. Thus a certain wash-out time is necessary in order to obtain reproducible output readings. This time depends on the diffusional restrictions imposed by the membranes and particularly by the polyurethane one. It is rather short (a few minutes) for the electrode covered with the enzyme membrane, while it

increases in the presence of the polyurethane membrane. Thus, when the electrodes are used at 10 min intervals, the observed hysteresis amounts to 10%. That is, even though the sensitivity remains constant, the current increase causes an error of 10% in the glucose concentration.

A further factor is the sensor mechanical stability. The solid-state part, in our case, being quite rugged, the final mechanical resistance will be that of the membrane part. In the presence of the polyurethane membrane the electrode's mechanical stability, which has been evaluated by mechanically tearing off the membranes, is very good.

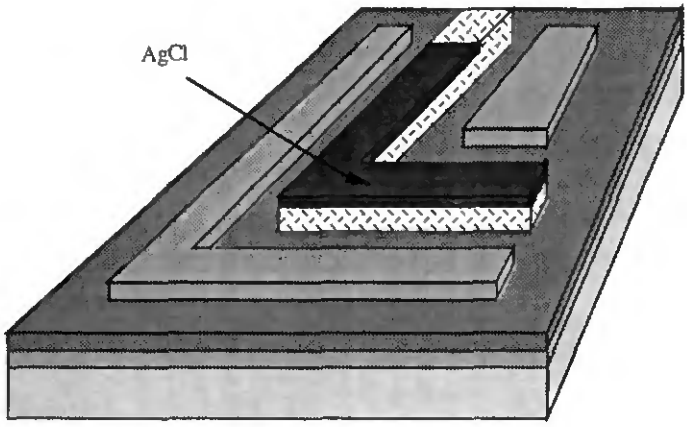

Fig. 5.33: Electrode configuration of the electrochemical cell.

The glucose oxidase membranes are patterned using the lift-off technique described in section 5.2.2. A typical procedure is as follows: A positive photoresist (Shipley Microposit S 1650) is spin-coated onto the wafer surface at 6000 rpm (4 µm). The coating thickness of the resist as a function of spin speed is shown in Fig. 5.34.

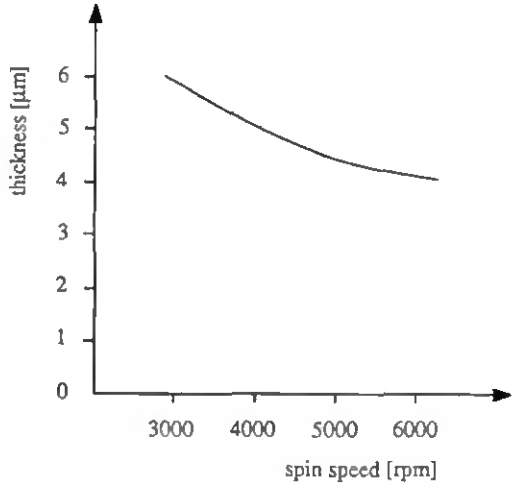

Fig. 5.34: Resist thickness vs. spin speed of Shipley Microposit S 1650.

5.4 On wafer deposited enzyme membranes

While the fabrication of electrochemical transducers by IC technology is well developed, their completion with an immobilized biocatalyst is still done manually. It should be pointed out that the reproducibility of the final sensor depends on the reproducibility of the solid-state part and that of the enzymatic membrane. The use of IC technology results in batch to batch reproducible devices. The enzymatic membranes, on the other hand, are usually deposited on each individual device using a μ-pipette. This process is obviously difficult to control. Another technique is the membrane fabrication on wafer level. The aim of this technique is the improvement of the reproducibility due to a better control of the membrane thickness and the precision of the membrane patterning.
Recently, several papers concerning on-wafer deposited enzyme membranes on ISFET's [5] and planar amperometric sensors [3] have been published. Water-soluble photo-crosslinkable polymers have been employed allowing thus patterning of enzymatic membranes (typical thickness: 0.5-1 μm) by usual photolithographic technique. Kuriyama et. al. [29, 30] reported for the first time a lift-off method for patterning enzyme membranes on ISFET's and planar amperometric sensors.
The study of patterning enzymatic membranes on wafer level by the IC compatible lift-off technique is described in this section. Special attention in the characterization of as-prepared membranes is given to their fabrication procedure in order to improve the membrane uniformity and response reproducibility. Hence, the current response of glucose electrodes from the same wafer as well as of those of different wafers are compared.

5.4.1 Standard procedure

The enzymatic membranes are fabricated onto the planar electrochemical cells detailed in section 5.2. Therefore, the standard mask layout SGL200 has been applied and the third mask (generally used for the partial chloridation of the Ag electrode) has been used for membrane patterning over the sensing area of all three electrodes.
The arrangement of the electrochemical cell with the two outer Pt electrodes and the inner Ag/ AgCl reference electrode is illustrated in Fig. 5.33. The picture shows clearly the difference in hight (thickness) between the Pt and the Ag/AgCl electrodes.

The exposure and development of the resist results in windows over the sensing region of all three electrodes. The enzyme containing solution is then prepared as follows. Glucose oxidase (70 mg/ml) and bovine serum albumin (80 mg/ml) are dissolved in a 10 mM phosphate buffer solution, mixed together, and then 0.1 ml of 2.5 % glutaraldehyde are added. 100 µl of this well-homogenized enzyme solution are then deposited, spread all over the wafer by a brush and spun at 1400 rpm. After being dried for 60 minutes in air, the enzyme membrane on top of the resist is lifted off in acetone assisted by ultrasonic vibration (1.5 s). After dicing the wafer, the individual sensor chips are mounted on a printed circuit board, bonded and encapsulated with an araldite-type epoxy. It should be pointed out that, during the packaging, no thermal treatment can be applied, and thus, the polymerization of the epoxy at room temperature takes about three days. Fig.5.35 shows an individual sensor chip with on wafer deposited membrane. The membrane measures 1.4 mm in length and 600 µm in width.

Fig. 5.35: Individual sensor chip with on-wafer deposited membrane.

Results and discussion

The aim of on-wafer membrane fabrication is to improve their reproducibility which depends on the uniformity of the membrane thickness all over the wafer and the precision of the membrane patterning. Important for a well defined membrane is the lift-off process. The parameters which influence this process are:

1.) substrate:
- insulating layers (glass, Al_2O_3, Si_3N_4)
- electrode thickness

2.) photoresist:
- thickness
- steepness and shape of the resist border (influenced by prebake, exposure, chlorobenzene soak and development)

3.) membrane:
- composition
- spinner speed (thickness)
- polymerization time

4.) lift-off in acetone (time of ultrasonic vibration)

Essential for a successful membrane patterning by the lift-off method is a sufficient adhesion of the membranes onto the passivating layer. It has been found that the best membrane adhesion results on Al_2O_3 which is due to its microscopic rough surface. Another critical factor related to the solid-state part is the electrode thickness. This problem concerns mainly the reference electrode which is much thicker than the Pt electrodes so that the membrane may easily crack at the electrode-substrate interface. Fig. 5.36 shows on the left the membrane coated passivating layer and on the right the membrane coated reference electrode.

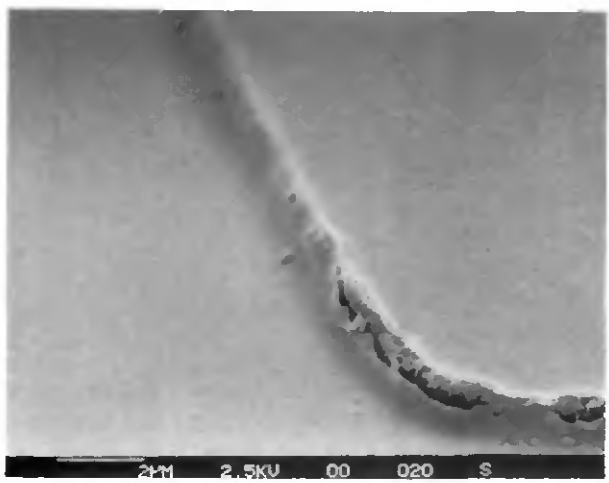

Fig.5.36: Membrane cracking at the side of the 1 µm thick Ag electrode.

The pboto illustrates the problem of membrane cracking due to mechanical stress and indicates therewith that the chosen electrode thickness of 1 μm is too high. Fig. 5.37, on the other hand, shows a membrane coated Pt electrode and thus, illustrates the smooth fit of the membrane at the layer interface between the electrode and the passivating layer. The photo shows in the background the enzymatic membrane and in the front the Pt electrode (on the right) and on the left the Al_2O_3 passivating layer.

Fig. 5.37: Membrane over the passivating layer - Pt electrode interface.

Decisive parameters are further the thickness of the photoresist layer and the resist profile which has to be overcut. Due to mechanical stresses occuring in the membrane during polymerization, thick and sharp patterned photoresist layers result in a membrane separation between the part on top of the resist and the part on the substrate. Fig. 5.38 illustrates this membrane separatioo. The photo shows on the right the membrane which has to stay and on the left the membrane coated photoresist.

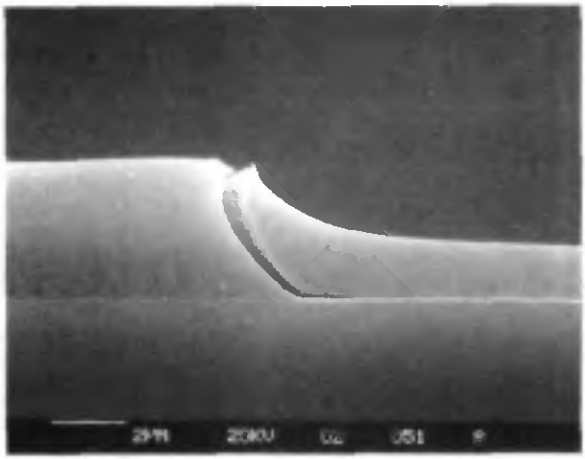

Fig. 5.38: Photo of a enzymatic membrane before lift-off, showing the membrane separation due to mechanical stresses during polymerization.

A disadvantage of the application of thick photoresists are the thick membrane sides which occure during the spinning procedure. Fig. 5.39 illustrates this behaviour. The membrane side shows a vertex of about 3.5 µm and a width of about 4 µm.

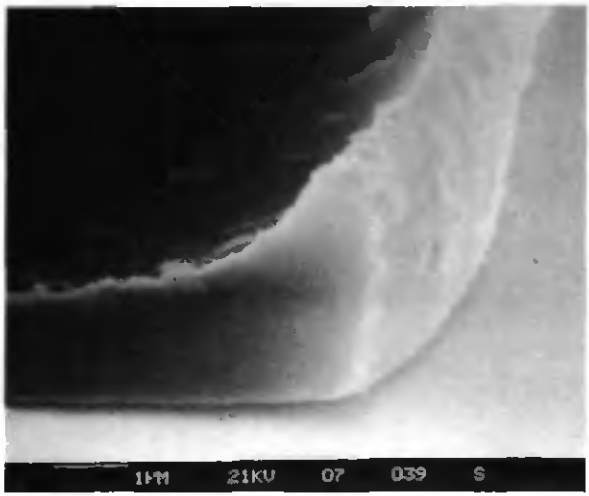

Fig. 5.39: Thick membrane sides resulting during spinning procedure.

The thickness of the photoresist, the spinning behavior (viscosity) of the enzymatic layer as well as the polymerization time and the lift-off procedure (time of ultrasonic vibration) have been adjusted in order to obtain well defined membranes. The application of ultrasonic vibration is a very critical procedure. In order to prevent mechanical destruction of the enzymatic membranes only a short-time ultrasonic vibration has to be used. This time can be minimized by optimization of the resist thickness and the resist profile. It has been found that times of about 1-2 s are already sufficient.

The membrane thickness and its reproducibility have been studied by SEM. We fabricated four wafers and tested five structures of each one. The membranes show a good uniformity and have a thickness of 9000 ±1000 Å for all four wafers. Moreover the membrane thickness over the passivating layer and over the electrode areas of Pt respectively Ag is the same.

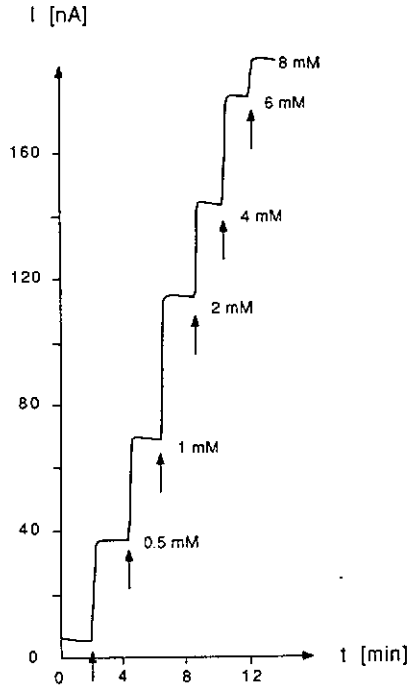

Fig.5.40: Typical response to a stepwise addition of glucose.

A typical smoothed glucose response curve to a stepwise addition of a 1 M glucose stock solution is presented in Fig. 5.40. The measurements are carried out in a stirred, air saturated Krebs solution at 37 °C. After stabilization of the background current, the glucose solution is added and the sensor current recorded. As can be seen, the sensor responds immediately and reaches the steady-state current within 10 s.
Fig. 5.41 shows the calibration curves of 5 different sensors from the same wafer. The sensors respond up to about 6 mM glucose and the output is linear up to 1.5 mM glucose. It can be seen that thus fabricated sensors show a rather good reproducibility of the sensor response. The sensor lifetime is about one week with one calibration curve a day.

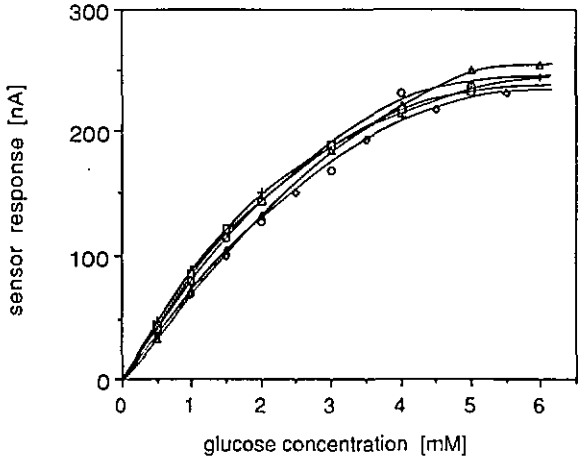

Fig. 5.41: Glucose calibration curves of five different sensors from the same wafer tested in a stirred, air saturated Krebs solution.

The response of such devices has further been compared with that of sensors with individually deposited membranes having the same membrane thickness (~ 1 µm) as on wafer deposited ones. No differences between individually and on wafer deposited membranes could be found which shows that the short-time treatment in acetone during the lift-off procedure does not affect the membrane behaviour.

5.4.2 Amelioration of the fabrication procedure

There are two possibilities to overcome the problem of membrane cracking at the electrode-substrate interface. The first one consists in reducing the thickness of the reference electrode and the second one consists in a modification of the membrane layout in order to cover only the working electrode with the enzymatic membrane. Applying the first possibility, we found that membrane cracking can be avoided with thicknesses of the reference electrodes between 4000 and 6000 Å. Unfortunately, those reference electrodes show rather poor stability. Thus, a new mask layout has been designed (see Fig. 5.42).

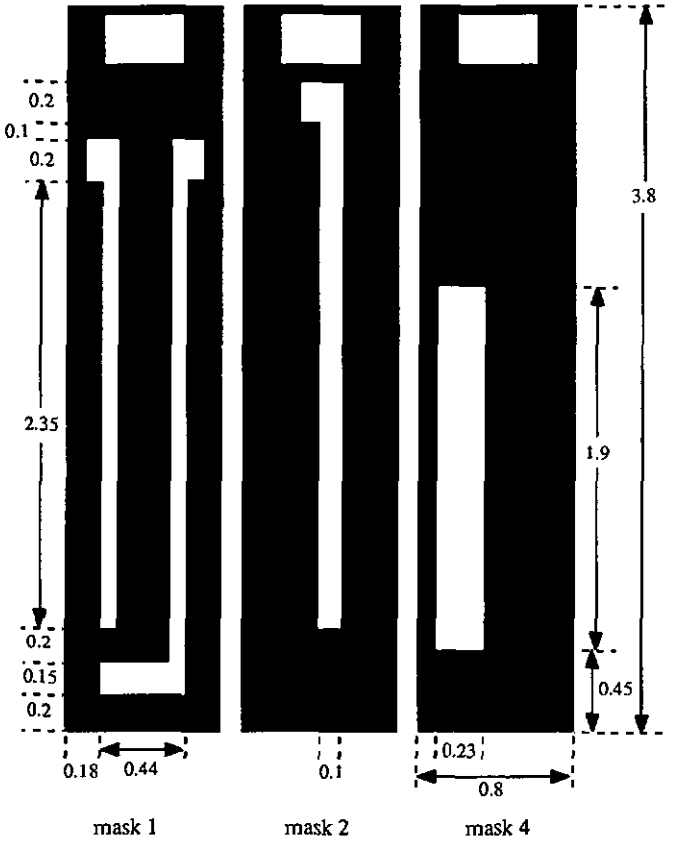

Fig. 5.42: Mask layout SGIMT400 (dimensions in mm).

The first mask defines the Pt electrodes, the second the Ag electrode and the fourth the enzymatic membrane. The third mask is used for partial chemical chloridation of the silver electrodes. Since its layout is quite simple and, moreover, its positioning relative to the other masks is not critical, its design is not presented in figure 5.42. It consists of a rectangular window of 0.6 mm x 2.25 mm over the sensing region of all three electrodes. Further, its upper side (against the bonding pads) coincides with the appropriate membrane side.

In order to prevent problems with imperfect membrane sides, a minimum extent of membrane overlapping beyond the working electrode is required. This is done by placing the reference electrode unsymmetrically between the Pt electrodes, thus lefting a large enough spacing between the working and reference electrodes for membrane patterning. The working electrode area exposed to the solution is 1.8 mm x 0.07 mm (0.126 mm^2) and the area of the counter electrode is 0.206 mm^2. Thus, the ratio r_A is about 0.6. The bonding pads of the Pt electrodes are 0.15 mm x 0.2 mm and that of the Ag electrode measures 0.2 mm x 0.2 mm.

In order to reduce the thick membrane sides, the resist thickness and the polymer concentration of the enzyme solution have been optimized. Optimal parameters has been found using the photoresist Microposit S 1400-27, spinning it at 4500 rpm (1.2 µm) and applying an enzyme solution consisting of 22 mg/ml GOD (224 U/mg), 120 mg/ml BSA and 200 µl/ml 2.5% GA. The components are mixed in a 10 mM phosphate buffer and the spinning of the homogenized enzyme solution is performed at 1400 rpm. The ideal polymerization time before the lift-off procedure is 45 min.

For some applications the response of those membranes is too low. One possibility to solve this problem is the deposition of two membranes. In this case, spreading of the enzyme solution by using a brush is not useable, otherwise the membranes are mechanically destroyed. An alternative procedure is as follows: A large amount of enzyme mixture (one wafer requires about 7 ml) is deposited onto the wafer surface and then spin-coated at 1400 rpm. Whereas membranes fabricated by spreading the enzyme solution by the use of a brush often include air bubbles or dust particles the alternative method (spin-coating) produces very clean membranes. Otherwise, no differences concerning membrane thickness or uniformity could be found.

Furthermore, a fabrication procedure for depositing double membranes has been evaluated. The Microposit S 1400-27 photoresist is applied at a spin speed of 3000 rpm (1.5 µm). The composition of the enzyme solution is 22 mg/ml GOD (224 U/mg), 60 mg/ml BSA and 125 µl/ml 2.5% GA. The components are mixed in a 10 mM phosphate buffer and then well homogenized. After spinning the enzyme mixture at 1400 rpm, the membranes are left to polymerize during 20 min before the second

membrane spinning is performed. The ideal polymerization time after the second membrane coating is 35 min.

In order to improve the membrane adhesion, a pretreatment of the wafer surface just prior to the deposition of the enzymatic solution is carried out. Therefore, 7 ml of the 10 mM phosphate buffer solution is deposited and spin-coated at 2400 rpm. A photo of an electrochemical cell with a thus prepared membrane is shown in Fig. 5.43. The chip measures 3.8 mm in length and 0.8 mm in width.

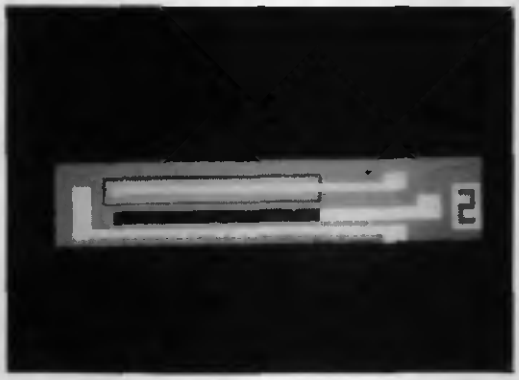

Fig. 5.43: Photo of a on wafer deposited membrane covering only the working electrode.

A SEM study has shown that the thicknesses of simple membranes measure 7000±1000 Å. The double membranes, on the other hand, have an average thickness of about 1.3 µm. The glucose response of 12 sensors from three different wafers have been measured. Their average response is shown in Fig. 5.44. The reproducibility of the sensitivity is about ± 15%.

In Fig. 5.45 typical responses of devices with (a) a simple membrane, (b) a double enzymatic membrane and, additionally, (c) of a membrane sandwich consisting of an enzymatic membrane and a BSA membrane (using 80 mg/ml BSA) are compared.

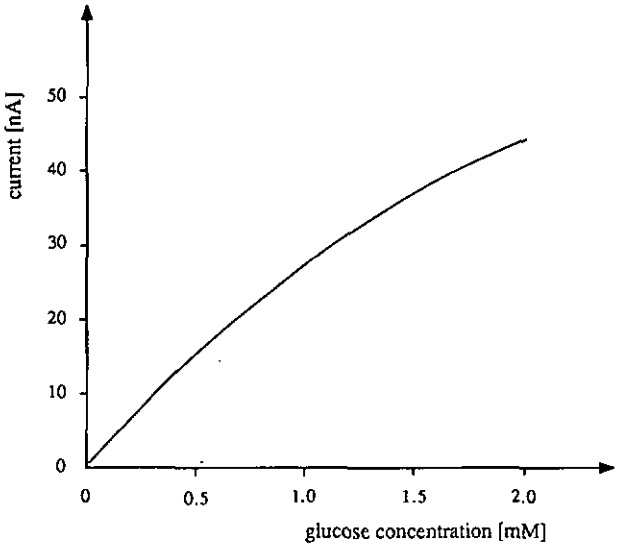

Fig. 5.44: Average glucose response of 12 devices from three different wafers with simple enzyme membranes.

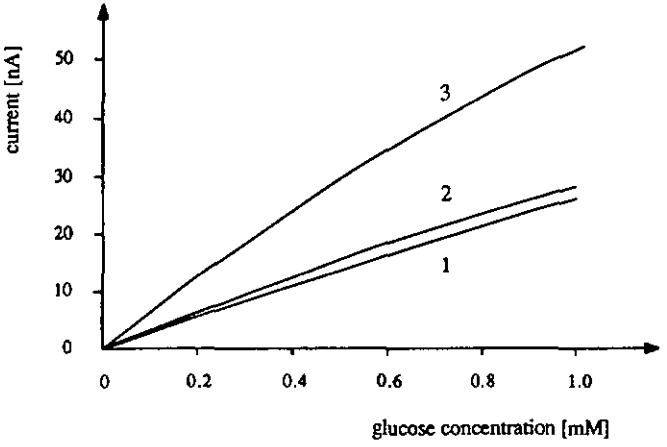

Fig. 5.45: Sensor responses of different on wafer deposited membranes.
1: one enzymatic membrane
2: one enzymatic and one BSA membrane
3: double enzymatic membrane

5.5 Biomedical applications

In order to complete the sensor characterization, a short description of its on vivo testing is also presented. Since the sensor's in vitro characteristics fulfill several of the physiological requirements, e.g. linear range, response time, low influence of O_2 on the sensor response and several days lifetime, it has been possible to progress toward their in vivo evaluation. Although implanting the sensor in a vessel would be optimal, from the practical point of view, the subcutaneous tissue is probably a more favorable site as it is considerably less detrimental for the sensor. The tissue implantation site was validated rather recently [31, 32], although some controversy concerning the exact relationship between blood and tissue glycaemia still remains.
The sensors are implanted subcutaneously in anesthetized normal rats (Fig. 5.23). Two silastic catheters are inserted via the right jugular vein to reach, respectively, the right auricle (blood samplings), or the vena cava inferior (glucose or insulin infusions). During experiments, the rats are ventilated (CO_2/ O_2 mixture) and warmed using a heating blanket.

Fig. 5.23: Implantation of the planar glucose microsensor in subcutaneous tissue of a rat.

Following implantation and after one hour of resting period to reach a more or less stable value of the sensor current, glycaemia is changed using one of the following methods:

1.) glucose or insulin infusions to obtain hyper- or hypoglycaemic plateau levels;

2.) intraperitoneal glucose loads (1 g / kg body weight);

3.) IVGTT (intravenous glucose tolerance test)

Blood is sampled at 5 min intervals and periodically the rat's blood volume is compensated for by blood from a donor rat. As an example, Fig. 5.24 shows the sensor response, represented by closed circles, and corresponding plasma glucose levels (measured using a Beckman glucose analyzer), represented by open circles, following an intraperitoneal glucose load. As it can be seen, the sensor mirrors correctly the plasma glucose levels.

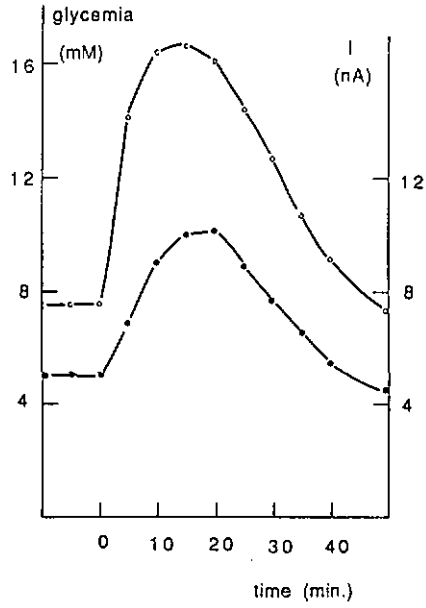

Fig. 5.24: Sensor output (closed circles) and plasma glucose levels (open circles) following an intraperitoneal glucose load.

Results of a large series (more than 50 sensors tested) of such short-term in vivo experiments has been quite encouraging. The behavior of the sensor during longer implantation times, as well as the lifetime of the chronically implanted sensor are now under investigation.

5.6 Conclusions

Thin film technology is a suitable method to realize planar electrochemical devices by reproducible mass fabrication. However, the control of thin film surface properties has to be included in the fabrication procedure to ascertain that no Pt contamination occurs. Periodical checks of the thin film Pt electrodes by cyclic voltammetry and even more important that of the reference electrode potential are nevertheless necessary during a long time use of these planar electrochemical cells. When care is taken during the fabrication procedure they exhibit good electrochemical behaviour, reproducibility and stability over several weeks. Upon completion by an immobilized glucose oxidase and a polyurethane membrane the glucose amperometric electrodes have a linear response range up to 40 mM glucose, short response time $t_{90} \approx 1$ min. and a life-time of several days.

In order to obtain precisely patterned membranes with good uniformity of membrane thickness, miniaturized glucose enzyme electrodes have been fabricated by means of the IC compatible lift-off technique. The membrane adhesion on Al_2O_3 is sufficient. The thickness and uniformity of such prepared membranes are very reproducible all over the wafer and from wafer to wafer. The technique of patterning on wafer deposited membranes can only be used for the fabrication of thin membranes (0.5 - 1.5 μm) which are not suitable for in-vivo testing. On the other hand , they can be used for flow injection analysis with predilution of the sample.

5.7 References

[1] M. Shichiri, Glycaemic control in pancreatectomized dogs with a wearable artificial endocrine pancreas, Diabetologia 24 (1983) 179-184.

[2] W. Sansen, M. Lambrechts and J. Suls, Fabrication of voltammetric sensors with planar techniques, Transducers'85, International Conference on Solid-State Sensors and Actuators, Philadelphia, USA, Digest of Technical Papers, 1985, pp. 344-347.

[3] I. Takatsu and T. Moriizumi, Solid state biosensors using thin-film electrodes, Sensors and Actuators 11 (1987) 309-317.

[4] M. Koudelka, S. Gernet and N.F. de Rooij, Planar amperometric enzyme-based glucose microelectrode, Sensors and Actuators, 18 (1989) 157.

[5] Y. Hanazato, M. Nakako, M. Maeda and S. Shiono, Proc. of the 2nd int. meeting on chemical sensors, Bordeaux, France, 1986, p. 576.

[6] S. Gernet, M. Koudelka and N.F. de Rooij, A planar glucose enzyme electrode, Sensors and Actuators, 17 (1989) 537-540.

[7] S. Gernet, M. Koudelka and N.F. de Rooij, Fabrication and characterization of a planar electrochemical cell and its application as a glucose sensor, Sensors and Actuators, 18 (1989) 59-70.

[8] W.M. Moreau, Semiconductor lithography: principles, practices, and materials, Plenum Press, New York, 1988.

[9] R.F. Bunshah, Deposition technologies for films and coatings, Noyes Publications, New Jersey, U.S.A., 1982.

[10] R.C. Weast, Handbook of chemistry and physics, CRC Press, Cleveland, Ohio, U.S.A., 1977, D-173.

[11] L.I. Maissel and R. Glang, Handbook of thin film technology, McGraw-Hill, New York, U.S.A., 1970, 6-32.

[12] W. Kern, R.S. Rosler, Advances in deposition processes, J. Vac. Sci. Technol., 14 (1977).

[13] R.M. Cohen, R.J. Huber, J. Janata, R.N. Ure and S.D. Moss, A study of insulator materials used in ISFET gates, Thin Solid Films, 53 (1978) 169-173.

[14] S.D. Moss, J. Janata and C.C. Johnson, Potassium ion sensitive field effect transistor, Anal. Chem. 47 (1975) 2238.

[15] S.J. Schepel, N.F. de Rooij, G. Koning, B. Oeseburg and G. Zijlstra, In vivo experiments with a pH-ISFET electrode, Med. Biol. Eng. Comput. 22 (1984) 6.

[16] C. Arnoux, Fabrication et étude des phénomènes de dérive de capteurs du type pH-ISFET à membrane en oxyde d'aluminium, dissertation at the Institute de Microtechnique de l'Université de Neuchâtel (CH), 1988.

[17] M. Hatzakis, B.J. Canavello and J.M. Shaw, Single-step optical lift-off process, IBM J. Res. Develop. 24 (1980) 452-460.

[18] W. Tomassi and W. Jodzewicz, O tatwym sposobie wytwarzania niektórych elektrod drugiego rodzaju i o zachowaniu sie tych elektrod w rodowisku nietypowym, Prz. Chemiczny 11 (1955), 129-132.

[19] A.J. Bard and L.R. Faulkner, Electrochemical Methods: Fundamentals and applications, Academic Press, New York, 1980, pp. 213-248.

[20] M- Koudelka, Performance characteristics of a planar 'Clark-type' oxygen sensor, Sensors and Actuators, 9 (1986) 249-258.

[21] D.J.G. Ives and G.J. Janz, Reference electrodes, Academic Press, New York, 1961, p. 217.

[22] A.J. Bard and L.R. Faulkner, Electrochemical Methods: Fundamentals and applications, Academic Press, New York, 1980, pp. 538-540.

[23] M. Jozowicz, J. Janata and M. Levy, Electrochemical pretreatment of thin film platinum electrodes, J. Electrochem. Soc., 135 (1988) 112-115.

[24] E. Gileadi, E. Kirowa-Eisner and J. Penciner, Interfacial Electrochemistry, Addison-Wesley, New York, 1975.

[25] R. Woods, in A.J. Bard (ed.), Electroanalytical Chemistry Series, Vol. 9, Marcel Dekker, New York, 1976, pp. 27-58.

[26] K. Mosbach, Methods in Enzymology, vol. 44, Academic Press, New York, 1976, p. 263.

[27] P.T. Kissinger and W.R. Heineman, Laboratory techniques in electro-analytical chemistry, Marcel Dekker, New York, 1984.

[28] S. Krishnaswamy and J.R. Kittrell, Deactivation studies of immobilized glucose oxidase, Biotechnol. Bioeng., 20 (1978) 821-835.

[29] T. Murakami, S. Nakamoto, J. Kimura, T. Kuriyama and I. Karube, A micro planar amperometric glucose sensor using an ISFET as a reference electrode, Anal. Lett., (1986) 19.

[30] S. Nakamoto, N. Ito, T. Kuriyama and J. Kimura, A lift-off method for patteming enzyme-immobilized membranes in multi-biosensors, Sensors and Actuators, 13 (1988) 165-172.

[31] U. Fischer et al., Diabetologia, 30 (1987) 940-945.

[32] K. Rebrin, U. Fischer, T. v. Woedtke, P. Abel and E. Brunstein, Automated feedback control of subcutaneous glucose concentration in diabetic dogs, Diabetologia, 32 (1989) 573-576.

VI

Model of the planar amperometric two-substrate enzyme electrode

6.0 Summary

The amperometric response of a glucose sensitive electrode is modelized by combining the two-substrate ping-pong enzyme kinetics and internal mass transport described by the two Fick's laws. An analytical solution of the resulting differential equations for substrate, cosubstrate and product can easily be found for the case of low bulk substrate concentrations. The only parameter to characterize the sensor response is a membrane design parameter V_S, which describes the ratio between the enzymatic transformation rate of substrate and the rate of substrate diffusion. Thus, this mathematical treatment allows the determination of V_S for any measured calibration curve.

In order to calculate the sensor response for any bulk substrate concentration, the method of finite differences is applied to solve the differential equations numerically. This digital simulation is then used to fit theoretical calibration curves to experimental ones by varying the Michaelis-Menten constant of substrate for the immobilized enzyme and the membrane design parameter V_C of the cosubstrate. The as-determined values allow then the calculation of the Michaelis-Menten constant of cosubstrate, so that the enzymatic membrane is completely characterized.

6.1 Introduction

Mell and Maloy proposed in 1975 for the first time a mathematical model of an amperometric enzyme electrode [1]. They considered an one-substrate reaction and used digital simulation to model the amperometric response of a glucose sensitive electrode. Two types of calibration curves have been predicted, depending upon whether the current was controlled by enzyme catalysis or by diffusion. Gough and Leypoldt [2] treated theoretically the bisubstrate enzyme electrode taking into account the effects of partitioning as well as internal and external diffusion. Thus, this latter approach represents a rather complete treatment of the amperometric enzyme electrode. Unfortunately, it is given in a generalized form, i.e., in terms of several dimensionless design parameters, so that the comparison of measured calibration curves with simulated ones is hardly possible because appropriate membrane parameters cannot be found in the literature and are difficult to determine experimentally.

The aim of this chapter is the modelization of the amperometric response of bisubstrate enzyme sensors using the ping-pong reaction mechanism and internal mass transport by diffusion. Since experimental data of partitioning effects, generally, are not available for concrete membranes, these effects are not considered. Furthermore, because all measurements reported in chapter 5 have be done in stirred analyte solutions, external diffusion resistances are neglected. The resulting model is given in terms of two dimensionless design parameters for substrate and cosubstrate as well as the Michaelis-Menten constants for both species. The goal of this theoretical treatment is then the determination of these parameters and constants for any measured calibration curve, allowing thus a better analysis of sensor responses.

In section 6.2, the differential equations describing substrate, cosubstrate and product profiles within the catalytic layer are deduced. Based on the measured current response, a mathematical treatment is then proposed (section 6.3) that allows the direct determination of the membrane design parameter for the substrate.

In order to solve the time dependent differential equations, a discretized model of the enzyme membrane is presented in section 6.4. Hence, in section 6.5, the membrane design parameter for cosubstrate as well as the Michaelis-Menten constant for substrate are determined by fitting digital simulated calibration curves to measured sensor responses. In section 6.6, the as-calculated responses are then compared with measured calibration curves of sensors with on wafer deposited enzyme membranes.

6.2 Differential equations describing substrate, cosubstrate and product diffusion within the enzymatic membrane

The subject of this modelisation is a planar enzyme sensor so that the theoretical treatment can be restricted to an one dimensional problem. Figure 6.1 shows the geometrical relationship.

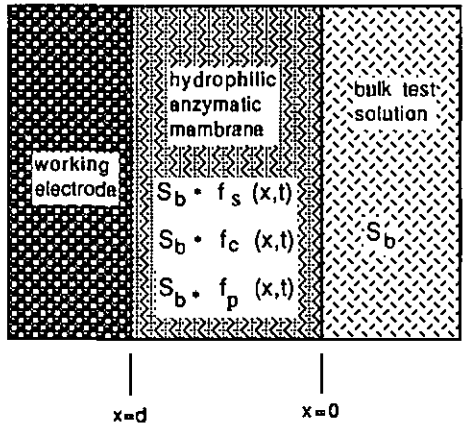

Fig. 6.1: Geometrical relationship

The origin of the homogeneous membrane of thickness d is taken as the interface between the membrane and the bulk test solution, briefly called the membrane-solution interface. The other membrane boundary , called the membrane-electrode interface, is taken at x=d.

The following discussion assumes that the enzyme is uniformly distributed in the catalytic membrane. Moreover, conformational and steric effects as well as microenvironmental effects are neglected. The latter assumption means that the solubilities of species in the bulk analyte solution are the same as those within the membrane. Thus, the following treatment of the kinetic behaviour of an immobilized GOD membrane is reduced to the description of the enzymatic reaction and the mass-transfer effects. In section 4.4 two modes of mass-transfer have been distinguished: external and internal transport. Because all measurements are carried out in stirred

solutions and because the consumption of glucose by the enzymatic reaction is relatively low compared to the amount of glucose in the sample solution, we assume that the overall reaction rate is governed by the enzymatic reaction and internal transport, i.e., by diffusion within the enzymatic membrane.
Writing S_b for substrate concentration in the bulk solution, S(x,t) for substrate, C(x,t) for cosubstrate and P(x,t) for product concentration at a given location x in the membrane at time t, the normalized fractional concentrations are:

$$f_S(x,t) = \frac{S(x,t)}{S_b} \quad , \quad f_C(x,t) = \frac{C(x,t)}{S_b} \quad , \quad f_P(x,t) = \frac{P(x,t)}{S_b} \tag{6.1}$$

The metabolite transformation causes a flux of substrate, cosubstrate and products. If the enzyme kinetics follows the bisubstrate ping-pong mechanism, also the action of the cosubstrate has to be considered. According to eq. (3.1) the oxidation of one mol glucose requires one mol oxygen, so that:

$$\frac{d\,S(x,t)}{dt} = \frac{d\,C(x,t)}{dt} \tag{6.2}$$

Due to the principle of conservation of mass, the amount of substrate loss is equal to that of product formation:

$$\frac{d\,S(x,t)}{dt} = -\frac{d\,P(x,t)}{dt} \tag{6.3}$$

The time dependent diffusion is now described by combining the ping-pong reaction scheme (eq. 3.22) and the mass transfer by diffusion (2nd Fick's law). To distinguish between the two Michaelis-Menten constants, we write K_M^S for the substrate (glucose) and K_M^C for the cosubstrate (oxygen).

$$\frac{dS(x,t)}{dt} = \frac{v_{max}}{1 + \dfrac{K_M^S}{S_b \cdot f_S(x,t)} + \dfrac{K_M^C}{S_b \cdot f_C(x,t)}} = S_b \cdot D_S \frac{d^2 f_S(x,t)}{dx^2} \tag{6.4}$$

$$\frac{dC(x,t)}{dt} = \frac{v_{max}}{1 + \dfrac{K_M^S}{S_b \cdot f_S(x,t)} + \dfrac{K_M^C}{S_b \cdot f_C(x,t)}} = S_b \cdot D_C \frac{d^2 f_C(x,t)}{dx^2} \tag{6.5}$$

$$\frac{dP(x,t)}{dt} = -\frac{v_{max}}{1 + \frac{K_M^S}{S_b \cdot f_S(x,t)} + \frac{K_M^C}{S_b \cdot f_C(x,t)}} = S_b \cdot D_P \frac{d^2 f_P(x,t)}{dx^2} \qquad (6.6)$$

D_S is the diffusion coefficient for substrate, D_C for cosubstrate and D_P for product. Thus, eqs. (6.4 - 6.6) are the differential equations describing the linear diffusion of substrate, cosubstrate and product through an enzymatic membrane taking into account the appropriate loss of substrate and cosubstrate as well as the product formation calculated with the bisubstrate ping-pong kinetics.

6.3 Steady-state behaviour

The fractional concentrations $f_S(x,t)$, $f_C(x,t)$ and $f_P(x,t)$ are time dependent, but at steady-state they become independent of time so that $f_S(x,t) = f_S(x)$, $f_C(x,t) = f_C(x)$ and $f_P(x,t) = f_P(x)$. To simplify eqs. (6.4 - 6.6) we define a reaction rate r(S,C) per unit volume:

$$r(S,C) \equiv \frac{v_{max}}{1 + \frac{K_M^S}{S(x)} + \frac{K_M^C}{C(x)}} \tag{6.7}$$

Hence, eqs. (6.4 - 6.6) can be written as:

$$r(S,C) = D_S \frac{d^2 S(x)}{dx^2} \tag{6.8}$$

$$r(S,C) = D_C \frac{d^2 C(x)}{dx^2} \tag{6.9}$$

$$r(S,C) = - D_P \frac{d^2 P(x)}{dx^2} \tag{6.10}$$

We consider now the denominator of the fraction in eq. (6.7) in the case when one term dominates the other ones.

$$\text{If} \quad \frac{K_M^C}{C(x)} >> \frac{K_M^S}{S(x)} + 1 , \tag{6.11}$$

e.g., when the sample solution is saturated with substrate and at low cosubstrate concentration, i.e., $C(x) << K_M^C$, it is:

$$r(S,C) = \frac{v_{max} \cdot C(x)}{K_M^C} \tag{6.12}$$

$$\text{If, on the other hand,} \quad \frac{K_M^S}{S(x)} >> \frac{K_M^C}{C(x)} + 1 , \tag{6.13}$$

e.g., when the analyte solution is saturated with cosubstrate and at low substrate concentration, i.e., $S(x) << K_M^S$, we get:

$$r(S,C) = \frac{v_{max} \cdot S(x)}{K_M^S} \qquad (6.14)$$

Further, the following dimensionless parameters can be introduced:

$$V_S \equiv \frac{v_{max}\, d^2}{D_S\, K_M^S} \qquad \text{and} \qquad V_C \equiv \frac{v_{max}\, d^2}{D_C\, K_M^C} \qquad (6.15)$$

For the general discussion of these parameters the designation V is used, i.e., V may design V_S or V_C. The diffusion coefficients D_S and D_C are generalized in the same way and, thus, are represented by the parameter D.

The membrane design parameter V is proportional to the product of the maximum rate of the enzyme reaction with the time associated with the diffusion through the enzymatic layer ($t = \frac{d^2}{2D}$).

$$V = \frac{2}{K_M}\, v_{max}\, t, \qquad t = \frac{d^2}{2\,D} \qquad (6.16)$$

v_{max} designs the maximum rate of enzyme reaction, i.e. the reaction rate under saturation. Since the rate of diffusion is proportional to 1/t, the parameter V compares the maximum rate of enzymatic reaction in the membrane to the rate of diffusion through the membrane and represents therefore a characteristic membrane parameter.

In the case of eq. (6.11), i.e., r(S,C) depends linearly on C(x), the steady-state fractional concentration of the cosubstrate can be described by the following differential equation:

$$\frac{d^2 f_C(x)}{dx^2} - \frac{V_C}{d^2} f_C(x) = 0 \qquad (6.17)$$

Eq. (6.17) yields the profile of the fractional cosubstrate concentration as a function of V_C. This differential equation is of second order and contains only one function $f_C(x)$ so that an analytical solution can easily be found.

In the case of eq. (6.13), i.e., r(S,C) depends linearly on S(x), the steady-state concentration of the substrate can be described by:

$$\frac{d^2 f_S(x)}{dx^2} - \frac{V_S}{d^2} f_S(x) = 0 \qquad (6.18)$$

The differential equation (6.18) is similar to eq. (6.17) so that the solutions of both equations have the same form. In order to generalize these differential equations, the parameter V and a function f(x), which replaces $f_S(x)$ or $f_C(x)$, are used:

$$\frac{d^2f(x)}{dx^2} - \frac{V}{d^2}f(x) = 0 \qquad (6.19)$$

A solution of the differential equation (6.19) is:

$$f(x) = c_1 e^{\frac{\sqrt{V}}{d}x} + c_2 e^{-\frac{\sqrt{V}}{d}x} \qquad (6.20)$$

Assuming that no diffusion gradient exists in the bulk solution, particularly near the membrane-solution interface, the boundary condition at x=0 (membrane-solution interface) is $f(0) = f_{bulk}$. This is quite a strong assumption that may be valid only approximatively and depends on the stirring conditions. Assuming now this boundary condition, we get one of the two constants of eq.(6.20):

$$c_2 = f_{bulk} - c_1 \qquad (6.21)$$

The electroinactivity of the species is a further assumption we make, but easy to check experimentally. When taking just an electrochemical cell without any membrane and applying the operational voltage, the current can be measured. Performing this test, we could find only a slight response for glucose so that this assumption is justified. Mathematically, this second boundary condition at x=d (electrode-membrane interface) can be written as:

$$\left.\frac{df(x)}{dx}\right|_{x=d} = c_1\frac{\sqrt{V}}{d}e^{\sqrt{V}} - c_2\frac{\sqrt{V}}{d}e^{-\sqrt{V}} = 0 \qquad (6.22)$$

Thus, the two constants of eq.(6.20) can be expressed as follows:

$$c_1 = f_{bulk}\cdot\frac{e^{-\sqrt{V}}}{e^{\sqrt{V}} + e^{-\sqrt{V}}}, \qquad c_2 = f_{bulk}\cdot\frac{e^{\sqrt{V}}}{e^{\sqrt{V}} + e^{-\sqrt{V}}} \qquad (6.23)$$

Inserting c_1 and c_2 in eq.(6.20) we get an analytical solution of the differential equation (6.19).

$$f(x) = \frac{f_{bulk}}{e^{\sqrt{V}} + e^{-\sqrt{V}}}\cdot\left(e^{\sqrt{V}(\frac{x}{d}-1)} + e^{-\sqrt{V}(\frac{x}{d}-1)}\right) \qquad (6.24)$$

It has to be pointed out that V is the only parameter of f(x) at a given location x/d in the membrane which can be emphasized by the designation of f(x) to f(x/d,V). The value of f_{bulk} in the case of eq. (6.13) is equal to one whereas in the case of eq. (6.11) f_{bulk}

coresponds to the oxygen concentration in the sample solution normalized by the bulk substrate concentration. A graphical illustration of eq. (6.24) is given in Fig. 6.2.

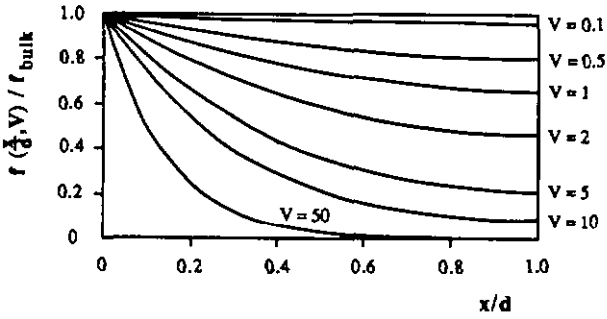

Fig. 6.2: Graphical illustration of eq. (6.24).

The concentration profiles drop from a value of unity at the membrane-solution interface to the respective values at the membrane-electrode interface, where no flux across the boundary occurs. High values of V result in a stronger decrease of the profiles, since the bulk of the enzymatic reaction takes place closer to the membrane-solution interface. As shows the profile for V = 50, there is no substrate or cosubstrate that reaches the electrode surface, since all molecules diffusing into the membrane have already been consumed before. Using eq. (6.24), the fractional concentration at the membrane-electrode interface can be expressed as:

$$f(d) = \frac{2}{e^{\sqrt{V}} + e^{-\sqrt{V}}} = \frac{1}{\cosh V} \qquad (6.25)$$

Hence, the greater V the smaller f(x) at the electrode surface, because increased values of V represent elevated enzyme catalysis and result therefore in small amounts of nonconverted substrate or cosubstrate at the electrode-membrane interface.

6.3.1 Estimation of V_S and V_C

As shown above, an appropriate knowledge of the values of V allows the prediction of the substrate or cosubstrate concentration profiles. Exact values of the different parameters contained in eq. (6.15) are not known for the specific membrane of our sensor. Approximated values, however, can be found in the literature.
Thus, the value of K_M^S given by Boehringer is 33 mM and that of K_M^C is 0.2 mM.

These are values measured for free enzyme in solution. The corresponding values for immobilized enzymes are generally lower (see chapter 4). The value of K_M^S found by Mell and Maloy [1] is about 6.8 mM. For an estimation of V_S and V_C, we need an upper and a lower limit of the Michaelis-Menten constants. From the values above we see that that the true Michaelis-Menten constants are very probably in the ranges:

$$2\ \text{mM} < K_M^S < 20\ \text{mM} \qquad 0.02\ \text{mM} < K_M^C < 0.2\ \text{mM}$$

The diffusion coefficient for glucose can be approximated [3] by $D_S = 6.7 \cdot 10^{-6}$ cm^2/s and that of oxygen by $D_C = 3 \cdot 10^{-5}$ cm^2/s. The maximum rate of enzyme activity v_{max} is the maximum velocity of the enzymatic reaction per unit volume and can be estimated by the enzyme concentration in the membrane. This is done for on wafer deposited enzyme layers.
According to the fabrication procedure for spin-coated membranes (section 5.4.2), 7.5 ml of the final enzyme solution contain about 30'000 U so that the polymerized membrane has an enzyme concentration of about 4000 U/ml. Since 1 U corresponds to the amount of enzyme that converts 1 µmol glucose per minute at 25 °C and pH 7, the maximum reaction rate is about 67 mM glucose per second.
Using a membrane thickness of 7000 Å and applying eq.(6.15), the maximum and minimum values of V_S^{spin} and V_C^{spin} for spin coated membranes are:

$$2.4 \cdot 10^{-3} < V_S^{spin} < 2.4 \cdot 10^{-2} \quad \text{and} \quad 5.4 \cdot 10^{-2} < V_C^{spin} < 5.4 \cdot 10^{-1} \qquad (6.26)$$

so that the overall kinetics is governed by the enzymatic reaction.
These membrane design parameters are now compared to those of on wafer deposited membranes fabricated by spreading the enzyme solution using a brush. According to the fabrication procedure described in section 5.4.1, the deposited enzyme solution contains about 12'700 U/ml. Hence, the maximum reaction rate is about 212 mM

glucose per second. Taking the membrane thickness as 9000 Å and applying eq.(6.15), the maximum and minimum values of V_S^{brush} and V_C^{brush} are:

$$1.2 \cdot 10^{-2} < V_S^{brush} < 1.2 \cdot 10^{-1} \quad \text{and} \quad 0.28 < V_C^{brush} < 2.8 \qquad (6.27)$$

From Fig. 6.2 it can be verified that the substrate concentration within the membrane is nearly constant for both cases (eqs. 6.26, 6.27) and, thus, corresponds approximately to that of the bulk sample solution. Further, in the case of eq.(6.26), the maximum decrease of cosubstrate concentration within the enzyme layer can be approximated by 20% of the bulk value whereas the maximum decrease in case of eq.(6.27) is about 60%. Hence, referring to the oxygen solubility found in appendix A, the oxygen concentration in both types of on wafer deposited membranes is similar to the value of K_M^C. Consequently, the overall reaction rate depends also on the cosubstrate concentration. Thereby, it should be noted that, due to the planar thin membrane geometry, even in the case where the enzyme layer covers all three electrodes, the oxygen formed at the counter electrode diffuses mainly into the bulk solution and thus serves only to maintain the oxygen concentration in the sample.

6.3.2 Steady-state behaviour at low substrate concentrations

V_S and V_C are characteristic membrane parameters and, thus, do not depend on the substrate or cosubstrate concentrations. Hence, when they can be calculated for special conditions, they are completely determined.

According to appendix A, the oxygen concentration in air saturated Krebs solution at 37 °C is 5.4 mg/l or 0.17 mM and, thus, is similar to the value of K_M^C given by Boehringer. Hence, it is easy to verify from eq. (6.7) that the reaction rate for low substrate concentrations can be approximated (see eq. 6.14) by:

$$r(S,C) = \frac{v_{max} \cdot S(x)}{K_M^S}$$

For the sake of simplicity we assume now that all three diffusion coefficients D_S, D_C and D_P are identical and equal to D_S. Hence, the steady-state of an enzyme electrode at low substrate concentrations can be described according to eqs. (6.8 - 6.10) and eq. (6.14):

$$\frac{d^2 f_S(x)}{dx^2} - \frac{V_S}{d^2} f_S(x) = 0 \qquad (6.28)$$

$$\frac{d^2 f_C(x)}{dx^2} - \frac{V_S}{d^2} f_S(x) = 0 \qquad (6.29)$$

$$\frac{d^2 f_P(x)}{dx^2} + \frac{V_S}{d^2} f_S(x) = 0 \qquad (6.30)$$

These differential equations (6.28 - 6.30) describe the change in fractional concentrations as a function of the dimensionless parameter V_S. Whereas eq. (6.28) contains only one function, i.e. $f_S(x)$, the two other ones are equations of two different functions.

6.3.2.1 Fractionol substrate concentration profile

Eqs. (6.28) describes the substrate concentration profile within the membrane thin layer for low substrate concentrations and has already been solved (see eq. 6.19). Hence, it is:

$$f_S(x) = \frac{1}{e^{\sqrt{V_S}} + e^{-\sqrt{V_S}}} \cdot \left(e^{\sqrt{V_S}\left(\frac{x}{d}-1\right)} + e^{-\sqrt{V_S}\left(\frac{x}{d}-1\right)} \right) \qquad (6.31)$$

The graphical illustration of this curve is shown in Fig. 6.2.

6.3.2.2 Fractionol cosubstrate concentrotion profile

Using eq. (6.31), the steady-state differential equation describing the fractional cosubstrate concentration profile can be expressed as function of $f_C(x)$ alone. Thus, taking eq.(6.29) and applying eq.(6.31) we obtain:

$$\frac{d^2}{dx^2} f_C(x) = \frac{V_S}{d^2} \cdot \frac{1}{e^{\sqrt{V_S}} + e^{-\sqrt{V_S}}} \left(e^{\sqrt{V_S}\left(\frac{x}{d}-1\right)} + e^{-\sqrt{V_S}\left(\frac{x}{d}-1\right)} \right) \qquad (6.32)$$

The integration results in:

$$\frac{d}{dx} f_C(x) = \frac{\sqrt{\nu_S}}{d} \cdot \frac{1}{e^{\sqrt{\nu_S}} + e^{-\sqrt{\nu_S}}} \left(e^{\sqrt{\nu_S}\left(\frac{x}{d}-1\right)} - e^{-\sqrt{\nu_S}\left(\frac{x}{d}-1\right)} \right) + A_1 \qquad (6.33)$$

$$f_C(x) = \frac{1}{e^{\sqrt{\nu_S}} + e^{-\sqrt{\nu_S}}} \left(e^{\sqrt{\nu_S}\left(\frac{x}{d}-1\right)} + e^{-\sqrt{\nu_S}\left(\frac{x}{d}-1\right)} \right) + A_1 x + A_2 \qquad (6.34)$$

To determine the two constants A_1 and A_2 in eq.(6.34), the behaviour of $f_C(x)$ at the membrane-electrode and the membrane-solution interface has to be borne in mind. At the latter interface, $f_C(x)$ corresponds to the oxygen solubility $S(O_2)$ divided by S_b:

$$f_C(0) = \frac{S(O_2)}{S_b} = 1 + A_2, \text{ so that:} \qquad A_2 = \frac{S(O_2)}{S_b} - 1 \qquad (6.35)$$

Since the oxygen is not consumed at the electrode surface, the boundary condition at the membrane-electrode interface is:

$$\left.\frac{df_C(x)}{dx}\right|_{x=d} = 0, \text{ so that:} \qquad A_1 = 0 \qquad (6.36)$$

Hence, the fractional cosubstrate concentration profile is given by:

$$f_C(x) = \frac{1}{e^{\sqrt{\nu_S}} + e^{-\sqrt{\nu_S}}} \left(e^{\sqrt{\nu_S}\left(\frac{x}{d}-1\right)} + e^{-\sqrt{\nu_S}\left(\frac{x}{d}-1\right)} \right) + \frac{S(O_2)}{S_b} - 1 \qquad (6.37)$$

$$= f_S(x) + \frac{S(O_2)}{S_b} - 1$$

According to appendix A, it is $S(O_2) = 0.17$ mM for an air saturated Krebs solution at 37 °C. Thus, $f_C(x)$ shows the same profile as that of the fractional substrate concentration (see Fig. 6.2) but is shifted in the ordinate.

6.3.2.3 Fractional praduct cancentration profile

The fractional product concentration within the membrane is given by eq. (6.30). Using the $f_S(x)$-profile (eq. 6.31), the steady-state differential equation becomes:

$$\frac{d^2}{dx^2} f_P(x) = -\frac{V_S}{d^2} \cdot \frac{1}{e^{\sqrt{V_S}} + e^{-\sqrt{V_S}}} \left(e^{\sqrt{V_S}\,(\frac{x}{d}-1)} + e^{-\sqrt{V_S}\,(\frac{x}{d}-1)} \right) \qquad (6.38)$$

Its integration results in:

$$\frac{d}{dx} f_P(x) = -\frac{\sqrt{V_S}}{d} \cdot \frac{1}{e^{\sqrt{V_S}} + e^{-\sqrt{V_S}}} \left(e^{\sqrt{V_S}\,(\frac{x}{d}-1)} - e^{-\sqrt{V_S}\,(\frac{x}{d}-1)} \right) + A_1 \qquad (6.39)$$

$$f_P(x) = -\frac{1}{e^{\sqrt{V_S}} + e^{-\sqrt{V_S}}} \left(e^{\sqrt{V_S}\,(\frac{x}{d}-1)} + e^{-\sqrt{V_S}\,(\frac{x}{d}-1)} \right) + A_1 x + A_2 \qquad (6.40)$$

The f_p-concentration at the membrane-solution interface can be neglected, since the initial product concentration is zero and stirring serves to dilute the product concentration at the membrane surface. Thus, the first boundary condition of f_p at x=0 can be expressed as:

$$f_p(0) = 0 \text{ , so that } A_2 = 1 \qquad (6.41)$$

With amperometric electrodes the electroactive solute is consumed rapidly at the electrode surface with the result that the product concentration at the membrane-electrode interface is maintained at zero:

$$f_P(d) = 0 \qquad (6.42)$$

Using eq.(6.40), we obtain the second constant:

$$A_1 = \frac{1}{d} \cdot \left(\frac{2}{e^{\sqrt{V_S}} + e^{-\sqrt{V_S}}} - 1 \right) \qquad (6.43)$$

Inserting now A_1 and A_2 into eq.(6.40), the analytical solution of eq.(6.30) can be written as:

$$f_P(x) = -\frac{1}{e^{\sqrt{\nabla_S}} + e^{-\sqrt{\nabla_S}}}\left(e^{\sqrt{\nabla_S}\,(\frac{x}{d}-1)} + e^{-\sqrt{\nabla_S}\,(\frac{x}{d}-1)}\right) \qquad (6.44)$$

$$+\left(\frac{2}{e^{\sqrt{\nabla_S}} + e^{-\sqrt{\nabla_S}}} - 1\right)\cdot\frac{x}{d} + 1$$

The profiles of the fractional product concentration as function of V_S is visualized graphically in Fig. 6.3.

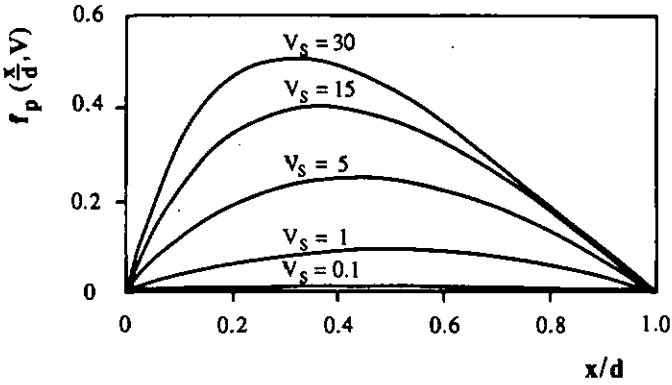

Fig.6.3: Fractional product concentration profiles at steady-state for $\frac{S(x)}{K_M^S} << 1$.

The fractional product profiles rise from a value of zero at the membrane-solution interface through a maximum and return to zero at the membrane-electrode interface where the product is consumed. The maximum of the product profile is higher and displaced further towards the membrane-solution interface with increasing values of V_S. Especially at elevated values of V_S, all profiles are assymmetrical in respect to the two membrane boundaries. To emphasize this behaviour, the locations of the respective product maximums are now calculated.

The maximum of a curve is located where the first derivative becomes zero and the second negative. Thus, according to eqs.(6.39) and (6.43), we write:

$$\frac{d}{dx} f_P(x) = 0 \qquad (6.45)$$

$$= -\frac{\sqrt{\nabla_S}}{d} \cdot \frac{1}{e^{\sqrt{\nabla_S}} + e^{-\sqrt{\nabla_S}}} \left(e^{\sqrt{\nabla_S}\left(\frac{x}{d}-1\right)} - e^{-\sqrt{\nabla_S}\left(\frac{x}{d}-1\right)} \right)$$

$$+ \frac{1}{d} \cdot \left(\frac{2}{e^{\sqrt{\nabla_S}} + e^{-\sqrt{\nabla_S}}} - 1 \right)$$

Reshaping eq.(6.45) and combining the respective terms, we obtain:

$$\left(e^{-\sqrt{\nabla_S}\left(\frac{x}{d}-1\right)} \right)^2 - \frac{e^{\sqrt{\nabla_S}} + e^{-\sqrt{\nabla_S}} - 2}{\sqrt{\nabla_S}} \cdot \left(e^{-\sqrt{\nabla_S}\left(\frac{x}{d}-1\right)} \right) - 1 = 0 \qquad (6.46)$$

This is a quadratic equation in $\left(e^{-\sqrt{\nabla_S}\left(\frac{x}{d}-1\right)} \right)$. The solution of such equations are summarized in any mathematical book, so that:

$$\frac{x}{d} = 1 - \frac{1}{\sqrt{\nabla_S}} \cdot \ln \left(\frac{e^{\sqrt{\nabla_S}} + e^{-\sqrt{\nabla_S}} - 2}{2\sqrt{\nabla_S}} \pm \sqrt{\left(\frac{e^{\sqrt{\nabla_S}} + e^{-\sqrt{\nabla_S}} - 2}{2\sqrt{\nabla_S}} \right)^2 + 1} \right) \qquad (6.47)$$

Obviously, eq.(6.46) yields two solutions from which we use the one with the negative second derivative. The f_P-maximums of the profiles presented in Fig.6.3 are listed in table 6.1.

Table 6.1: Location of the f_P-maximums within the enzymatic membrane.

membrane design parameter V_S	dimensionless position within the membrane: $\frac{x}{d}$
0.01	0.500
0.05	0.499
0.1	0.498
0.5	0.490
1	0.481
5	0.425
15	0.359
30	0.312
50	0.277
100	0.230

At moderate enzyme reaction velocity (with respect to diffusion) a symmetrical distribution of f_P occurs. On the other hand, an asymmetrical distribution of f_P results when V_S is large. This is due to an elevated product diffusion out of the membrane, since the bulk of the enzyme reaction takes place closer to the membrane-solution interface. Computing all locations of the f_P-maximums, it is found that for values of V_S greater than 0.023, the maximum is shifted near to the membrane boundary at x=0.

6.3.2.4 Calculation of the sensor response

In the following, the different diffusion coefficients for substrate, cosubstrate and product are distinguished again. The measured variable is the current, which is related through Faraday's and Fick's laws to the flux of product at the electrode surface. Thus, the first derivative of the product concentration determines the electrode current [4]:

$$i = -n F A D_P \frac{d}{dx} P(x)\Big|_{x=d} \qquad (6.48)$$

All terms have their usual meaning: n is the number of electrons involved in the electrochemical oxidation of the product, F is the Faraday constant and A represents the electrode surface covered by the membrane. Eq.(6.48) contains the derivative of the product concentration at the electrode surface (x=d). Using eqs.(6.8 - 6.10) and eq.(6.14) it is easy to verify that :

$$\frac{d}{dx}P(x)\Big|_{x=d} = S_b \frac{1}{d} \frac{D_S}{D_P} \left(\frac{2}{e^{\sqrt{V_S}} + e^{-\sqrt{V_S}}} - 1 \right) \qquad (6.49)$$

so that:

$$i = n F A D_S S_b \frac{1}{d} \left(1 - \frac{2}{e^{\sqrt{V_S}} + e^{-\sqrt{V_S}}} \right) \qquad (6.50)$$

It can easily be seen that this relationship deduced for low bulk substrate concentrations depends linearly on S_b.

6.3.2.5 Calculation of the membrane design parameter V_S

The membrane design parameter V_S is the ratio between the rate of enzymatic reaction and the rate of diffusion. The larger is V_S, the faster is the enzyme catalysis with respect to diffusion. At small values of V_S the overall membrane process is reaction controlled and depends on the enzyme concentration and kinetics. High values of V_S represent an overall transport controlled reaction because the diffusion is the slowest step, and properties such as the permeability of the membrane largely determine the response. Hence, this parameter V_S is a decisive parameter for describing membrane characteristics. It should be pointed out, that for a specific membrane the value of V_S is constant for any substrate concentration. Thus, when V_S can be measured or calculated for a special case, e.g. at low substrate concentrations, the membrane will be characterized completely.

Looking at eq.(6.50), the current depends at low bulk substrate concentrations beyond the well known physical constants only on the diffusion constant D_S, the membrane thickness d, the working electrode area A, the bulk substrate concentration S_b and the value of V_S. As described in the previous chapters, the dry membrane thickness can be measured by SEM. Further, Mell and Maloy [1] found the diffusion coefficient D_S in the membrane matrix nearly identical to the value reported for glucose in aqueous

solution D_{sol} [3]. Thus, making the assumption that $D_S \cong D_{sol}$, the diffusion coefficient can be regarded as known, so that the only unknown parameter of the sensor response for $S_b / K_M^S << 1$ is V_S. Consequently, the aim of this theory is a mathematical formalism allowing us to calculate the value of V_S for any measured calibration curve.

The slope s of such a calibration curve indicates the sensitivity to substrate concentration changes. According to eq.(6.50), there is:

$$\frac{\Delta i}{\Delta S_b} = - n F A D_S \cdot \frac{1}{d} \left(\frac{2}{e^{\sqrt{V_S}} + e^{-\sqrt{V_S}}} - 1 \right) \qquad (6.51)$$

Taking into account that $\frac{1}{e^{\sqrt{V_S}} + e^{-\sqrt{V_S}}} = \frac{e^{\sqrt{V_S}}}{e^{V_S} + 1}$ and with $s = \frac{\Delta i}{\Delta S_b}$ the equation (6.50) can be written as:

$$\left(e^{\sqrt{V_S}}\right)^2 + \frac{2 e^{\sqrt{V_S}}}{\frac{s d}{n F A D_S} - 1} + 1 = 0 \qquad (6.52)$$

This is a quadratic equation in $\left(e^{\sqrt{V_S}}\right)$ with the respective solution:

$$\sqrt{V_S} = \ln \left(- \frac{1}{\left(\frac{s d}{n F A D_S} - 1 \right)} \pm \sqrt{\left(\frac{1}{\left(\frac{s d}{n F A D_S} - 1 \right)} \right)^2 - 1} \right) \qquad (6.53)$$

Based on measured calibration curves, this equation (6.53) enables us to determine the membrane parameter V_S for any enzyme membrane.

According to eq.(6.53), the calculation of V_S requires the slope s of the calibration curve. To improve the accuracy of this value, a straight line has to be drawn trough the measured i-S_b points in the range of low bulk substrate concentrations. According to eq.(6.50), the current may be expressed as linear function of S_b. Writing the background current as i_0, we obtain:

$$i = i_0 + s S_b \qquad (6.54)$$

Taking into account t measured i-S_b points at low S_b values, we get a set of t linear equations:

$$i^m = i_0 + s\, S_b^m \quad , \quad 1 \le m \le t \tag{6.55}$$

This is a linear system of t equations and two unknowns, so that the problem is overdetermined. Such a system can be treated by the method of least squares. Applying this method (see appendix B) we get the two constants i_0 and s:

$$s = \frac{\sum_{m=1}^{t} S_b^m\, i^m \; - \; \frac{1}{t}\left(\sum_{m=1}^{t} S_b^m\right)\left(\sum_{m=1}^{t} i^m\right)}{\sum_{m=1}^{t} \left(S_b^m\right)^2 \; - \; \frac{1}{t}\left(\sum_{m=1}^{t} S_b^m\right)^2} \tag{6.56}$$

$$i_0 = \frac{1}{t}\left(\sum_{m=1}^{t} i^m \; - \; s \sum_{m=1}^{t} S_b^m\right) \tag{6.57}$$

Eq.(6.57) represents the background current and eq.(6.56) the slope of the calibration curve, so that we are able to calculate the value of V_S for any measured calibration curve.

6.3.3 *Steady-state behaviour at high substrate and low cosubstrate concentrations*

In principle, the membrane design parameter V_C, characterizing the membrane behaviour with respect to the cosubstrate, can be calculated in a similar way as that for V_S. Using the condition (6.11), so that r(S,C) can be expressed by eq.(6.12), the appropriate system of differential equations (see eqs.6.8 - 6.10) is given by:

$$\frac{d^2 f_S(x)}{dx^2} - \frac{D_C}{D_S} \cdot \frac{V_C}{d^2} f_C(x) = 0 \tag{6.58}$$

$$\frac{d^2 f_C(x)}{dx^2} - \frac{V_C}{d^2} f_C(x) = 0 \tag{6.59}$$

$$\frac{d^2 f_P(x)}{dx^2} + \frac{D_C}{D_P} \cdot \frac{V_C}{d^2} f_C(x) = 0 \tag{6.60}$$

This system can be solved by inserting the solution of eq.(6.59) in eqs.(6.58, 6.60). The first derivative of P(x) can then be applied to calculate the current as function of

V_C. The resulting expression of V_C is only correct for the condition (6.11), i.e., at high substrate and low cosubstrate concentrations. Since most glucose calibration curves are measured in air saturated solutions, the condition of low cosubstrate concentration may not always be fulfilled. Thus, to ensure condition (6.11), the measurements should be carried out under special conditions, e.g., nearly N_2 saturated samples.

6.3.4 Numerical calculotian of V_S for different enzyme membranes

A Pascal program has been written to fit calibration curves at low substrate concentrations by straight lines according to eqs.(6.56, 6.57). Applying then eq.(6.53) the membrane design parameters V_S can easily be calculated. The values used for the different constants and parameters are F = 96485 As/mol, n = 2 and $D_S = 6.7 \cdot 10^{-10}$ m^2/s. The working electrode area A as well as the membrane thickness d depend on the mask design and the fabrication procedure of the membrane. Thereby, it should be mentioned, that, for thin membranes, only the hydrogen peroxide formed in the membrane part over the working electrode contributes to the sensor current. From this point of vue, it is insignificant whether the membrane covers the sensing region of all three electrodes or only that of the working electrode.

A first determination of the membrane design parameter V_S has been done for on wafer fabricated membranes deposited by spreading the enzyme solution using a brush. The mask design applied was SGL200. Thus, the working electrode area is $8.5 \cdot 10^{-8}$ m^2 and the membrane thickness measures $9 \cdot 10^{-7}$ m (see section 5.4.1). The arithmetical mean of the five calibration curves shown in Fig. 5.41 has been applied for the determination of V_S. The value found is $V_S = 1.2 \cdot 10^{-2}$ which is at the lower limit of the estimated values in section 6.3.1.

The membrane design parameter V_S has also been calculated for spin coated membranes using the average calibration curve of 12 devices from three different wafers (Fig. 5.44). These membranes have a thickness of about 7000 Å and the working electrode area measures $1.26 \cdot 10^{-7}$ m^2. Hence, the resulting V_S-value is $2.5 \cdot 10^{-3}$ and thus is also at the lower limit of the estimated values.

6.4 Digital simulation of the sensor response

Differential equations describing substrate, cosubstrate and product concentration profiles have been derived in chapter 6.2. They are based on mass transfer by diffusion and the two-substrate ping-pong enzyme reaction. The resulting exact differential equations (6.4 - 6.6) are of second order and are, in this general form, difficult to solve analytically. As seen in section 6.3, a solution in closed form can only be found in the case of low bulk substrate concentrations.

Mell and Maloy [1] proposed in 1975 a model of an amperometric one-substrate enzyme electrode applying the method of finite differences [5]. This method allows one to attack these complex problems numerically by digital simulation techniques [6, 7], so that predictions may be made concerning the current response. Usually, the results are presented in terms of dimensionless working curves using the dimensionless parameters V_S and S_b/K_M^S. The same method, but applying the two-substrate ping-pong enzyme kinetics, is now used to simulate numerically the amperometric response of glucose sensitive electrodes.

6.4.1 Discretized madel of the enzymatic membrane

A numerical simulation of the enzymatic reaction and Fick's laws cannot be handled by continuous functions so that the problem has to be attacked by the method of finite differences. Consequently, the enzymatic membrane is considered in terms of small, discrete volume elements [8]. For this purpose, the membrane layer of thickness d is divided into m equal volume elements:

$$\Delta x = \frac{d}{m} \qquad (6.61)$$

Throughout any element, the concentration E(x,t) of any species E is regarded as uniform, but may vary from element to element. Further, if edge diffusion is prevented, the concentration of any species is constant over any plane parallel to the electrode.

The fraction d^2/D_S can be used as time parameter (see eq. 6.16). This time is now devided into L equal intervals:

$$\Delta t = \frac{d^2}{D_S L} \qquad (6.62)$$

To model the system's evolution the reaction and mass transport laws are expressed in finite difference form:

1st Fick's law:

$$J(x,t) = D_E \frac{E(x+\Delta x,t) - E(x,t)}{\Delta x} = \frac{D_E}{\Delta x}\left[E(x+\frac{\Delta x}{2},t) - E(x-\frac{\Delta x}{2},t) \right] \qquad (6.63)$$

2nd Fick's law:

$$\frac{E(x,t+\Delta t) - E(x,t)}{\Delta t} = \frac{J(x+\frac{\Delta x}{2},t) - J(x-\frac{\Delta x}{2},t)}{\Delta x} \qquad (6.64)$$

These algebraic relations describe the concentration changes over one interval! Δt. The combination of (6.63) and (6.64) gives:

$$E(x,t+\Delta t) = E(x,t) + \frac{D_E \Delta t}{(\Delta x)^2} [E(x+\Delta x,t) - 2\,E(x,t) + E(x-\Delta x,t)] \qquad (6.65)$$

This is the general law defining diffusion effects on any species in any volume element, except the first one. The proportionality factor $\frac{D_E \Delta t}{(\Delta x)^2}$, called the model diffusion coefficient D_M^E, is calculated by the equations (6.61) and (6.62):

$$D_M^E = \frac{D_E \Delta t}{(\Delta x)^2} = \frac{m^2}{L} \cdot \frac{D_E}{D_S} \qquad (6.66)$$

Since m and L are input parameters of the numerical simulation, some care must be exersized in their selection to prevent simulated diffusion between non-adjacent volume elements:

The maximum mass transport occurs if $E(x,t)=0$ and $E(x+\Delta x,t)=0$, but $E(x-\Delta x,t)>0$. Hence, according to eq.(6.65), it is:

$$E(x,t+\Delta t) - E(x,t) = D_M^E \cdot E(x-\Delta x,t) \qquad (6.67)$$

In this case, when the amount of species E in volume x extends to the double volume, the maximum mass transport is:

$$E(x,t+\Delta t) - E(x,t) = \frac{1}{2} \cdot E(x-\Delta x,t) \qquad (6.68)$$

Thus, in order to prevent diffusion between non-adjacent volume elements, it is:

$$D_M^E \leq 0.5 \qquad (6.69)$$

The membrane is now envisioned as sequence of volume elements i $(0 \leq i \leq m)$ as shown in fig.6.4.

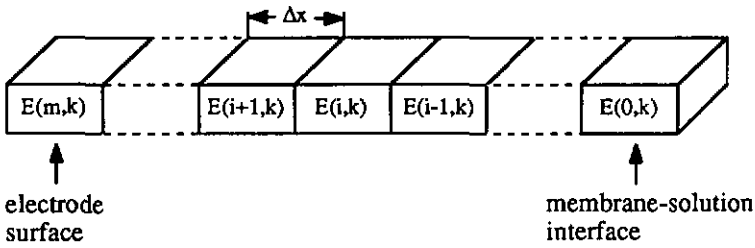

Fig. 6.4: Discrete model of a membrane adjacent to an electrode.

The outer membrane boundary is in the center of box zero, and each box i is taken to characterize the membrane at $x = i\ \Delta x$ from this membrane-solution interface.
The time is also broken into segments of a duration Δt. The time evolution of the continuous reaction and mass transport laws is approximated by applying these transformation laws k times. The k^{th} iteration therefore yields the model for $t = k\ \Delta t$.
Using the two model variables i and k, equation (6.65) can be written as:

$$E(i,k+1) = E(i,k) + D_M^E \left[E(i+1,k) - 2\,E(i,k) + E(i-1,k)\right] \qquad (6.70)$$

For any box i the concentration resulting from iteration k+1 is calculated from the concentrations produced in boxes (i-1), i and (i+1) by iteration k.
Using eqs.(6.7 and 6.62), the change of substrate, cosubstrate and product concentrations in each volume element during each iteration can be expressed as:

$$\Delta S(i,k) = \frac{v_{max}\ \frac{d^2}{D_S}\ L}{1 + \frac{K_M^S}{S(x)} + \frac{K_M^C}{C(x)}} = \frac{S(i,k)\ C(i,k) / L}{\frac{S(i,k)}{K_M^S} \cdot \frac{C(i,k)}{V_S} + \frac{C(i,k)}{V_S} + \frac{S(i,k)}{V_C} \cdot \frac{D_S}{D_C}} \qquad (6.71)$$

According to eqs.(6.2, 6.3): $\Delta S(i,k) = \Delta C(i,k) = -\Delta P(i,k)$ (6.72)

Thus, the concentrations of the different species can be written as:

$$S(i,k+1) = S(i,k) + D_M^S \left[S(i+1,k) - 2\,S(i,k) + S(i-1,k)\right] - \Delta S(i,k) \qquad (6.73)$$

$$C(i,k+1) = C(i,k) + D_M^C \left[C(i+1,k) - 2\,C(i,k) + C(i-1,k)\right] - \Delta S(i,k) \qquad (6.74)$$

$$P(i,k+1) = P(i,k) + D_M^P \left[P(i+1,k) - 2\,P(i,k) + P(i-1,k)\right] + \Delta S(i,k) \qquad (6.75)$$

Eqs.(6.73 - 6.75) are the general formulas describing substrate, cosubstrate and product diffusion in a discretized enzymatic membrane.
Further, the appropriate boundary conditions have to be satisfied. For box zero, which represents the membrane-solution interface, there is:

$$\left.\begin{aligned} S(0,k) &= S_{bulk} \\ C(0,k) &= S(O_2) \end{aligned}\right\} \quad \text{at any iteration k.} \tag{6.76}$$

According to assumption (6.41), the initial P(0,k) is zero and stirring serves to dilute the product concentration. Thus:

$$P(0,k) = 0 \quad \text{for any k.} \tag{6.77}$$

According to eqs.(6.22, 6.36), there is no flux of substrate or cosubstrate at the membrane-electrode interface. This is taken into account by:

$$S(m,k+1) = S(m,k) + D_M^S \left[S(m-1,k) - S(m,k)\right] - \Delta S(m,k) \tag{6.78}$$

$$C(m,k+1) = C(m,k) + D_M^C \left[C(m-1,k) - C(m,k)\right] - \Delta S(m,k) \tag{6.79}$$

Finally, according to eq.(6.42), the electroactive product is consumed rapidly at the electrode surface, so that:

$$P(m,k) = 0 \quad \text{at any iteration k.} \tag{6.80}$$

6.4.2 Time evolution of the sensor response

A pascal program has been written to simulate the response of an amperometric one-substrate enzyme electrode using the considerations outlined above. To describe the initial situation at k=1, the following conditions have been defined:

substrate:	$S(i,1) = 0$,	$0 \le i < m$	(6.81)
cosubstrate:	$C(i,1) = S(O_2)$,	$0 \le i \le m$	(6.82)
product:	$P(i,1) = 0$,	$0 \le i \le m$	(6.83)

Typical values used for the calculation are m=25 and L=7000, so that:

$$D_M^S = 0.09 \tag{6.84}$$

Further, the following values of the diffusion coefficients are used [3]:

$$D_S = 6.7 \cdot 10^{-10} \frac{m^2}{s}$$
$$D_C = 3 \cdot 10^{-9} \frac{m^2}{s} \qquad (6.85)$$
$$D_P = 1.5 \cdot 10^{-9} \frac{m^2}{s}$$

Thus, the model diffusion coefficients of the cosubstrate and the product can be calculated to be:

$$D_M^C = 0.4 \qquad (6.86)$$

$$D_M^P = 0.2 \qquad (6.87)$$

The flux of product across the boundary between boxes m-1 and m is given by:

$$J(k+1) = D_P \frac{P(m-1,k) - P(m,k)}{\Delta x} \qquad (6.88)$$

Taking into account the boundary condition P(m,k)=0, we get:

$$J(k+1) = D_P \frac{P(m-1,k)}{\Delta x} \qquad (6.89)$$

According to eq.(6.48) the current is given by:

$$i(k+1) = n\,F\,A\,J(k+1) = n\,F\,A\,D_P \frac{P(m-1,k)}{\Delta x}$$

$$= n\,F\,A\,D_P \frac{m}{d} \cdot P(m-1,k) \qquad (6.90)$$

Fig. 6.5 shows the time evolution of as-calculated sensor responses to a 1 mM glucose solution. Therefore, the membrane design parameters V_S and V_C are held constant and the influence of the Michaelis-Menten constant for substrate is studied. Further, the electrode design SGL200 and a membrane thickness of 0.9 µm are assumed. The curves in the upper panel are calculated using $V_S = 0.1$ and $V_C = 1$ whereas for the curves in the lower panel the values applied are $V_S = 0.01$ and $V_C = 0.01$. Typical current vs. time curves illustrating the approach to steady-state are shown in Fig. 6.5. In each simulation attempted, a steady-state current is obtained after about 14'500 iterations or in a time interval less than 2.5 ms, regardless of V_S, V_C and K_M^S.

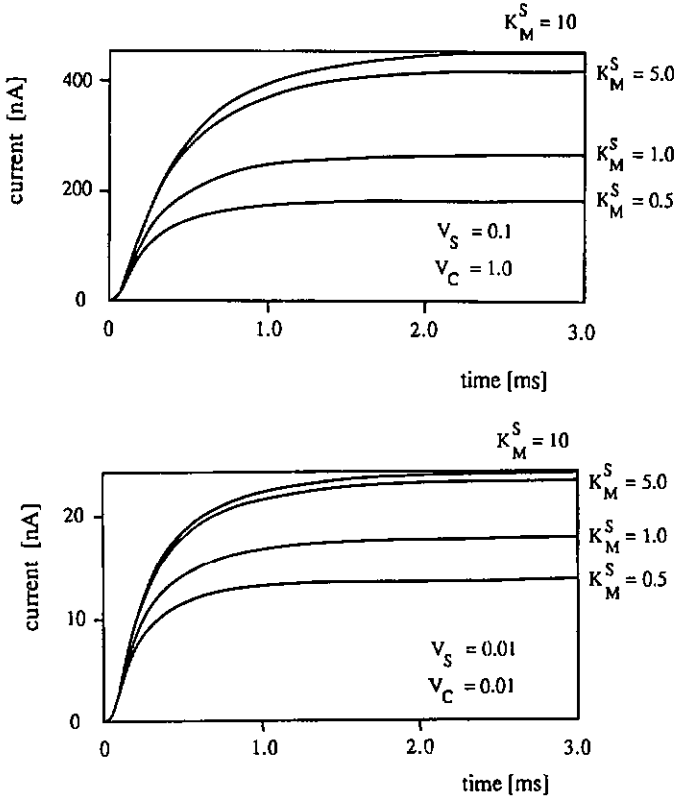

Fig. 6.5: Time evolution of sensor responses using the electrode design SGL200 and assuming a membrane thickness of 0.9 µm.

6.4.3 Simulated calibration curves

The method used above can also be applied to obtain simulated calibration curves. Assignment of values for V_S, V_C and K_M^S allows one to study the current response under the influence of all possible reaction velocity combinations. Representative simulated calibration curves for equal V_S and V_C are presented in Fig. 6.6 whereas

Fig. 6.7 shows curves with different membrane design parameters for substrate and cosubstrate. Thereby, for all curves presented in the two figures, the electrode design SGL200 and a membrane thickness of 0.9 µm are assumed.

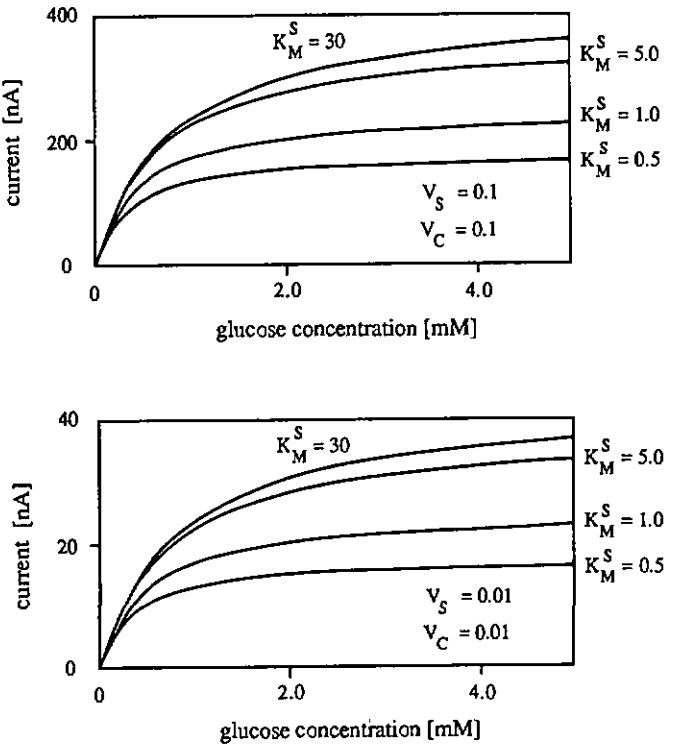

Fig. 6.6: Simulated calibration curves as function of the Michaelis-Menten constant of substrate for equal assignment of V_S and V_C. All sensor responses are simulated using the electrode design SGL200 and assuming a membrane thickness of 0.9 µm. All curves in the upper panel are calculated with V_S=V_C= 0.1 and those in the lower panel with V_S=V_C=0.01.

Fig. 6.6 shows that, in the case of equal membrane design parameters for substrate and cosubstrate, the shape of the calibration curves depends only on K_M^S. Thereby,

care should be taken of the different division of the ordinates in the upper and lower panel. The different order of magnitude of the currents in the two cases corresponds to the expected behaviour of increased enzyme reaction velocity in the case of the upper panel where the membrane design parameters are ten times greater than those used for the curves in the lower panel.

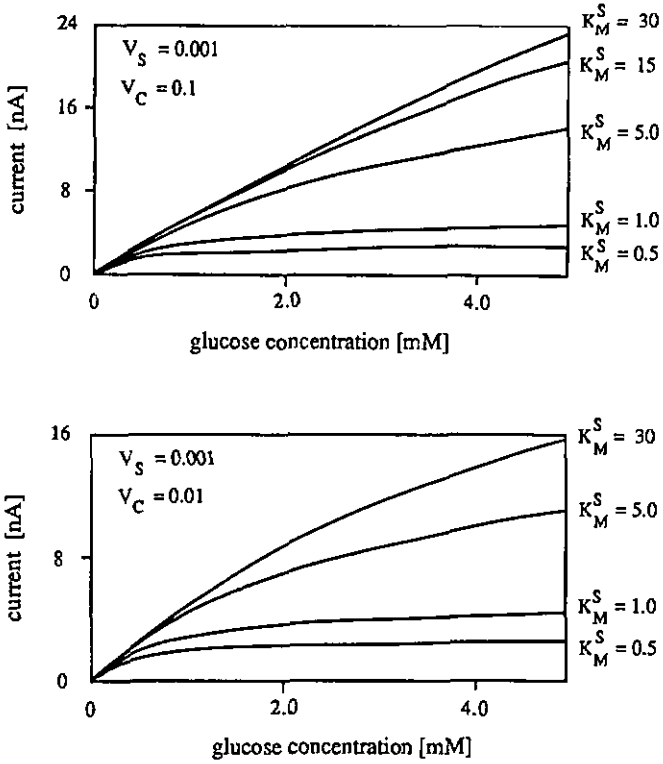

Fig. 6.7: Simulated calibration curves as function of the Michaelis-Menten constant of substrate for different assignments of V_S and V_C. The design SGL200 and a membrane thickness of 0.9 µm are assumed. The curves in the upper panel are calculated with V_C=0.1 and those in the lower panel with V_C=0.01. V_S is the same for all curves in both panels and is taken as 0.001.

Due to the assignment of V_S and V_C used in Fig. 6.7, the sensor responses are diffusion controlled and, thus, show an extended linear region compared to those presented in Fig. 6.6. Moreover, it should be noted that all calibration curves in Fig.6.6 and Fig.6.7 show typical behavior of enzyme kinetics: At very low bulk substrate concentrations, a linear relationship between current and bulk substrate concentration results. On the other hand, at high bulk substrate concentrations, the steady-state current approaches a limiting value dependent upon V_S, V_C and K_M^S.

6.4.4 Fitting simulated calibration curves to meosured ones

According to section 6.4.3, calibration curves are completely characterized by assigning the values of V_S, V_C and the Michaelis-Menten constant for substrate. Thereby, the membrane design parameter V_S can easily be calculated according to the method described in section 6.3.2.5.

The goal of this chapter is the determination of V_S, V_C and the Michaelis-Menten constants for substrate and cosubstrate. Hence, the method of least squares is applied to fit simulated calibration curves to measured ones by varying the assignment of V_C and K_M^S. In principle, the determination of V_C requires only the fit of one measured $i(S_b)$-point since the slope of the calibration curve at low bulk substrate concentrations (linear range) is given by the values of V_S and V_C. In order to ensure the accuracy of the V_C-value, currents at two different bulk substrate concentrations are used, i.e., the first $i(S_b)$-point and the value at about half the highest measured bulk substrate concentration. The determination of the Michaelis-Menten constant for substrate requires also current values at higher substrate concentrations. Hence, in addition to the two points used already for the determination of V_C, also the current at the highest measured substrate concentration is considered.

Applying eq.(6.15), the Michaelis-Menten constant for cosubstrate can then be evaluated by calculating the maximum reaction rate of the best fitted curve, i.e., using the values for V_C and K_M^S of the best fitted current response.

Due to section 6.4.3, the simulated curves show typical behavior of enzyme kinetics, i.e., they approach a limiting current at high bulk substrate concentrations. Thus, the maximum current response for any simulated calibration curve can easily be calculated using the steady-state value at high substrate concentration. For the values indicated below, the current response at 100 mM glucose is taken.

This numerical treatment is now applied to determine the different parameters and constants of on wafer deposited membranes. Moreover, in order to certify this numerical method, each measured current response is compared visually with the best fitted curve. Thus, Fig. 6.8 shows the comparison of the measured with the fitted calibration curve of on wafer fabricated membranes deposited by spreading the enzyme solution using a brush (design: SGL200, d = 0.9 µm). The arithmetical mean of the five calibration curves shown in Fig. 5.41 has been taken as measured calibration curve. Hence, the determined values are:

$$V_S = 0.0125\,,\quad V_C = 1.25\,,\quad K_M^S = 26.2\ \text{mM}\,,\quad K_M^C = 0.06\ \text{mM}$$
$$v_{max} = 0.271\ \text{M/s}\,,\qquad i_{max} = 1126\ \text{nA} \tag{6.91}$$

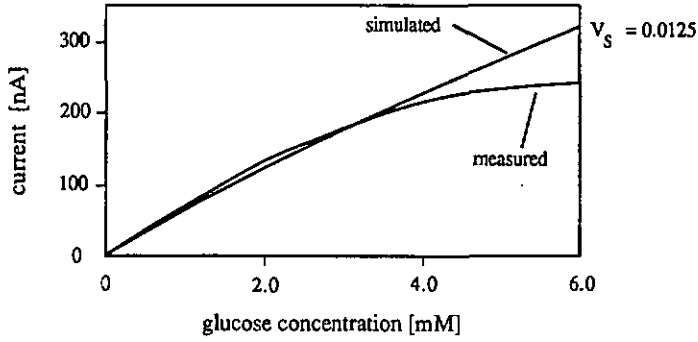

Fig. 6.8: Comparison of fitted and measured calibration curves of a sensor with on wafer fabricated membrane deposited by spreading the enzyme solution using a brush .

It should be pointed out that the first $i(S_b)$-point of any measured sensor response should be taken at about K_M^C, i.e. $S_b \approx 0.1$ mM, thus ensuring that the slope of the calibration curve used for the calculation of V_S is that of the linear region. Since the fist measured point in Fig. 5.41 has been taken at a bulk glucose concentration of about 0.6 mM, there may be a little inaccuracy of the calculated V_S-value. Hence, this calibration curve has also been fitted assigning a fixed V_S-value of 0.014. Fig. 6.9 shows the comparison of the as-obtained curve with the measured sensor response.

The corresponding values are:

$$V_S = 0.014\ ,\quad V_C = 0.719\ ,\quad K_M^S = 26.2\ \text{mM}\ ,\quad K_M^C = 0.11\ \text{mM}$$
$$v_{max} = 0.303\ \text{M/s}\ ,\qquad i_{max} = 1037\ \text{nA} \tag{6.92}$$

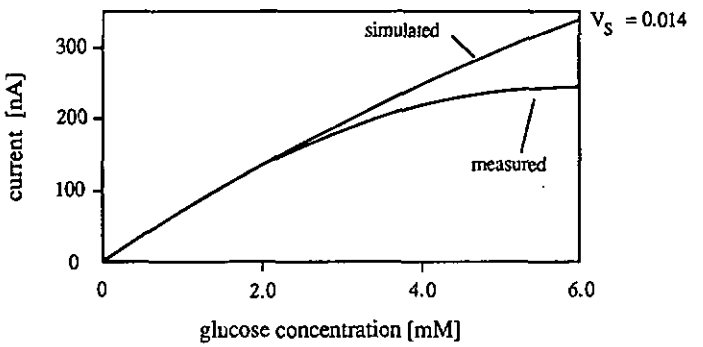

Fig. 6.9: Comparison of the measured calibration curve in Fig. 6.8 with the fitted one calculated using $V_S = 0.014$.

It is easy to see that the simulated curve fits the experimental one very well at low bulk substrate concentrations. More important, however, is the fact that there is no intersection of the two curves.

This fitting procedure is also applied for the characterization of spin-coated membranes (design: SGL400, d = 0.7 µm). Using the average calibration curve of 12 devices *from three different wafers (Fig. 5.44)*, the corresponding values are:

$$V_S = 0.0028\ ,\quad V_C = 0.144\ ,\quad K_M^S = 26.2\ \text{mM}\ ,\quad K_M^C = 0.11\ \text{mM}$$
$$v_{max} = 0.10\ \text{M/s}\ ,\qquad i_{max} = 408\ \text{nA} \tag{6.93}$$

The comparison of the experimental curve with the fined one is visualized in Fig. 6.10. The first measured $i(S_b)$-point of this curve has been taken at 0.1 mM glucose so that the calculated V_S-value should be close-fitted which is confirmed by the absence of any intersection of the two curves.

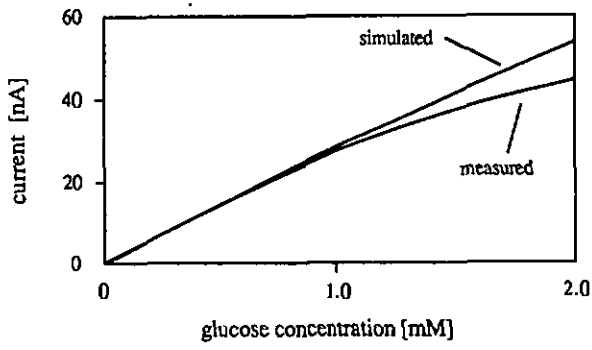

Fig. 6.10: Comparison of fitted and measured calibration curves of devices with spin-coated membranes.

Applying the fitting procedure to the response of a device with a double enzymatic membrane (Fig. 5.45 / 3, design: SGL400, d = 1.3 µm), we get:

$$V_S = 0.0102\ ,\quad V_C = 1.02\ ,\quad K_M^S = 26.2\ \text{mM}\ ,\quad K_M^C = 0.06\ \text{mM}$$
$$v_{max} = 0.10\ \text{M/s}\ ,\qquad i_{max} = 948\ \text{nA} \tag{6.94}$$

The comparison of the measured and fitted curve at low glucose concentrations (see Fig. 6.11) shows a little difference in the slope of the two curves. However, assigning a fixed V_S-value of 0.0107 results already in a perfect agreement of both slopes. The appropriate values are:

$$V_S = 0.0107\ ,\quad V_C = 0.55\ ,\quad K_M^S = 26.2\ \text{mM}\ ,\quad K_M^C = 0.11\ \text{mM}$$
$$v_{max} = 0.11\ \text{M/s}\ ,\qquad i_{max} = 822\ \text{nA} \tag{6.95}$$

Comparing the values of eq.(6.93) and eq.(6.95), i.e. simple and double enzyme membrane, it is easy to verify that, in the case of double enzyme membranes, the maximum current is doubled. Further, examining the Michaelis-Menten constant of substrate, we find excellent conformity of the determined values. Using improved V_S-values, i.e. no intersections of the measured with the simulated calibration curve, even the Michaelis-Menten constant of cosubstrate is the same for all membranes tested (see eqs. 6.92, 6.93 and 6.95). Moreover, it should be pointed out that the K_M^S-value is

only little diminished after immobilization, i.e., compared to the value given by Boehringer. On the other hand, the vale of K_M^C is about half the value indicated by the furnisher.

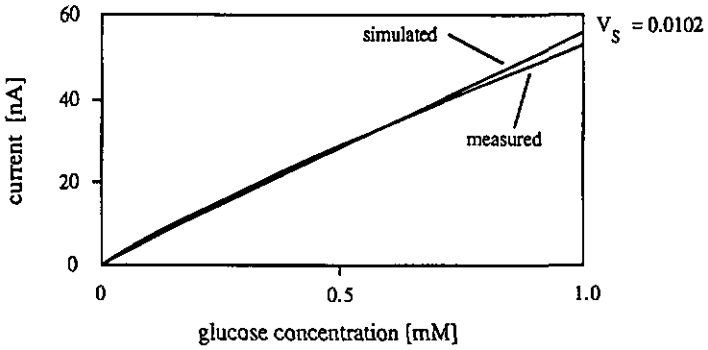

Fig. 6.11: Comparison of fitted and measured calibration curves of devices with double enzymatic membranes.

6.5 Conclusions

In this chapter, digital simulation is used to model the amperometric response of a glucose sensitive electrode. The model takes into account the competitive effects of diffusion and enzymatic reaction which is treated in the simulation by allowing ordinary two-substrate enzyme kinetics to occur in each volume element during each iteration. The numerical treatment permits the evaluation of the Michaelis-Menten constants for substrate and cosubstrate for any measured calibration curve. The only requirement is one measured current value at low substrate concentration, i.e., at a bulk glucose concentration smaller or equal the Michaelis-Menten constant of oxygen.
The determination of the membrane design parameters V_S and V_C allows one to characterize the enzyme membranes with respect to the ratio between the enzymatic reaction rate and the rate of diffusion. Further, the known parameters and constants allow one to evaluate the maximum reaction velocity and the saturation current. On the other hand, assignment of values for V_S, V_C and the Michaelis-Menten constant for substrate permits the study of the current response under the influence of all possible reaction velocity combinations.
The model presented in this chapter predicts successfully the current response of the glucose/ oxygen-GOD system at low and moderate bulk substrate concentrations. Moreover, the Michaelis-Menten constants are the same for all membranes tested and are only little smaller than the values indicated by Boehringer. At higher glucose concentrations the simulated sensor responses are always higher than the measured ones. This may be due to a change of the oxygen solubility in the membrane by altering the ionic strength of the analyte solution in the membrane caused by the formation of hydrogen peroxide.

6.6 References

[1] L.D. Mell and J.T. Maloy, A model for the amperometric enzyme electrode obtained through digital simulation and applied to the immobilized glucose oxidase system, Analytical Chemistry, 47 (1975) 299.

[2] D.A. Gough and J.K. Leypoldt, Theoretical aspects of enzyme electrode design, in Applied Biochemistry and Bioengineering, Vol. 3, Academic Press, 1981, p.175.

[3] R.C. Weast, CRC Handbook of Chemistry and Physics, 63rd ed., The Chemical Rubber Co., Florida, 1983, p. F-51.

[4] A.J. Bard and L.R. Faulkner, Electrochemical Methods: Fundamentals and Applications, Academic Press, New York, 1980.

[5] G. Dahlquist and A. Björck, Numerical Methods, Prentice Hall, Englewood Cliffs, 1973, Chapter 5.

[6] S.W. Feldberg, in A.J. Bard (ed.), Electroanalytical Chemistry, Vol.3, Marcel Dekker, New York, 1969, Chapter 4.

[7] J.T. Maloy, in J.S. Mattson, H.B. Mark and H.C. MacDonald (eds.), Electrochemistry: Calculations, Simulations and Instrumentation, Marcel Dekker, New York, 1972, Chapter 9.

[8] A.J. Bard and L.R. Faulkner, Electrochemical Methods: Fundamentals and Applications, Academic Press, New York, 1980, Appendix B.

VII
Conclusions

The goal of this thesis was the development and the study of a miniaturized amperometric glucose sensor for biomedical applications. Such an implantable biosensor may be used in clinical medicine allowing continuous measurement of rapidly varying blood glucose levels, without the need for added reagents or withdrawal of body fluids.

In this concluding chapter, the features of our in vivo glucose sensor are compared with those of other research groups all over the world. Hereby, it should be pointed out, that an exact comparison of published data of the different sensors is rather difficult since the sensor dimensions as well as the experimental conditions of characterization are not the same. Only five research groups currently work on glucose sensors designed especially for in vivo applications [1-4]. All of them use the enzyme glucose oxidase; but the sensor described in this thesis is the only one fabricated by means of thin film technology. Hence, it shows the most favorable degree of miniaturization. Further, the use of integrated circuit fabrication processes allows the realization of mass fabricated and well controlled electrochemical cells having reproducible characteristics with respect to response time and stability. However, the membrane part of our sensor applied so far for in vivo testing is still deposited manually limiting thus slightly the advantage obtained using well defined planar electrochemical cells.

Two approaches, generally, are known to minimize the dependence on fluctuating tissue oxygen tension: the use of a mediated electron transfer or the application of an outer hydrophobic membrane. Pickup et al. [1] represents the only group using a mediator, the dimethylferrocene, acting as a redox shuttle between immobilized glucose oxidase and a platinum electrode. Therewith, they demonstrated for the first time the feasibility of short-term metabolic monitoring in insulin-dependent diabetic patients.

The other groups measure the concentration of hydrogen peroxide and restrict the diffusion of glucose by a membrane, thus ensuring that the enzyme reaction is glucose-limited over a wide range of oxygen concentration. The comparison of the in vivo behaviour is even more critical than the in vitro characterization since the different research group do not use the same diabetic subjects and, moreover, implant the

sensors at different implantation sites. Shichiri et al. [2] described a needle-type sensor with an outer alginate-polylysine-alginate membrane as a hydrophilic biocompatible one. The sensor was applied to the continuous monitoring of tissue glucose concentrations in normal dogs. These results indicated an augmentation of the operational sensor life time by improvement of the biocompatibility. Reach et al. [3] modified the sensor design from Shichiri using an outer polyurethane membrane and investigated the kinetics of subcutaneous glucose concentration in anaesthetized rats. Fischer et al. [4] implanted Clark-type amperometric sensors consisting of a Pt anode and a Ag/AgCl cathode in insulin-dependent diabetic dogs. Their enzyme layer is covered with a perforated polyethylene membrane and cellulose. The recently published data demonstrated the principle effectiveness of feedback control of intracorporal glucose metabolism. But, all the sensors showed a continuous downward drift upon implantation, some of them even loosing their sensitivity already after a few hours. The in vivo characteristics of the sensor described in this thesis are comparable to those found by Fischer and Reach in that that the sensor response mirrors correctly blood glucose levels during one day. Also our devices show similar drift problems which may be due to tissue reaction to the implanted sensor. Thereby, it should be pointed out that the objective of very long-term implantation is unrealistic in the foreseeable future, due to the poor biocompatibility of materials currently available to package the sensor.

The thesis describes also another technique of membrane deposition resulting in on wafer level completed devices. This technique allows the realization of precisely patterned membranes with reproducible membrane thicknesses. Only Kuriyama et al. reported a similar lift-off method [5] for the patterning of enzyme membranes, but did not present data of the response reproducibility. Since the same design of electrochemical cells has been applied for both techniques of membrane deposition, for the first time a direct comparison of the quality of on wafer fabricated membranes with individual deposited ones could be carried out. The only drawback of this technique is that only thin membranes can be deposited so that this method is not suitable for in-vivo usable membranes. On the other hand, it allows the fabrication of membranes of different and well-defined thicknesses (e.g., simple and double membranes) which are well-suited for the study of sensor kinetics.

The comparison of measured calibration curves with calculated ones showed impressively that the model developed in the last chapter mirrors rather well the real behaviour of enzyme electrodes, thus indicating that the development has overcome the pure empiric stage.

7.1 References

[1] J,C. Pickup, G.W. Shaw and D.J. Claremont, In vivo molecular sensing in diabetes mellitus: an implantable glucose sensor with direct electron transfer, Diabetologia, 32 (1989) 213-217.

[2] M. Shichiri, H. Fukushima, K. Yamaguchi, R. Kawamori, Y. Yamasaki, N. Ueda and T. Kamada, Membrane design for extending the long-life of an implantable glucose sensor, Diab. Nutr. Metab., 2 (1989) 309-313.

[3] G. Velho, Ph. Froguel, D.R. Thévenot and G. Reach, In vivo calibration of a subcutaneous glucose sensor for determination of subcutaneous glucose kinetics, Diab. Nutr. Metab. (Diabetes, Nutrition & Metabolism), 3 (1988) 227-233.

[4] K. Rebrin, U. Fischer, T. v. Woedtke, P. Abel and E. Brunstein, Automated feedback control of subcutaneous glucose concentration in diabetic dogs, Diabetologia, 32 (1989) 573-576.

[5] S. Nakamoto, N. Ito, T. Kuriyama and J. Kimura, A lift-off method for patterning enzyme-immobilized membranes in multi-biosensors, Sensors and Actuators, 13 (1988) 165-172.

Acknowledgements

In the course of this work I have received highly appreciated help from the knowledge, experience and practical skill of many people. In particular, I wish to thank the following:

Professor de Rooij, for his support and continuous interest in this work;

Dr. M. Koudelka, for her decisive contribution to and guidance during the project as well as for reading and discussing the manuscript;

Ms. S. Pochon for wire bonding, chip encapsulation and some of the sensor measurements;

Mr. G. Mondin and Mr. C. Ketterer of the Centre Suisse d'Electronique et de Microtechnique (Neuchâtel), respectively for e-gun evaporation of thin metal films and for most of the SEM-photos;

Mr. S. Jeanneret for various technical advices;

All the collaborators of the Laboratoires de Recherches Métaboliques de la Faculté de Médecine (Geneva) for the in vivo characterization of the sensor;

All my collegues of the Sensors and Actuators Group of the Institute of Microtechnology;

Further I thank Prof. H.-L. Schmidt, Prof. A. Shah, Dr. J. Randin and Dr. M. Koudelka for kindly agreeing to be co-examiners.

The work was supported by grants of the AND (Association Neuchâteloise du Diabète) the Swiss National Science Foundation, The Foundation of Lord Michelham of Hellingly and the Committee for the Promotion of Applied Scientific Research for financial support of this project.

Appendix A
Oxygen solubility tables

If the values of the Bunsen absorption coefficient, α, and the vapor pressure of water, p_1, at a particular temperature are known, equation (3.40) allows the calculation of the oxygen solubility in air-saturated fresh water for any temperature and pressure. Therefore, the value of α can be obtained from eq. (3.31) or (3.33). The value of p_1 can either be calculated from eq.(3.39) or looked up in tables (see Ch. 3, Ref. [16]).

Table A.1: Oxygen solubility [mg/l] in air saturated fresh water.

	temperature [°C]						
P_T [torr]	15	20	25	30	35	37	40
610	8.03	7.23	6.56	5.99	5.50	5.32	5.06
620	8.16	7.35	6.67	6.10	5.60	5.41	5.15
630	8.30	7.47	6.78	6.20	5.69	5.51	5.24
640	8.43	7.59	6.90	6.30	5.79	5.60	5.33
650	8.57	7.72	7.01	6.41	5.89	5.69	5.42
660	8.70	7.84	7.12	6.51	5.98	5.79	5.51
670	8.84	7.96	7.23	6.62	6.08	5.88	5.60
680	8.97	8.08	7.34	6.72	6.18	5.98	5.69
690	9.11	8.20	7.45	6.82	6.27	6.07	5.78
700	9.24	8.33	7.57	6.93	6.37	6.17	5.88
710	9.37	8.45	7.68	7.03	6.47	6.26	5.97
720	9.51	8.57	7.79	7.13	6.56	6.36	6.06
730	9.64	8.69	7.90	7.24	6.66	6.45	6.15
740	9.78	8.81	8.01	7.34	6.76	6.54	6.24
750	9.91	8.93	8.13	7.44	6.86	6.64	6.33
760	10.05	9.06	8.24	7.55	6.95	6.73	6.42
770	10.18	9.18	8.35	7.65	7.05	6.83	6.51
780	10.32	9.30	8.46	7.76	7.15	6.92	6.60

Table A.1 gives oxygen solubilities in mg/l for temperature intervals of 5 °C from 15-40 °C and pressure intervals of 10 torr from 610-780 torr. Tables with smaller intervals and expanded temperature and pressure ranges can be found in the literature (Ch. 3, Ref. [11]).

The dependence of solubility on salt concentration can also be obtained from eq.(3.40) except that now values of α calculated from eq.(3.45) have to be used. For uni-univalent solutions, e.g. saline water, the ionic strength I in eq.(3.45) can be replaced by $[Cl^-]$ (according section 3.4.4).

The values of oxygen solubilities listed in table A.2 are based on an atmospheric pressure (at Neuchâtel) of 720 torr. The table gives the oxygen solubilities in mg/l for ionic strength intervals of 2 g/l from 0 - 20 g/l. According to section 3.4.4 the Krebs physiological solution has a ionic strength of 12.54 g/l. Hence, the air saturated Krebs solution at 720 torr and 37 °C has an oxygen solubility of about 5.4 mg/l.

Table A.2: Oxygen solubility [mg/l] in an air saturated electrolytic solution (P_T = 720 torr).

ionic strength [g/l]	temperature [°C] 0	10	15	20	25	30	37
2	13.49	10.44	9.32	8.41	7.65	7.00	6.20
4	13.18	10.21	9.13	8.25	7.50	6.85	6.05
6	12.87	9.99	8.94	8.08	7.35	6.71	5.89
8	12.56	9.77	8.75	7.92	7.20	6.57	5.73
10	12.24	9.54	8.57	7.75	7.06	6.43	5.58
12	11.93	9.32	8.38	7.59	6.91	6.28	5.42
14	11.62	9.10	8.19	7.43	6.76	6.14	5.26
16	11.31	8.88	8.00	7.26	6.61	6.00	5.11
18	11.00	8.65	7.81	7.10	6.47	5.86	4.95
20	10.69	8.43	7.62	6.93	6.32	5.71	4.79

Appendix B

Approximation of functions by the method of least squares

B.1 Basic concept

A linear system of t equations and n unknowns

$$\begin{aligned} &a_{11}x_1 + a_{12}x_2 + \ldots + a_{1n}x_n = b_1 \\ &a_{21}x_1 + a_{22}x_2 + \ldots + a_{2n}x_n = b_2 \\ &\ldots \\ &a_{t1}x_1 + a_{t2}x_2 + \ldots + a_{tn}x_n = b_t \end{aligned} \qquad \text{(B.1)}$$

can be written in matrix notation as $Ax = b$. We shall write matrices and vectors in boldface type. The matrix A is a collection of $t \times n$ real numbers ordered in a scheme

$$\mathbf{A} = \begin{bmatrix} a_{11} & a_{12} & \ldots & a_{1n} \\ a_{21} & a_{22} & \ldots & a_{2n} \\ \ldots & & & \\ a_{t1} & a_{t2} & \ldots & a_{tn} \end{bmatrix} \qquad \text{(B.2)}$$

The notation (t x n) means that the matrix has t rows and n columns. In an overdetermined system of linear equations there are more rows than columns, so that A is rectangular. The schematic representation of problem (B.1) is

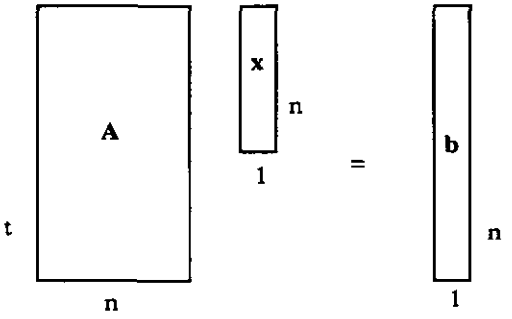

Fig.B.1: Schematic representation of eq.(B.1).

Two matrices are said to be equal, $\mathbf{A} = \mathbf{B}$, if $a_{ij} = b_{ij}$, i = 1,2,...,t, j = 1,2,...,o. The product of a matrix A and a scalar c is a matrix $c\,\mathbf{A} = (c\,a_{ij})$. The sum of two matrices, $\mathbf{C} = \mathbf{A}+\mathbf{B}$ is a matrix with elements $c_{ij} = a_{ij}+b_{ij}$. The product of two matrices A (t x n) and B (n x p) is a matrix C (t x p) with elements

$$c_{ij} = \sum_{k=1}^{n} a_{ik} b_{kj} .$$

Matrix multiplication satisfies the rules

$$\mathbf{A}\,(\mathbf{B}\,\mathbf{C}) = (\mathbf{A}\,\mathbf{B})\,\mathbf{C}\,, \qquad \mathbf{A}\,(\mathbf{B}+\mathbf{C}) = \mathbf{A}\,\mathbf{B} + \mathbf{A}\,\mathbf{C}.$$

However, in general $\mathbf{A}\,\mathbf{B} \neq \mathbf{B}\,\mathbf{A}$, i.e., multiplication is not commutative. The transpose, $\mathbf{A}^T$, of a matrix A is the matrix whose rows are the columns of A.

Inserting a vector x in the left side of (B.1), we get a residual vector

$$\mathbf{r} = \mathbf{A}\,\mathbf{x} - \mathbf{b}. \qquad \text{(B.3)}$$

A solution of an overdetermined system of equations according to the method of least squares is the vector x, for which the Euclidean norm of the residual vector is as small as possible [1]. This is simply a generalization of the well-known geometrical fact that the shortest distance from a point to a linear subspace is the length of the vector which is perpendicular to the subspace. The Euclidean norm of r is

$$\| \mathbf{r} \|^2 = \| \mathbf{A}\,\mathbf{x} - \mathbf{b} \|^2\,, \qquad \| \mathbf{r} \|^2 := \sum_{i=1}^{n} r_i^2 \qquad \text{(B.4)}$$

The square of a vector y can be written as:

$$\| y \|^2 = y^T y \qquad (B.5)$$

Thus, the method of least squares is based on the principle of minimizing the Euclidean norm of the residual vector r as function of x. We maintain now that the solution x_o of the equation

$$A^T A x = A^T b \qquad (B.6)$$

satisfy the condition according the method of least squares.

Proof: We write $x = x_o + y$

Then
$$\begin{aligned} r &= A x - b \\ &= A (x_o + y) - b \\ &= r_o + A y , \end{aligned}$$

where r_o represents the residual vector of the above defined vector x_o. The Euclidean norm of r can be written as:

$$\begin{aligned} \| r \|^2 &= (r_o^T + y^T A^T) (r_o + A y) \\ &= r_o^T r_o + r_o^T A y + y^T A^T r_o + y^T A^T A y \end{aligned}$$

With $r_o = A x_o - b$ and $x_o = (A^T A)^{-1} A^T b$ the middle terms become

$$\begin{aligned} y^T A^T r_o &= (r_o^T A y)^T \\ &= y^T A^T (A (A^T A)^{-1} A^T b - b) \\ &= y^T A^T b - y^T A^T b = 0 \end{aligned}$$

It remains $\| r \|^2 = \| r_o \|^2 + \| A y \|^2$,

consequently $\| r \| \geq \| r_o \|$.

Thus $\| r \|$ and $\| r_o \|$ are only equal if $y = 0$.

Therewith we proofed the theorem:

Theorem B.T.1: The solution of the overdetermined system of linear equations
$A x = b$ (t equations with $n < t$ unknowns)
according to the method of least squares is identical with the solution of the system
$A^T A x = A^T b$ (n equations with n unknowns).

These equations are called the normal equations and have a square matrix. Thus, this system of equations can be solved by applying the Gaussian elimination [2]. The aim of this method is to eliminate the unknowns in a systematic way, so that we end with a triangular system, which we know how to solve. We consider a system of linear equations

$$\begin{aligned} a_{11}\,x_1 + a_{12}\,x_2 + \ldots + a_{1n}\,x_n &= b_1 \\ a_{21}\,x_1 + a_{22}\,x_2 + \ldots + a_{2n}\,x_n &= b_2 \\ \ldots & \\ a_{n1}\,x_1 + a_{n2}\,x_2 + \ldots + a_{nn}\,x_n &= b_n \end{aligned} \qquad \text{(B.7)}$$

and assume that the system $A\,x = b$ with

$$A = \begin{bmatrix} a_{11} & a_{12} & \cdots & a_{1n} \\ a_{21} & a_{22} & \cdots & a_{2n} \\ \cdots & & & \\ a_{n1} & a_{n2} & \cdots & a_{nn} \end{bmatrix}, \quad x = \begin{bmatrix} x_1 \\ x_2 \\ \cdots \\ x_n \end{bmatrix}, \quad b = \begin{bmatrix} b_1 \\ b_2 \\ \cdots \\ b_n \end{bmatrix} \qquad \text{(B.8)}$$

has a unique solution. Introducing now a rectangular matrix

$$B = \begin{bmatrix} a_{11} & a_{12} & \cdots & a_{1n} & -b_1 \\ a_{21} & a_{22} & \cdots & a_{2n} & -b_2 \\ \cdots & & & & \\ a_{n1} & a_{n2} & \cdots & a_{nn} & -b_n \end{bmatrix} \qquad \text{(B.9)}$$

the vector x is then a solution of eq.(B.8) if the scalar product of $B\,v = 0$, where $v = (x_1, x_2, \ldots, x_n, 1)$. This system of equations remains the same if we interchange two raws, or if we multiply one row with a constant $\neq 0$, or if we add one row to another. Now assume that $a_{11} \neq 0$, so that the first row of matrix B can be devided by a_{11}. Hence we get the matrix

$$B^* = \begin{bmatrix} 1 & a_{12}^{(1)} & \dots & a_{1n}^{(1)} & -b_1^{(1)} \\ a_{21} & a_{22} & \dots & a_{2n} & -b_2 \\ \dots & & & & \\ a_{n1} & a_{n2} & \dots & a_{nn} & -b_n \end{bmatrix} \qquad (B.10)$$

where $a_{1i}^{(1)} = \frac{a_{1i}}{a_{11}}$, $b_1^{(1)} = \frac{b_1}{a_{11}}$, $i = 2,3,...,n.$ (B.11)

Then we can eliminate a_{i1} for $i = 2,3,...,n$ by subtracting from the i^{th} row the multiple a_{i1} of the first row:

$$B^{(1)} = \begin{bmatrix} 1 & a_{12}^{(1)} & \dots & a_{1n}^{(1)} & -b_1^{(1)} \\ 0 & a_{22}^{(1)} & \dots & a_{2n}^{(1)} & -b_2^{(1)} \\ \dots & & & & \\ 0 & a_{n2}^{(1)} & \dots & a_{nn}^{(1)} & -b_n^{(1)} \end{bmatrix} \qquad (B.12)$$

where the new coefficients are given by

$$a_{ij}^{(1)} = a_{ij} - a_{i1}\, a_{1j}^{(1)}, \quad b_i^{(1)} = b_i - a_{i1}\, b_1, \quad i = 2,3,...,n, \quad j = 2,3,...,n. \qquad (B.13)$$

This is a system of (n-1) equations in the (n-1) unknowns $x_2,...,x_n$. If $a_{22}^{(1)} \neq 0$, we can in a similiar way eliminate $a_{i2}^{(1)}$ for $i = 3,4,...,n$ from the last (n-2) of these equations. Otherwise, if $a_{22}^{(1)} = 0$ we have to interchange the rows, so that $a_{22}^{(1)} \neq 0$. The elements $a_{11}^{(1)}, a_{22}^{(2)}, a_{33}^{(3)}, \dots$ which appear during the elimination are called pivot elements. If all these are nonzero, we can continue the elimination. After the n^{th} step we get:

$$B^{(n)} = \begin{bmatrix} 1 & a_{12}^{(1)} & \dots & a_{1n}^{(1)} & -b_1^{(1)} \\ 0 & 1 & \dots & a_{2n}^{(2)} & -b_2^{(2)} \\ \dots & & & & \\ 0 & 0 & \dots & 1 & -b_n^{(n)} \end{bmatrix} \qquad \text{(B.14)}$$

Thus we have reduced eq. (B.9) to the triangular system of eq.(B.14), from which the unknowns can be calculated as follows:

$$x_n = b_n^{(n)}, \qquad x_{n-1} = b_{n-1}^{(n-1)} - a_{n-1\,n}^{(n-1)}\, x_n$$

in general $$x_i = b_i^{(i)} - \sum_{m=i+1}^{n} a_{im}^{(i)} x_m , \qquad i = n,n-1,\dots,1. \qquad \text{(B.15)}$$

The algorithme described by (B.15) is called back substitution.

B.2 Special matrices

B.2.1 Approximotion of linear functions

The problem of drawing a straight line trough a number of t measured points $b_1(x_1),b_2(x_2),...,b_n(x_n)$, where the b_i are functions of the x_i , can be treated by the above reviewed method of least squares. The appropriate system of linear equations can be written as

$$\begin{aligned} a_0 + a_1 x_1 &= b_1 \\ a_0 + a_1 x_2 &= b_2 \\ &\cdots \\ a_0 + a_1 x_t &= b_t \end{aligned} \qquad \text{(B.16)}$$

or in matrix notation: $\mathbf{A}\,\mathbf{y} = \mathbf{b}$
with

$$\mathbf{A} = \begin{bmatrix} 1 & x_1 \\ 1 & x_2 \\ \cdots & \\ 1 & x_t \end{bmatrix}, \quad \mathbf{y} = \begin{bmatrix} a_o \\ a_1 \end{bmatrix}, \quad \mathbf{b} = \begin{bmatrix} b_1 \\ b_2 \\ \cdots \\ b_t \end{bmatrix} \qquad \text{(B.17)}$$

According to the theorem B.T.1 we write $\mathbf{A}^T\mathbf{A}\,\mathbf{y} = \mathbf{A}^T\mathbf{b}$, or in explicit form:

$$\begin{bmatrix} 1 & 1 & \cdots & 1 \\ x_1 & x_2 & \cdots & x_t \end{bmatrix} \begin{bmatrix} 1 & x_1 \\ 1 & x_2 \\ \cdots & \\ 1 & x_t \end{bmatrix} \begin{bmatrix} a_o \\ a_1 \end{bmatrix} = \begin{bmatrix} 1 & 1 & \cdots & 1 \\ x_1 & x_2 & \cdots & x_t \end{bmatrix} \begin{bmatrix} b_1 \\ b_2 \\ \cdots \\ b_t \end{bmatrix} \qquad \text{(B.18)}$$

$$\mathbf{A}^T\mathbf{A} = \begin{bmatrix} t & \sum_{i=1}^{t} x_i \\ \sum_{i=1}^{t} x_i & \sum_{i=1}^{t} (x_i)^2 \end{bmatrix}, \qquad \mathbf{A}^T\mathbf{b} = \begin{bmatrix} \sum_{i=1}^{t} b_i \\ \sum_{i=1}^{t} x_i b_i \end{bmatrix} \qquad \text{(B.19)}$$

so that eq.(B.18) becomes

$$\begin{bmatrix} t & \sum_{i=1}^{t} x_i & -\sum_{i=1}^{t} b_i \\ \sum_{i=1}^{t} x_i & \sum_{i=1}^{t} (x_i)^2 & -\sum_{i=1}^{t} x_i b_i \end{bmatrix} \begin{bmatrix} a_o \\ a_1 \\ 1 \end{bmatrix} = \begin{bmatrix} 0 \\ 0 \\ 0 \end{bmatrix} \tag{B.20}$$

Applying the Gaussian elimination this system of equations can be reduced to a triangular system. The first row of the (2x3)-matrix on the left side of eq.(B.20) can be devided by t, resulting in

$$\begin{bmatrix} 1 & \frac{1}{t}\sum_{i=1}^{t} x_i & -\frac{1}{t}\sum_{i=1}^{t} b_i \\ \sum_{i=1}^{t} x_i & \sum_{i=1}^{t} (x_i)^2 & -\sum_{i=1}^{t} x_i b_i \end{bmatrix} \tag{B.21}$$

Subtracting from the second row the multiple $\sum_{i=1}^{t} x_i$ of the first one we get

$$\begin{bmatrix} 1 & \frac{1}{t}\sum_{i=1}^{t} x_i & -\frac{1}{t}\sum_{i=1}^{t} b_i \\ 0 & \sum_{i=1}^{t} (x_i)^2 - \frac{1}{t}\left(\sum_{i=1}^{t} x_i\right)^2 & -\sum_{i=1}^{t} x_i b_i + \frac{1}{t}\left(\sum_{i=1}^{t} x_i\right)\left(\sum_{i=1}^{t} b_i\right) \end{bmatrix} \tag{B.22}$$

Thus from the second row

$$a_1 = \frac{\sum_{i=1}^{t} x_i b_i - \frac{1}{t}\left(\sum_{i=1}^{t} x_i\right)\left(\sum_{i=1}^{t} b_i\right)}{\sum_{i=1}^{t} (x_i)^2 - \frac{1}{t}\left(\sum_{i=1}^{t} x_i\right)^2} \tag{B.23}$$

which represents the slope of the linear function. The constant a_o can be calculated from the first row using eq.(B.15) and taking into account eq.(B.23)

$$a_o = \frac{1}{t}\left(\sum_{i=1}^{t} b_i - a_1 \sum_{i=1}^{t} x_i\right) \qquad (B.24)$$

so that the best linear fit of problem (B.16) according to the method of least squares is

$$b(x) = a_o + a_1 x .$$

B.2.2 Approximation of square functions

Assuming that calibration curves of amperometric sensors are continuous functions without local maximums, they can be approximated by square functions of the form

$$f(x) = a_o + a_1 x + a_2 x^2 .$$

The method of fitting measured calibration curves by square functions has been used extensively in the chapters three to five. A Pascal program has been written to perform this approximation using the theorem B.T.1 and the procedure of Gaussian elimination, so that we restrict us to present the system of equations required for the application of the method of least squares.

Assuming that, i.g., the current i depends only on the bulk substrate concentration c, we write

$$\begin{aligned} i(c_1) &= a_0 + a_1 c_1 + a_2 (c_1)^2 \\ i(c_2) &= a_0 + a_1 c_2 + a_2 (c_2)^2 \\ &\cdots \\ i(c_n) &= a_0 + a_1 c_n + a_2 (c_n)^2 \end{aligned} \qquad (B.25)$$

and in matrix notation:

$$\begin{bmatrix} 1 & c_1 & (c_1)^2 \\ 1 & c_2 & (c_2)^2 \\ \cdots & & \\ 1 & c_n & (c_n)^2 \end{bmatrix} \begin{bmatrix} a_o \\ a_1 \\ a_2 \end{bmatrix} = \begin{bmatrix} i_1 \\ i_2 \\ \cdots \\ i_n \end{bmatrix} \qquad (B.26)$$

which can be solved applying the procedure reviewed above.

B.3 References

[1] G. Dahlquist and A. Björck
Numerical Methods.
Prentice Hall, Englewood Cliffs, 1973, chapter 5.

[2] H. Rutishauser
Vorlesungen über numerische Mathematik.
Birkhäuser Verlag, Basel, 1976.